

ISSN 2074-272X

науково-практичний  
журнал

2018/6



# **EIE** Електротехніка і Електромеханіка

**Electrical Engineering**

**& Electromechanics**

**Електротехніка. Визначні події. Славетні імена  
Електричні машини та апарати**

**Електротехнічні комплекси та системи.**

**Силова електроніка**

**Теоретична електротехніка та електрофізика**

**Техніка сильних електричних та магнітних полів.**

**Кабельна техніка**

**Електричні станції, мережі і системи**

**З 2015 р. журнал індексується у міжнародній  
наукометричній базі Web of Science  
Core Collection: Emerging Sources  
Citation Index**



# «ELECTRICAL ENGINEERING & ELECTROMECHANICS»

SCIENTIFIC & PRACTICAL JOURNAL

Journal was founded in 2002

## Founders:

National Technical University «Kharkiv Polytechnic Institute» (Kharkiv, Ukraine)

State Institution «Institute of Technical Problems of Magnetism of the NAS of Ukraine» (Kharkiv, Ukraine)

## INTERNATIONAL EDITORIAL BOARD

<b>Klymenko B.V.</b>	<b>Editor-in-Chief</b> , Professor, National Technical University "Kharkiv Polytechnic Institute" (NTU "KhPI"), Ukraine
<b>Sokol Ye.I.</b>	<b>Deputy Editor</b> , Professor, Corresponding member of NAS of Ukraine, Rector of NTU "KhPI", Ukraine
<b>Rozov V.Yu.</b>	<b>Deputy Editor</b> , Professor, Corresponding member of NAS of Ukraine, Director of State Institution "Institute of Technical Problems of Magnetism of the NAS of Ukraine"(SI "ITPM NASU"), Kharkiv, Ukraine
<b>Batygin Yu.V.</b>	Professor, Kharkiv National Automobile and Highway University, Ukraine
<b>Bíró O.</b>	Professor, Institute for Fundamentals and Theory in Electrical Engineering, Graz, Austria
<b>Bolyukh V.F.</b>	Professor, NTU "KhPI", Ukraine
<b>Colak I.</b>	Professor, Nisantasi University, Istanbul, Turkey
<b>Doležel I.</b>	Professor, University of West Bohemia, Pilsen, Czech Republic
<b>Féliachi M.</b>	Professor, Technological Institute of Saint-Nazaire, University of Nantes, France
<b>Gurevich V.I.</b>	Ph.D., Honorable Professor, Central Electrical Laboratory of Israel Electric Corporation, Haifa, Israel
<b>Ida N.</b>	Professor, The University of Akron, Ohio, USA
<b>Kildishev A.V.</b>	Associate Research Professor, Purdue University, USA
<b>Kuznetsov B.I.</b>	Professor, SI "ITPM NASU", Ukraine
<b>Kyrylenko O.V.</b>	Professor, Member of NAS of Ukraine, Institute of Electrodynamics of NAS of Ukraine (IED of NASU), Kyiv, Ukraine
<b>Nacke B.</b>	Professor, Gottfried Wilhelm Leibniz Universität, Institute of Electrotechnology, Hannover, Germany
<b>Podoltsev A.D.</b>	Professor, IED of NASU, Kyiv, Ukraine
<b>Rainin V.E.</b>	Professor, Moscow Power Engineering Institute, Russia
<b>Rezynkina M.M.</b>	Professor, NTU "KhPI", Ukraine
<b>Shkolnik A.A.</b>	Ph.D., Central Electrical Laboratory of Israel Electric Corporation, member of CIGRE (SC A2 - Transformers), Haifa, Israel
<b>Trichet D.</b>	Professor, Institut de Recherche en Energie Electrique de Nantes Atlantique, Nantes, France
<b>Yatchev I.</b>	Professor, Technical University of Sofia, Sofia, Bulgaria
<b>Yuferov V.B.</b>	Professor, National Science Center "Kharkiv Institute of Physics and Technology", Ukraine
<b>Zagirnyak M.V.</b>	Professor, Member of NAES of Ukraine, rector of Kremenchuk M.Ostrohradskiy National University, Ukraine
<b>Zgraja J.</b>	Professor, Institute of Applied Computer Science, Lodz University of Technology, Poland

## ISSUE 6/2018

### TABLE OF CONTENTS

#### *Electrical Engineering. Great Events. Famous Names*

<b>Baranov M.I.</b> An anthology of the distinguished achievements in science and technique. Part 46: Thermonuclear power engineering. Thermonuclear reactors and power plants: retrospective view of investigations of the controlled thermonuclear synthesis, their state-of-the-art and future .....	3
---	---

#### *Electrical Machines and Apparatus*

<b>Bolyukh V.F., Schukin I.S.</b> An optimization approach to the choice of parameters of linear pulse induction electromechanical converter .....	18
--	----

#### *Electrotechnical Complexes and Systems. Power Electronics*

<b>Zhemerov G.G., Krylov D.S.</b> Concept of construction of power circuits of a multilevel modular converter and its transistor modules .....	26
<b>Kuznetsov B.I., Nikitina T.B., Kolomiets V.V., Bovdui I.V.</b> Improving of electromechanical servo systems accuracy ....	33
<b>Yarovenko V.A., Chernikov P.S., Varbanets R.A., Zaritskaya E.I.</b> Optimal control of the electric ships' propulsion motors during reversal .....	38

#### *Theoretical Electrical Engineering and Electrophysics*

<b>Suprunovska N.I., Shcherba M.A.</b> Application of Vyshnegradky's diagrams for transient analysis in electric discharge installations with stochastic load .....	47
<b>Chunikhin K.V.</b> On the influence of the level of an external magnetic field and the length on the magnetic moment of cylindrical cores .....	51

#### *High Electric and Magnetic Field Engineering. Cable Engineering*

<b>Baranov M.I.</b> A choice of sections of electric wires and cables in circuits of devices of high-voltage high-current impulse technique .....	56
<b>Bezprozvannykh G.V., Boyko A.N., Roginskiy A.V.</b> Effect of a dielectric barrier on the electric field distribution in high-voltage composite insulation of electric machines .....	63

#### *Power Stations, Grids and Systems*

<b>Dehghani M., Mardaneh M., Montazeri Z., Ehsanifar A., Ebadi M.J., Grechko O.M.</b> Spring search algorithm for simultaneous placement of distributed generation and capacitors .....	68
---	----

**Editorial office address:** Dept. of Electrical Apparatus, NTU «KhPI», Kyrpychova Str., 2, Kharkiv, 61002, Ukraine  
**phones:** +380 57 7076281, +380 67 3594696, **e-mail:** a.m.grechko@gmail.com (**Grechko O.M.**)

**ISSN (print) 2074-272X**

© National Technical University «Kharkiv Polytechnic Institute», 2018

**ISSN (online) 2309-3404**

© State Institution «Institute of Technical Problems of Magnetism of the NAS of Ukraine», 2018

Printed 17 December 2018. Format 60 x 90 1/8. Paper – offset. Laser printing. Edition 200 copies.

Printed by Printing house «Madrid Ltd» (11, Maksymilianivska Str., Kharkiv, 61024, Ukraine)

M.I. Baranov

## AN ANTHOLOGY OF THE DISTINGUISHED ACHIEVEMENTS IN SCIENCE AND TECHNIQUE. PART 46: THERMONUCLEAR POWER ENGINEERING. THERMONUCLEAR REACTORS AND POWER PLANTS: RETROSPECTIVE VIEW OF INVESTIGATIONS OF THE CONTROLLED THERMONUCLEAR SYNTHESIS, THEIR STATE-OF-THE-ART AND FUTURE

*Purpose. Preparation of brief scientific and technical review about the retrospective view of investigations, state-of-the art, problems and possible prospects of development in the world of thermonuclear power engineering. Methodology. Known scientific methods of collection, analysis and analytical treatment of the opened scientific and technical information of world level in area of the controlled thermonuclear synthesis (CTS) and thermonuclear power engineering, resulted in scientific monographs, journals and internet reports. Results. A brief analytical scientific and technical review is resulted about the retrospective view of researches, modern state, basic achievements, existent problems and possible prospects of development of thermonuclear power engineering in the leading countries of the world. Nuclear physical bases of process of flowing of CTS are resulted in mixture of light nuclei. Information is presented about the results of the initial and modern stages of world researches in area of CTS. Basic constructions and technical descriptions of thermonuclear reactors (TNR), utilizing the magnetic and inertia withholding of hot plasma are described. World progress is analyzed in area of development, creation and research of experimental TNR, being based on the systems of withholding of hot plasma in toroidal magnetic «traps» (options: tokamaks and stellarators) and inertia systems of laser-impulse technology of microscopic explosions of targets-capsules of thermonuclear fuel. Information is resulted about the basic types of thermonuclear fuel, which can be used in the duty cycles of TNR, and safety of TNR. The basic systems and devices of the largest in the world of experimental TNR-tokamak of ITER type (with a reference cost of EUR 15 billion and term of putting into an experimental operation in 2025), erected now within the framework of international project in France are described. Basic problems are indicated in area of CTS in experimental TNR and creations in the future of the thermonuclear power plants (TNPP). The important role of TNPP and thermonuclear power engineering is marked on the whole in providing of humanity in a long-term prospect electric energy. Originality. Certain systematization of the scientific and technical materials touching the problem of CTS of light nuclei and practical application in the peaceful aims of thermonuclear energy known from the sources opened in outer informative space is executed. It is shown on the basis of approach of the systems, that, in spite of row of existent technical problems in area of creation of industrial TNR and practical commercial capture thermonuclear energy, thermonuclear power engineering has an important value for providing in remote future electric energy of all of humanity. Practical value. Scientific popularization and deepening for the students of technical universities, engineering, technical and scientific workers, working in the power sector of economy, scientific and technical knowledge in area of CTS and thermonuclear power engineering, extending their scientific range of interests and further development of scientific and technical progress in society. References 29, figures 16, tables 2.*

*Key words:* thermonuclear synthesis and reactor, thermonuclear power engineering, tokamak, stellarator, laser-impulse reactor, safety of thermonuclear reactor, thermonuclear power plant of the future, problems and possible prospects of development of world thermonuclear power engineering.

*Приведен научно-технический обзор о ретроспективе исследований в ведущих странах мира управляемого термоядерного синтеза (УТС) легких ядер, современном состоянии разработок и возможных перспективах мирового развития наукоемкой техники в области термоядерной энергетики. Приведены ядерно-физические основы процесса протекания УТС в смеси легких ядер. Представлены данные о результатах начального и современного этапов исследований в области УТС. Описаны основные конструкции и технические характеристики термоядерных реакторов (ТЯР), использующих магнитное и инерционное удержание горячей плазмы. Проанализирован мировой прогресс в области разработки, создания и исследования экспериментальных ТЯР, базирующихся на системах удержания горячей плазмы в тороидальных магнитных «ловушках» (установки-токамаки и стеллараторы) и инерционных системах лазерно-импульсной технологии микровзрывов мишеней-капсул термоядерного топлива. Приведены данные об основных видах термоядерного топлива, которое может применяться в рабочих циклах ТЯР, и безопасности ТЯР. Указаны основные проблемы в области УТС для экспериментальных ТЯР и создания в будущем термоядерных электрических станций (ТЯЭС). Отмечена важная роль ТЯЭС и термоядерной энергетики в обеспечении человечества в долгосрочной перспективе электроэнергией. Библ. 29, рис. 16, табл. 2.*

*Ключевые слова:* термоядерный синтез и реактор, термоядерная энергетика, токамак, стелларатор, лазерно-импульсный реактор, безопасность термоядерного реактора, термоядерная электрическая станция будущего, проблемы и возможные перспективы развития мировой термоядерной энергетики.

**Introduction.** From the world history of development on the planet Earth of modern civilization, it is clear that the needs of mankind in various types of energy are steadily increasing from year to year. In this regard, earthlings objectively face common planetary questions: how to satisfy the growing population's growing energy needs of people and industries around the world and on what principles to create further powerful

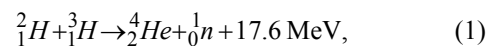
new and safe artificial energy sources? For several centuries, the main source of both thermal and electrical energy for the inhabitants of the Earth has been the use (as a rule, combustion) of planetary reserves of natural fossil fuels – wood, coal, oil and gas. It is known that the reserves of this fuel on our planet are very limited. It is believed that by 2050 energy production in the world will

© M.I. Baranov

increase by about three times compared with its current level and will be about  $10^{21}$  J/year [1]. Therefore, in the foreseeable future, such a source of energy as fossil fuels will have to be replaced by earthlings with other sources of energy and, accordingly, with other types of its production. In this regard, at present, nuclear power [2] and alternative energy with its renewable energy sources [3] have been actively introduced into the production of thermal and electrical energy throughout the world. According to reputable energy specialists, alternative energy is able to meet the energy needs of humanity only in a relatively small fraction of energy (now this share in the world does not exceed 10 % [3]). Therefore, objectively nuclear power remains for us the main candidate for the energy of the near future [1]. At present, nuclear physicists and power engineers have mastered only nuclear fission reactions of heavy nuclei of a number of isotopes of such radioactive chemical elements as uranium  ${}_{92}^{238}\text{U}$ , plutonium  ${}_{94}^{244}\text{Pu}$ , and thorium  ${}_{90}^{232}\text{Th}$  in this complex energy sector on an industrial scale [2]. These reactions are widely used at modern high-power nuclear power plants (NPPs) based on the use of *nuclear reactors* (NRs) operating on slow or fast neutrons in their technological cycle [2, 4]. A significant disadvantage of NRs is the presence from their work of long-lived radioactive waste in large quantities, representing a huge world problem. Huge financial resources are spent on disposal and safe storage of this waste in the world. In addition, this waste for tens of thousands of years poses a serious environmental threat to all life on Earth. Taking into account these features of the operation of nuclear radiation at nuclear power plants, nuclear physicists since the 1950s turned their attention to thermonuclear synthesis reactions occurring in *thermonuclear reactors* (TNRs). The main and fundamental difference of these nuclear synthesis reactions in the TNR from nuclear fission reactions in the NR is the absence of long-lived radioactive waste from the TNR operation. It is believed that after stopping the TNR, the induced radioactivity of the refractory walls of the protective *blanket* in its core will decrease in time to safe levels for  $\sim 30$  years [1]. In addition, there are inexhaustible fuel reserves on the Earth for thermonuclear synthesis reactions. Despite all the difficulties of the implementation of controlled thermonuclear synthesis (CTS) of light chemical elements (for example, such hydrogen  ${}^1_1\text{H}$  (protium) isotopes as deuterium D –  ${}^2_1\text{H}$  and tritium T –  ${}^3_1\text{H}$  [4] in the TNR, in the mid-1950s leading nuclear countries of the world, including the USSR, the USA, the UK and France, to launch large-scale studies on CTS [1, 5, 6]. Add to the above that by this time in the USA and the USSR for military purposes successful tests of the first powerful hydrogen charges and bombs [1, 7] used explosive-type thermonuclear reactions and confirmed the principal possibility of the realization in terrestrial conditions of thermonuclear deuterium D and Tritium T synthesis were carried out.

**The goal** of the paper is preparation of a scientific and technical review of a retrospective of research, the current state, problems and possible prospects for the development of thermonuclear energy in the world.

**1. Brief fundamentals of the physics of thermonuclear synthesis of light nuclei in the TNR.** To begin with, let us point out that CTS is a synthesis of heavier atomic nuclei from less light nuclei, non-explosive in the macrovolume of a substance, in order to obtain energy [4, 6]. In accordance with the laws of nuclear physics, energy in CTS is released due to the mass defect of the nuclei participating in it – the mass of the resulting nuclei and particles turns out to be less than the mass of the original nuclei [4]. Applying to the CTS the law of energy conservation and the Einstein principle of equivalence of mass and energy, we can verify the reliability of the physical fact of the release of the energy of a strong interaction in CTS. So, for the nuclear reaction of the synthesis of deuterium D and tritium T (Fig. 1), proceeding according to the scheme



for each act of synthesis (fusion) of these nuclei, energy releases equal to about 17.6 MeV [1, 4, 6]. As a result of this nuclear reaction, such a chemical element as helium with its  ${}^4_2\text{He}$  nucleus, having kinetic energy of 3.5 MeV, and a fast high-energy neutron  ${}^1_0\text{n}$ , which has kinetic energy of 14.1 MeV, «born». It is necessary to remind the reader of the well-known data that the off-system energy unit used in nuclear physics  $1 \text{ eV} = 1.602 \cdot 10^{-19} \text{ J}$  (one electron volt is the energy that an electron acquires, which overcomes a potential difference of one volt in the electric field) is practically equivalent to a micro-substance with absolute temperature of 11600 K [4]. We add that according to the laws of molecular physics, the absolute temperature of a gas (plasma) is a measure of the average kinetic energy of its molecules (atomic nuclei) [4]. In addition, we note that in order for (1) the D – T type reaction to proceed, in the TNR core a temperature of at least  $100 \cdot 10^6 \text{ K}$  should be maintained [4, 5, 8]. The reason for this is that to merge two nuclei into one, you first need to bring them closer to the distance between the forces of strong interaction, overcoming the Coulomb repulsion of their positively charged protons (from nuclear physics it is known that for all nuclei the forces of strong interaction have a radius of less than for their Coulomb repulsion [4]). For TNR, the only way to overcome these Coulomb forces is to use the energy of the thermal motion of the nuclei [4-8].

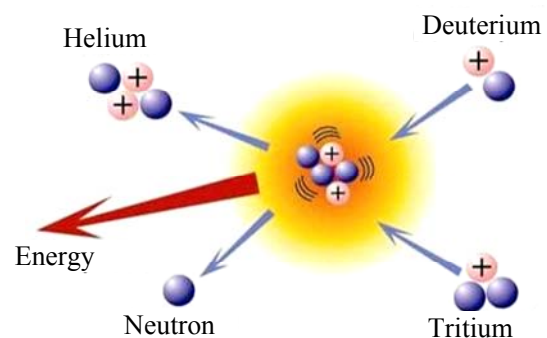


Fig. 1. Schematic representation of a promising thermonuclear synthesis reaction in TNR of deuterium D and tritium T [6]

In the course of many years of research by nuclear physicists from leading scientific centers of the world, it

has been established that at least the following three basic conditions must be fulfilled simultaneously for a reliable flow of CTS in a high-temperature plasma (a mixture of light nuclei used) of the TNRs:

- the rate of nuclear collisions in a plasma should correspond to its temperature  $T_p$  in the TNR chamber (in this case, for a D – T reaction, the temperature  $T_p > 10^8$  K);
- the Lawson criterion formulated for a D – T type thermonuclear reaction in the form of the following mathematical relationship:  $n_p \tau_p > 10^{14}$  cm<sup>-3</sup>·s, where  $n_p$ ,  $\tau_p$  are the density and retention time of a high-temperature plasma in the active zone of the TNR, respectively;
- the criterion for «ignition» of a mixture of light nuclei.

Here we need to note that the value of  $\tau_p$  is not the time during which a hot plasma is maintained in the TNR with temperature  $T_p$  indicated above. It should be pointed out that the time  $\tau_p$  of plasma confinement in the TNR is equal to the ratio of the thermal energy stored in the plasma under consideration to the power losses of this energy [9]. For a better understanding of this special material from the field of high-temperature plasma physics, let us point out that, according to the Lawson criterion at a temperature  $T_p$  a mixture of deuterium D and tritium T in the TNR core equal to 10 keV (approximately  $116 \cdot 10^6$  [4]), for flow in it (in this zone) of the CTS we need to obtain in TNR a product of the number  $n_p$  of particles of the indicated thermonuclear fuel of 1 cm<sup>3</sup> by the time  $\tau_p$  of their retention (in seconds), numerically equal to at least  $10^{14}$  cm<sup>-3</sup>·s. In this case, it is unimportant that a plasma with concentration of about  $n_p = 10^{14}$  cm<sup>-3</sup> and its confinement time  $\tau_p = 1$  s or with concentration  $n_p = 10^{23}$  cm<sup>-3</sup> and its confinement time  $\tau_p = 1$  ns will be in the TNR [9]. It is believed that the Lawson criterion is responsible for obtaining in the TNR an energetically favorable thermonuclear synthesis reaction in a mixture of light nuclei. The fulfillment of the plasma «ignition» criterion for the TNR means that the fraction of thermonuclear energy that remains in the plasma is enough to maintain the required temperature  $T_p$  in it and additional heating of the plasma from light nuclei in the TNR is not required [9].

**2. The initial stage of research on controlled thermonuclear synthesis.** In 1950, at the suggestion of Academician of the Academy of Sciences of the USSR I.V. Kurchatov (1903-1960), Corresponding Member of the Academy of Sciences of the USSR L.A. Artsimovich (1909-1973) was appointed by the Chairman of the USSR Council of Ministers I.V. Stalin as scientific supervisor of the Soviet experimental studies on the CTS [10]. Since that time, research began in the world on the CTS. It is generally accepted that the initial idea and the first scheme of building a laboratory unit for obtaining the CTS were proposed in 1950 by a talented Soviet self-taught physicist, then serving as a sergeant for military service in the Far East of the country, O.A. Lavrentiev (1926-2011), worked for many years after the turning point for him and the whole USSR the year 1953 (the time of I.V. Stalin's death, the execution of L.P. Beria and

the actual «expulsion» of this physicist by his detractors-scientists from Moscow) at the Ukrainian Institute of Physics and Technology (UPhTI, now the National Scientific Center «KhPhTI» of the National Academy of Sciences of Ukraine, Kharkiv) and which first became Candidate of Physical and Mathematical Sciences in the USSR and then Doctor of Physical and Mathematical Sciences in independent Ukraine [7, 11, 12]. A surprising fact is that it would seem that the amateur physicist O.A. Lavrentiev proposed in complete isolation on Sakhalin Island the installation scheme for the implementation of the CTS in 1951 which was refined by professional physicists then still Candidate of Physical and Mathematical Sciences A.D. Sakharov (1921-1989) and Corresponding Member of the Academy of Sciences of the USSR I.E. Tamm (1895-1971), who worked at the P.N. Lebedev Physical Institute of the Academy of Sciences of the USSR and both of them later became Academicians of the Academy of Sciences of the USSR and the Heroes of Labor for the outstanding results of the work on the USSR Atomic Project, and finally received the name TOKAMAK, which is widely known in the scientific world [11-14]. This abbreviation of purely Soviet origin is decoded as «TOroidal CAmera with MAgnetic COils» [5, 9]. Since the 1950s, in the field of controlled synthesis, the era of tokamak installations began in the scientific physical world, which continues to this day.

We emphasize that the technical proposals of O.A. Lavrentiev on the CTS, set forth by him in a number of letters to the Central Committee of the Communist Party and personally to I.V. Stalin, served as a kind of «catalyst» for the appearance in the USSR of the government program of CTS research [15]. So, on May 5, 1951, I.V. Stalin approved the secret Resolution of the Council of Ministers of the USSR No. 1463-732cc/on «*On the conduct of research and experimental work to clarify the possibility of a magnetic thermonuclear reactor*» (it is now declassified) [15]. This document was the first not only in the USSR, but also the first government act in the world, indicating the beginning of the exploratory works of physicists on the CTS. It is interesting to note that the author on official business in the 2000s was fortunate enough to personally communicate with the legendary physicist O.A. Lavrentiev, who left a noticeable «trace» in domestic atomic science and technology, despite all adversities and upheavals in his rich creative life. Getting acquainted with the materials of the mid-1950s on the CTS [12, 15], proposed by this talented nugget man with a seven-year education, alone at the remote edge of the USSR, along with other scientists, one is struck by his intuition and abilities.

**2.1. Thermonuclear tokamak installations.** Fig. 2 in general form shows the scheme for constructing the thermonuclear installation TOKAMAK used at the initial stage of studies of the CTS [9-14].

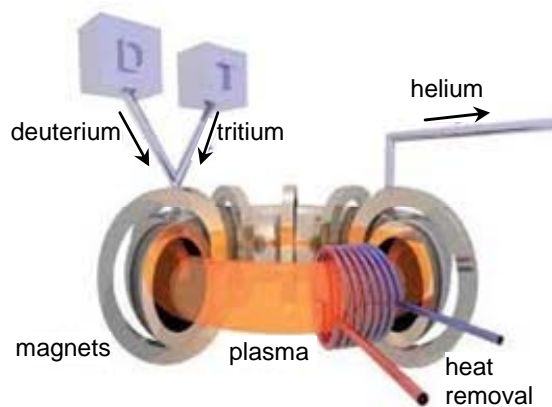


Fig. 2. Schematic representation of the TOKAMAK thermonuclear facility with superconducting coils of toroidal magnetic field, which uses in its vacuum toroidal chamber a high-temperature plasma from Mixture of interacting nuclei of deuterium D and tritium T [9]

We point out that from 1951, M.A. Leontovich (1903-1981), future Academician of the Academy of Sciences of the USSR, headed theoretical studies on the problem of the CTS in the USSR [12]. It is important to note that in 1956, by special order of the Chairman of the USSR Council of Ministers N.S. Khrushchev, works on the CTS in the USSR were completely declassified [10]. This allowed Academician of the Academy of Sciences of the USSR I.V. Kurchatov in the same 1956 when he traveled to the UK as part of a government delegation make a presentation at the British Nuclear Center (Harwell) on the first results of the CTS research obtained by Soviet physicists. This event for the West has become a real sensation (their own work on the CTS was secretly «behind the seal»). From Fig. 2 it can be seen that ring-shaped superconducting coils cooled by liquid helium create a toroidal magnetic field in tokamak, isolating the high-temperature D – T plasma from the walls of its toroidal chamber [5, 8]. In this regard, high-temperature plasma in the TNR is not held by the walls of the toroidal chamber with a refractory blanket, which is not able to withstand its temperature of hundreds of millions of degrees, but by specially created crossed magnetic fields: toroidal and poloidal (Fig. 3). A special feature of the TOKAMAK was the use of a ring electric current flowing directly through the D – T plasma and intended both for its ohmic heating and creating around the cord of a hot plasma of an azimuthal magnetic field necessary for its additional radial compression and reliable confinement.

According to Fig. 3 lines of force of the total magnetic field in the tokamak installation have the shape of spirals, covering the central annular axis of the plasma torus, in which the CTS reactions should occur. The Lorentz force acting on the charged particles of hot plasma (ions and electrons) in a magnetic field causes them to rotate along so-called Larmor circles around the indicated spirals-lines of force of the total magnetic field in the toroidal plasma cord [4]. The greater the magnetic flux density in the tokamak hot plasma, the smaller the Larmor radius of these particles in the mixture of reactive nuclei of thermonuclear fuel. This circumstance will prevent the plasma from spreading across the total magnetic field in its toroidal cord. It should be noted that, together with plasma

particles, the considered magnetic field of a tokamak will keep charged products of a thermonuclear reaction in its «trap». If D – T mixture is used, these products will be helium  ${}^4_2\text{He}$  nuclei (alpha particles with energy of 3.5 MeV) [7]. When cooled during Coulomb collisions with plasma particles, these products of D – T reactions will transfer their energy to the plasma. This phenomenon opens up the possibility of obtaining a mode with self-sustaining thermonuclear burning in tokamaks [1].

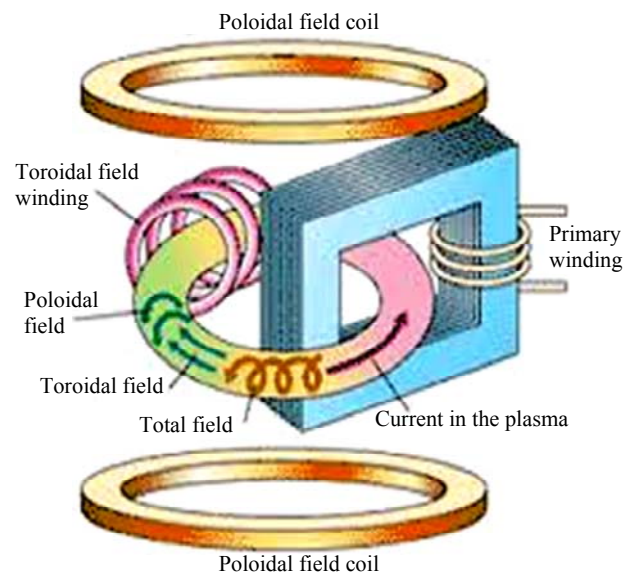


Fig. 3. An advanced scheme for constructing a TOKAMAK thermonuclear installation, containing superconducting coils of toroidal and poloidal magnetic fields, and also the excitation system in the plasma of the ring current [1, 5]

In 1968, a group of Soviet physicists under the supervision of Academician of the Academy of Sciences of the USSR L.A. Artsimovich at the TOKAMAK-3 facility (Fig. 4), for the first time in the world, make it possible to register «thermonuclear» neutrons, «born» as a result of a nuclear reaction of the CTS in a mixture of deuterium D and tritium T nuclei [10]. The highest temperature of the D – T plasma in a closed magnetic system («trap») of a toroidal type of the 1st generation of the Soviet tokamak installation of the TOKAMAK-3 type reached this period about 0.5 keV ( $5.8 \cdot 10^6$  K) [1, 16]. The principle of magnetic confinement of hot plasma in the implementation of the CTS, implemented in the scheme in Fig. 3, was also used in the creation in the 1970s of the 2nd generation of tokamak installations (T-7, T-10 and T-11 types) in the USSR [1]. We point out that the UPHTI-KhPhTI of the Ukrainian SSR Academy of Sciences (Kharkiv) was in the former USSR one of the leading scientific centers for the development, creation and research of experimental thermonuclear facilities.

For example, in 1978, the TOKAMAK-7 large research thermonuclear installation [7, 17] was put into operation at the KhPhTI of the Academy of Sciences of the Ukrainian SSR. In addition, this principle of building tokamaks was also applied when creating similar thermonuclear facilities abroad (for example, PLT and DIII-D types in the USA, ASDEX types in Germany, TER in France and JET-2 in Japan) [1]. At tokamaks installations of the 2nd generation, the temperature

levels in the thermonuclear plasma reached several keV (several tens of millions of degrees), and the density  $n_p$  of the hot plasma was  $\sim 10^{20} \text{ m}^{-3}$  [1]. In the 1980s, the 3rd generation of tokamak installations with large radius of a toroidal chamber up to 2-3 m and a plasma ring current of several megaamperes (for example, types JET and TORUS-SUPRA in Europe, JT60-U in Japan, TFTR in the USA and T-15 in the USSR) [1, 18] was developed. Fig. 5 shows a general view of the installation TOKAMAK-15 [18].

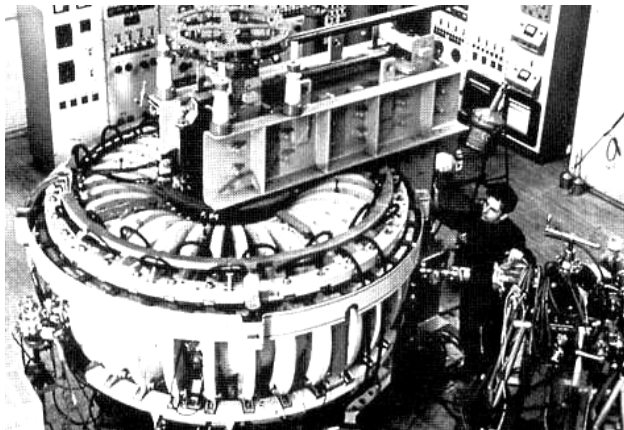


Fig. 4. General view of one of the world's first tokamak installations of the TOKAMAK-3 type built by Soviet physicists and electrical engineers at the I.V. Kurchatov Institute of Atomic Energy (1968, Moscow, USSR) [11]

Table 1 presents the main technical characteristics of the above mentioned experimental tokamaks of the 3rd generation, in which the parameter  $Q_f = P_{syn}/P_{cost}$ , where  $P_{syn}$ ,  $P_{cost}$  are, respectively, the values of the power of thermonuclear synthesis and the costs used, numerically did not exceed 1 [1, 18].

Note that in all thermonuclear tokamaks built as of 2017 in a number of industrialized countries of the world (Russia, Ukraine, USA, UK, Germany, France, Japan, China, Kazakhstan, etc.) in a total of up to 300, the ring megaampere current flowing in their high-temperature plasma provides its initial heating only to about  $30 \cdot 10^6 \text{ K}$  [5, 14]. Further heating of the hot plasma in these installations is performed by other physical methods [5].

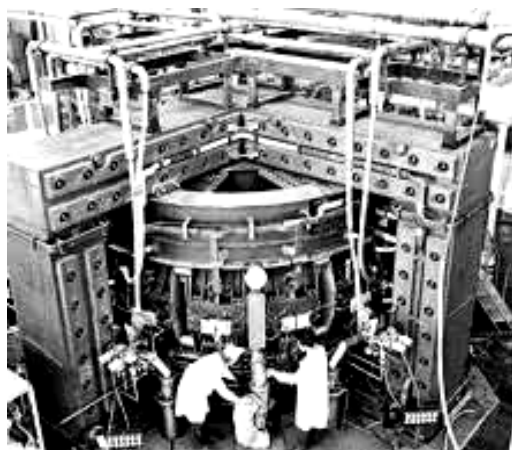


Fig. 5. General view of the largest Soviet research thermonuclear tokamak installation of the 3rd generation of the type TOKAMAK-15 (1980s, Moscow, USSR) [18]

Table 1  
The main technical characteristics of the world's largest tokamaks of the 3<sup>rd</sup> generation [1, 18]

Tokamak installation type	JET	JT60-U	T-15	TFTR	TORUS-SUPRA
Chamber large radius, m	3	3,3	2,4	2,6	2,4
Chamber small radius, m	1	1	0,7	0,9	0,8
Current in the plasma, MA	7	3	2,5	3	2
Plasma heating power, MW	30	30	20	50	15
Magnetic flux density in the plasma, T	3,5	4	3,5	6	4

Fig. 6 shows a general view of the powerful foreign tokamak installation of the 3rd generation JET (Joint European Torus), created in 1991 by the international organization Euratom in the UK [13, 18].

In the tokamak of JET type, a combined heating of its D – T plasma with a volume of  $100 \text{ m}^3$  to the temperature of  $150 \cdot 10^6 \text{ K}$  was used due to the injection of fast neutral particles (20 MW) into the active zone and the use of electromagnetic waves (32 MW) with frequency coinciding with rotation around the magnetic field lines in the TNR chamber of electrons and ions (electron-ion cyclotron resonance mode) [13]. As a result, for this tokamak, the Lawson criterion turned out to be only 4-5 times lower than the level of the «ignition» reaction of the mixture of light nuclei used in it [13, 19]. We point out that for the first time at tokamaks of JET (United Kingdom) and TFTR (Test Fusion Tokamak Reactor, USA) types, large values of developed thermonuclear power in plasma were obtained during synthesis reactions in D – T mixture: 11 MW in TFTR and 16 MW in JET [1, 13].



Fig. 6. General view of the world's largest operating thermonuclear tokamak JET, created by Euratom and located near Oxford in the nuclear research center Culham Lab (1997, Abingdon, UK) [18]

(Currently, the tokamak of JET type successfully continues its operation and has reached a record plasma temperature of  $300 \cdot 10^6 \text{ K}$  with duration of its confinement  $\tau_p \leq 1.2 \text{ s}$  [11]. Up to 350 leading European physicists and specialists are involved in it. According to experts, the current Brexit and the possible exit of Great Britain from Euratom (the European Atomic Energy Community

responsible for the safe use of nuclear energy) will significantly complicate further operation of the world's largest tokamak of JET type [13]. In addition, the decommissioning of the JET-type tokamak will lead to the formation of about 3000 m<sup>3</sup> of radioactive waste, the disposal of which will cost the European taxpayer up to USD 360 million [13].

An important problem for tokamak installations for a long time was the need to create the circular current in hot plasma. For this purpose, a massive magnetic core was installed inside their torus (see Fig. 3-6), the magnetic flux of which continuously changed in time [9]. The change of this flux in accordance with the laws of electrodynamics leads to the creation in the considered region of an eddy electric field, which induces a corresponding current in the plasma cord. This current had to flow continuously in the plasma in one direction, which was naturally impossible to implement. Therefore, the required current in the plasma was maintained only for a limited time, measured in fractions of a second, and in the limit by several seconds [9]. In the course of research on tokamak installations, by electrophysicists a so-called bootstrap current was detected, which appeared in plasma without the influence of an external eddy electric field. In addition, methods have been developed for cyclotron heating of plasma particles, at the same time causing in it to flow the necessary circular current. All this together gave a potential opportunity for long-term maintenance of hot plasma in the vacuum chamber of the experimental TNR. Currently, the record belongs to the large tokamak of the type «Tore Supra» (nuclear center in Cadarache, France), in which the plasma «burned» for up to 360 s [9, 19].

Taking into account the above information, it can be stated that the invention and research of tokamaks, requiring the attraction of huge creative forces of people and financial resources in a number of countries, allowed humanity to nevertheless approach the practical development of such an unlimited source of energy as CTS [5, 14].

## 2.2. Thermonuclear stellarator installations.

In the tokamak plasma torus, plasma ignition occurs due to the formation in it of a ring electric current of the megaampere range (see Fig. 3 and Table 1). Because of this, moving electrons and ions are formed in the torus («donut») of the tokamak installation, forming azimuthal magnetic fields. These fields strive to destroy the main toroidal magnetic field of the installation and destabilize its plasma cord. It is important to note that the circular current in the plasma in modern tokamaks is supported by a superhigh-frequency electric field created by the primary winding of an inductor located in the central region of the toroidal chamber. In this case, the plasma cord inside the chamber plays the role of a secondary single-turn winding of a step-down transformer. For the first time in the world, the thermonuclear stellarator facility was proposed in 1951 by the American physicist L. Spitzer [20]. This type of research thermonuclear reactor received its name from the Latin word «*stella*» – «*star*» [21]. Indeed, the planned temperature level in the active zone of this thermonuclear installation should have exceeded the temperature ( $\sim 15 \cdot 10^6$  K) inside the core of a

star like the Sun. Unlike a thermonuclear tokamak facility, in this thermonuclear stellarator unit plasma from a mixture of light nuclei (for example, from a D – T mixture) arising in a toroidal vacuum chamber is heated and held only by external electric currents and magnetic fields (Fig. 7) [9].

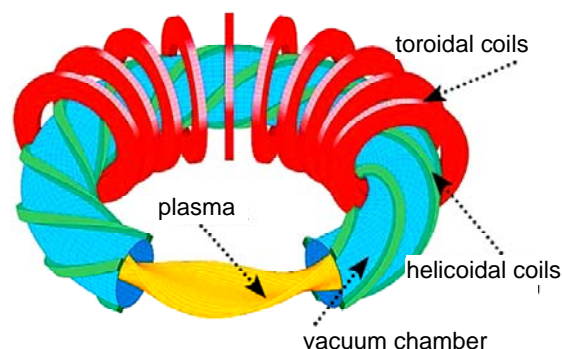


Fig. 7. Schematic diagram of the construction of a research thermonuclear stellarator installation containing a toroidal vacuum chamber with a plasma of light nuclei, helicoidal and toroidal superconducting coils for the formation of a complex-shaped magnetic field [9]

In this regard, the design of the stellarator required the use of superconducting helicoidal coils of complex shape (see Fig. 7). Exploratory studies of electrophysicists have shown that another possible way to create a thermonuclear stellarator installation may be the use of a vacuum chamber with a hot plasma not in the shape of a circular ring (torus) as in Fig. 7, but in the shape of the «eight» or even more complex shape – the «crumpled donut» (Fig. 8) [9].

The external magnetic field in such designs of the stellarator is formed of a «sly» shape, which ensures the stability of the plasma generated in its vacuum chamber. Compared with a tokamak, such a stellarator design is more complex and requires quite complex numerical calculations for the geometry of its magnetic field to be calculated.



Fig. 8. General view of a working vacuum metal chamber with a hot plasma of an experimental thermonuclear stellarator installation curved in the shape of complex 3D serpentine configuration («crumpled donut») [9]

In the second half of the 1950s, on the initiative of the supervisor of the USSR Atomic Project, Academician of the Academy of Sciences of the USSR I.V. Kurchatov In the UPhTI (the Physics and Technology Institute – PhTI which had become by this time) of the Ukrainian

SSR Academy of Sciences, research was started on a new scientific field related to the study of high-temperature plasma and the CTS [17, 22]. Academician of the Academy of Sciences of the Ukrainian SSR K.D. Sinelnikov (1901-1966) was appointed scientific supervisor of thermonuclear research at the PhTI of the Ukrainian SSR Academy of Sciences (Kharkiv) [22]. The apogee of these works was the creation in 1968 of a powerful experimental thermonuclear installation with superconducting magnets of the Uragan-2 type at the indicated Ukrainian institute (Fig. 9) [22, 23].

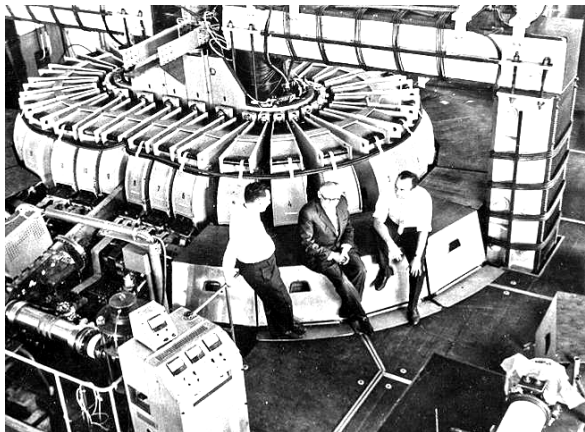


Fig. 9. General view of a powerful Uragan-2 type thermonuclear installation developed by the PhTI of the Ukrainian SSR Academy of Sciences (from left to right: famous Kharkiv physicists V.A. Suprunenko, A.I. Akhiezer and V.T. Tolok; 1968; PhTI of the Ukrainian SSR Academy of Sciences; Kharkiv) [22]

We also point out that in the 1980s, in the framework of experimental research on the CTS in the USSR at the KhPhTI of the Academy of Sciences of the Ukrainian SSR (Kharkiv), a superconducting torsatron of stellarator type Crystal-2 with magnetic flux density up to 5 T and stored magnetic energy up to 1 MJ in its vacuum chamber of complex geometric shape with a hot plasma [7, 24] was created. Fig. 10 shows a general view of a modern experimental thermonuclear stellarator installation with a camera made in the shape of a «crumpled donut» [6].

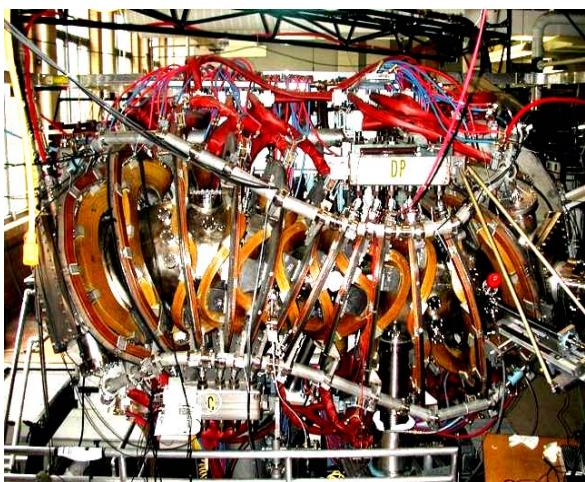


Fig. 10. External view of one of the laboratory constructions of a research thermonuclear stellarator containing a vacuum chamber in the shape of a «crumpled donut» [6, 13]

Despite the fact that today in the stellarator units, the retention time for hot plasma is less, and the cost of their construction is higher than for tokamak installations, research in the world of this type of TNR is actively continuing [1, 20]. One of the reasons for this is that the behavior of high-temperature plasma in them is quieter and more stable. This leads to a higher working life of the inner wall of the vacuum chamber with hot plasma. With the commercialization of the CTS, this technical fact can play a decisive role in choosing the design of the TNR, so it will determine its service life as part of a thermonuclear power plant (TNPP). In this regard, the designs of powerful thermonuclear stellarators being created at the present time have been substantially simplified. Their vacuum chambers in the shape of «crumpled donuts» had to be abandoned. They look like tokamaks [9].

**3. The modern stage of research in controlled thermonuclear synthesis.** As was noted above in subsection 2.1, experimental studies on the CTS at the largest JET tokamak-type thermonuclear facility are currently being actively pursued as part of the Euratom program [1, 13]. With the reached «life» time of the hot plasma in the vacuum chamber of the tokamak of JET type up to 1.2 s, its energy parameter  $Q_f$  was numerically 0.65 [12]. It can be seen that the European nuclear physicists on the JET-type tokamak came close to the «threshold», beyond which a positive energy balance begins when implementing CTS. Experimental data on thermonuclear power and temperature in the D – T mixture (respectively, up to 16 MW and 300 million K [1, 13]) obtained at this TNR give us some hope for the reality of the creation in the 21st century of industrial TNR and practical receiving energy from CTS ( $Q_p \gg 1$ ).

In Germany, at the Max Planck Institute for Plasma Physics (Greifswald) on December 10, 2015, the world's largest thermonuclear «Wendelstein 7-X» type thermonuclear stellarator installation (Fig. 11) was successfully put into its pilot operation which cost the German state EUR 1.06 billion [20].



Fig. 11. General view of the construction site at the time of final assembly of unique electrophysical devices of the world's largest experimental thermonuclear stellarator installation «Wendelstein 7-X» (2015, M. Planck Institute for Plasma Physics, Greifswald, Germany) [20]

In this stellarator, the large radius of the vacuum chamber with plasma is 5.5 m, and its small radius is 0.53 m. The volume of its hot plasma is 30 m<sup>3</sup>, and its density will reach a level of 3·10<sup>20</sup> m<sup>-3</sup> [20]. This experimental TNR contains 50 superconducting niobium-titanium coils of 3.5 m high, the total weight of which is about 425 tons. The magnetic flux density in the working vacuum chamber of the TNR reaches 3 T, and the plasma temperature maintained by such a magnetic field will be up to 130·10<sup>6</sup> K [20]. The entire construction of the world's largest stellarator is surrounded by a cryostat (durable heat insulating shell) with a diameter of 16 m. A major technical problem in the construction of a «Wendelstein 7-X» type stellarator was a shortage of superconducting magnets with special geometry and cooled by liquid helium [20]. In 2003, during the tests, up to 30 % of the magnets were rejected and returned to the supplier. The project by 2007 was on the verge of closure. The long-term construction led to an almost 2-time increase in the planned cost of the stellarator (from EUR 500 to 1,060 million) [20].

In the first experiments on «Wendelstein 7-X» type stellarator, physicists was able to heat one milligram of gaseous helium to a temperature of 1·10<sup>6</sup> K using a 1.3 MW microwave external electromagnetic pulse and hold the resulting hot plasma for 0.1 s [20]. The immediate work plans for this facility are a gradual increase in the power of the source of electromagnetic radiation and an increase in the temperature of the plasma investigated in the chamber [20].

The German research TNR stellarator «Wendelstein 7-X» is not a competitor to the world's largest tokamak ITER (International Thermonuclear Experimental Reactor) currently under construction in France (nuclear center Cadarache), which will be discussed below in section 7. One of the goals of the German project in the field of controlled synthesis is to work out the confinement mode of hot hydrogen plasma to half an hour and bring the parameter  $\beta$ , equal to the ratio of the plasma pressure to the pressure of the magnetic field holding it, to (0.04-0.05). Another goal of this important high-tech project is to develop a number of promising thermonuclear technologies [20].

In the mid-1960s, a fundamentally new approach appeared as an alternative to magnetic confinement of hot plasma in the field of the CTS: its inertial confinement based on the use of high-power lasers – sources of directed ultra short-wave electromagnetic radiation [4, 9]. This approach initially used small target balls of frozen D – T fuel, uniformly irradiated from all sides by a multitude of laser beams. The irregular heating of such thermonuclear fuel required a significant change in the design of the ball target [5]. Currently, these fusion fuel targets are placed inside a hollow spherical hohlraum chamber (from the German word «*hohlraum*» – «*cavity*») with holes through which laser beams fall into it. In addition, in the laser-pulse technology of the CTS, they began to use crystals that convert infrared laser radiation into ultraviolet radiation. This ultraviolet radiation is absorbed by a thin layer of the target hohlraum material, heated to an enormous temperature and emitted soft X-rays [9]. This P-radiation is absorbed by the thinnest layer

of the thermonuclear fuel capsule, which leads to the flow of the CTS in it.

Fig. 12 shows a general view of a thermonuclear installation that uses laser pulse technology of microexplosions of thermonuclear fuel enclosed in separate capsules in its TNR [9, 18].



Fig. 12. General view of an experimental TNR of a modern thermonuclear installation using laser-pulse technology for microexplosions of D-T fuel capsules [5, 18]

At present, this promising technology for the implementation of the CTS due to the simultaneous volumetric impact on spherical target microcapsules of frozen thermonuclear D – T fuel of high-power laser pulses is at the stage of conducting laboratory experiments [9, 25]. It should be noted that over the past ten years there has been a qualitative leap in the development of world laser technology, which has managed to increase the efficiency of high-power lasers by a factor of ten [9]. Moreover, their power at the same time managed to increase hundreds and thousands of times [9]. Therefore, it can be said that the inertial version of the CTS in the world does not «stand» in place, but is successfully developing [5, 18, 25].

In 2006, the first successful tests of an experimental advanced superconducting tokamak of the EAST type (Experimental Advanced Superconducting Tokamak) were carried out in China, the general view of which is shown in Fig. 13 [5, 18]. In 2007, the first «break-even» CTS in the world, characterized by the parameter  $Q_f = 1.25$ , equal to the ratio of obtained in the toroidal chamber of this reactor that is a deep modernized design of the Russian tokamak of HT-7 type thermonuclear energy to spent on receiving and combined heating to ultra-high temperature (about 100·10<sup>6</sup> K) of a plasma string of electrons and relatively light heavy and super-heavy isotopes of hydrogen (nuclei of deuterium D and tritium T) [5] was carried out. In the near future, Chinese nuclear physicists will try to bring the  $Q_f$  parameter to a value of ~50 [5]. At present, the experimental TNR of EAST type is also used in the framework of research activities related to the development and creation of a more powerful international tokamak of ITER type.

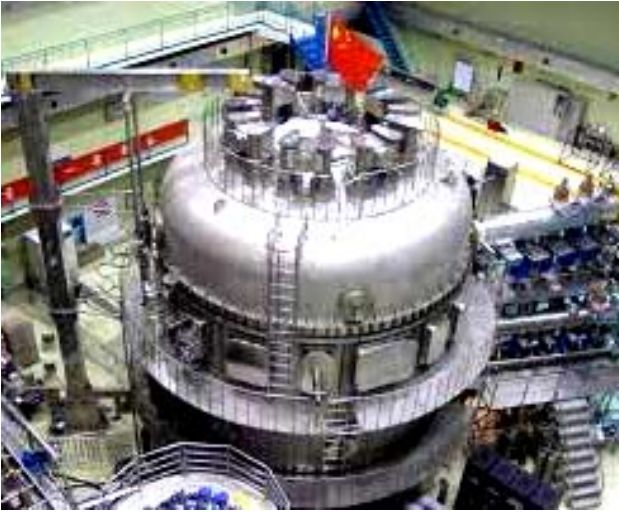


Fig. 13. General view of a powerful experimental TNR of EAST type, created according to the tokamak scheme in the People's Republic of China (2006, Institute of Plasma Physics, Chinese Academy of Sciences, Hefei, Anhui Province) [5, 18]

**4. The main problems in the creation of the TNR and the shortcomings of the TNR.** Let us further dwell on the TOKAMAK design of the TNR which is the most studied and advanced in the world now [5, 14]. For tokamak installations, in which thermonuclear fuel with density of up to  $10^{20} \text{ m}^{-3}$  must be heated to temperature of  $(100-300) \cdot 10^6 \text{ K}$ , the main disadvantages and problems in creating industrial TNR based on them are the following [5, 19, 26]:

- the instability of a hot plasma (the plasma cord in the toroidal chamber tends to be thinner somewhere, thicker somewhere, or interrupted somewhere else with the cessation of the flow of the ring megaampere current). The use of a poloidal magnetic field (see Fig. 3) and an increase in the geometric dimensions of the vacuum chamber became possible proven ways to increase the stability of plasma combustion. The improved plasma confinement mode open by physicists will also contribute to the above mentioned stability, when at high power of its additional heating the losses of hot plasma energy sharply decreases (two or more times) [20];

- the main scientific problem for tokamak installations is that, as the pressure in the hot plasma increases, complex and dangerous instabilities arise in it, leading to an unstable operating mode of the TNR (physicists will have to take this path without fail, since the rate of fusion of light nuclei at a given plasma temperature is directly proportional to the square of its pressure);

- the high cost of tritium  ${}^3\text{H}$ , a superheavy radioactive isotope of hydrogen  ${}^1\text{H}$  with a half-life of 12.3 years [1, 4] (1 kg of this substance was worth about USD 30 million by 2010 [27]). In 2014, the world stock of tritium was about 20 kg, with its annual consumption in the world of about 7 kg [27]. For the future put into operation of the tokamak of ITER type being constructed in France, it will take about 3 kg of tritium to charge all of its tritium subsystems, as well as about 1 kg of tritium for each year of its operation [27];

- the minimum power of the TNR should be hundreds and thousands of megawatts (the main reasons for this are

that the hot plasma in the reactor loses a lot of energy for electromagnetic radiation, and its vacuum chamber must have relatively large geometrical dimensions in order to ensure the stability of the plasma cord behavior in it);

- the high cost of the Tokamak type TNR (for example, the creation of an experimental ITER type TNR with 1500 MW thermonuclear power will cost the participants of an international project about EUR 15 billion which is unacceptable today for an industrial CTS reactor installed at the TNPP);

- the presence of powerful neutron radiation in the TNR, which negatively affects its working life (for comparison, we point out that the neutron flux in the TNR is up to ten times more powerful than a similar flux in the NR). In this regard, the expected service life of the TNR can be no more than 5 years instead of 50 years characteristic of NR;

- specialists have no confidence in the operation of industrial TNRs based on their construction according to the principle of tokamak (up to the present, not a single tokamak worked even for several hours, not to mention the years typical of industrial reactors; there is no certainty that materials of the blanket of the inner wall of the vacuum chamber of the reactor is able to withstand the effects of hot plasma for a long time; there is also no confidence in the thermal and mechanical resistance of a number of other structural materials of the reactor experiencing prolonged exposure to intense flux of fast high-energy neutrons and powerful flux of electromagnetic radiation of particles of its high-temperature plasma);

- the design of the TNR, based on the tokamak scheme, is today quite complex (therefore, nuclear physicists and power engineers have a problematic task of special importance – ensuring the high reliability of operation of TNR as a part of the TNPP; its design and construction tasks require that whole complex of various complicated technological problems from a number of branches of knowledge should be rigorously solved).

**5. Thermonuclear fuel and the main types of nuclear reactions used in TNR.** As is well known, hot plasma in the TNR, using magnetic confinement of the initial products of the CTS, has a low density (of the order of  $10^{20} \text{ m}^{-3}$  [1, 5]). This density of hot plasma is about  $10^5$  times less than the density of atoms and molecules in the air under normal atmospheric conditions [4]. In this regard, the Lawson criterion for tokamaks is achieved due to a good retention of thermal energy in their chamber and, accordingly, a large energy «life time» of their hot plasma. Therefore, a relatively small amount of thermonuclear fuel is required for the operation of the TNR. For example, for the largest ITER-type TNR tokamak with the specified density of the fusion gas mixture in its chamber, the initial thermonuclear cycle of the CTS requires an initial fuel of only (0.5–1) g [5, 19]. Note for reference that to heat 0.5 g of conventional  ${}^1\text{H}$  hydrogen protium to temperature of  $100 \cdot 10^6 \text{ K}$ , it is necessary to expend as much energy as it needs to heat ordinary  $\text{H}_2\text{O}$  water with a volume of 186 l to its boiling temperature of  $100^\circ \text{ C}$  [19]. At present, the main types of

nuclear reactions in CTS, which determine the choice of thermonuclear fuel, are the following [1, 5, 8]:

- $D + T \rightarrow {}^4_2\text{He} (3.5 \text{ MeV}) + {}^1_0n (14.1 \text{ MeV})$ ;
- $D + D \rightarrow {}^3_2\text{He} (0.82 \text{ MeV}) + {}^1_0n (2.45 \text{ MeV})$ ;
- $D + D \rightarrow T (1.01 \text{ MeV}) + {}^1_1p (3.02 \text{ MeV})$ ;
- $D + {}^3_2\text{He} \rightarrow {}^4_2\text{He} (3.6 \text{ MeV}) + {}^1_1p (14.7 \text{ MeV})$ ;
- ${}^6_3\text{Li} + {}^1_0n \rightarrow {}^4_2\text{He} + T + 4.8 \text{ MeV}$ .

In the above nuclear reactions involving deuterium D and tritium T, which are of particular interest for CTS, the symbol  ${}^2_2\text{He}$  denotes the light isotope of ordinary helium  ${}^4_2\text{He}$ ,  ${}^1_0n$  is the fast neutron,  ${}^6_3\text{Li}$  is the light isotope of natural lithium  ${}^7_3\text{Li}$ , and  ${}^1_1p$  is the stable proton [4]. From these nuclear reactions it can be seen that all of them occur with the release of energy in the form of the kinetic energy of the products of these reactions flying in all directions of the TNR core. The last nuclear reaction plays a special role in the CTS. It is used in the industrial production of unstable tritium T (in the liquefied state, tritium is 6 times lighter than water  $\text{H}_2\text{O}$  [4]), which does not exist in nature in the free state (due to its relatively fast radioactive  $\beta$ -decay [5]). From the analysis of these nuclear reactions, it follows that the first reaction of the type (D + T) is the most «easy» for its implementation (for its flow in the working chamber of the TNR, the temperature of about 100 million K is required) [19]. For reactions of synthesis of the type (D + D), approximately

the same ultrahigh temperatures are required, but they proceed about 100 times slower than reactions of the type (D + T). In addition, the energy released during their flow is much less (about 5 times) than in the deuterium-tritium synthesis reaction. Nuclear reactions of the type (D +  ${}^3_2\text{He}$ ) go faster than competing reactions of the type (D + D). However, for their realization it is required to create limiting temperatures in the working chamber of a powerful TNR – about 1 billion K [19]. Therefore, we can conclude that for industrial use of the CTS, only nuclear fusion reactions of the type (D + T) are even remotely accessible to mankind with all their shortcomings (for example, the difficulties of obtaining radioactive tritium  ${}^3_1\text{H}$  using the presented fifth nuclear reaction and radioactivity induced by fast neutrons from their course in used in the construction of the cores of the TNR materials) [19]. In this regard, it is expected that in the coming decades (possibly centuries), in the industrial application of CTS in powerful TNR of a particular design, only a mixture of heavy (deuterium  ${}^2_1\text{H}$ ) and superheavy (tritium  ${}^3_1\text{H}$ ) hydrogen isotope  ${}^1_1\text{H}$  (protium) will be used as thermonuclear fuel [5, 14, 19].

Fig. 14 shows a schematic diagram of the production of electricity at the future TNPP using in its powerful TNR the considered TCS in a mixture of light nuclei of deuterium D and tritium T [1].

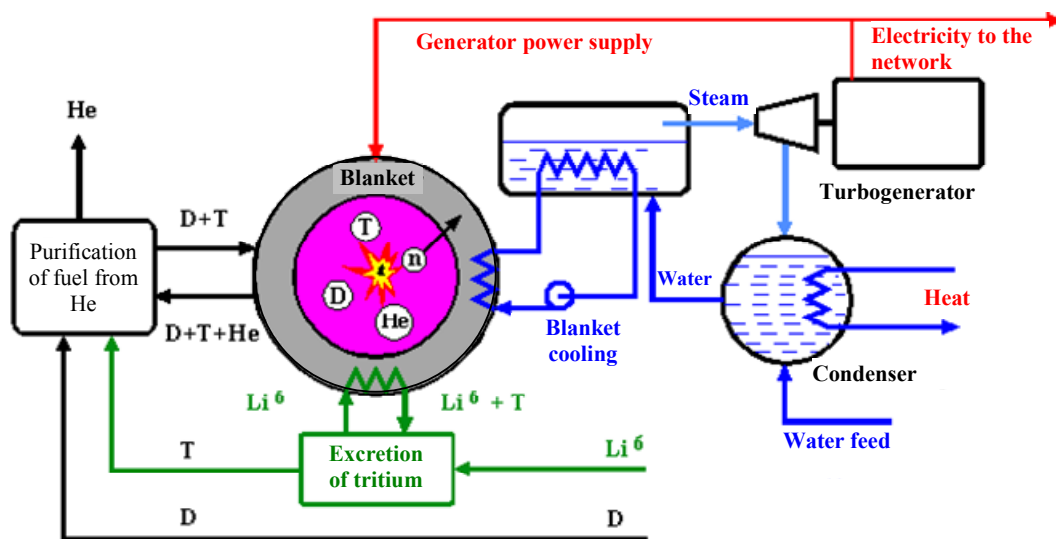


Fig. 14. Diagram of industrial production of electric power on a TNPP using large-sized TNR of controlled thermonuclear synthesis of light nuclei of deuterium D and tritium T [1, 5]

According to this scheme, the energy of thermonuclear reactions occurring in the deuterium-tritium plasma of the TNR chamber, mainly due to the intense flow of high-energy neutrons  ${}^1_0n$ , is removed from the reactor core and absorbed by the massive refractory blanket (up to 1 m thickness) of the vacuum chamber case. The released thermal energy in the TNR blanket is removed by superheated coolant (for example, distilled water  $\text{H}_2\text{O}$ ) of the primary reactor cooling circuit, which gives its heat in the steam generator to the liquid coolant (for example, the same  $\text{H}_2\text{O}$  water purified from the impurities) of the second reactor circuit. Further, according to the classical scheme of operation of energy devices of a thermal power plant or NPP, superheated steam formed in the second circuit of the TNR is directed

to the blades of a steam turbine rotating a massive steel shaft-rotor of a synchronous turbogenerator, producing a corresponding electromotive force and, accordingly, electric power in the windings of its stator.

Presented in Fig. 14 TNR requires supplying its core with deuterium D and tritium T. Deuterium D is produced industrially from ordinary natural water  $\text{H}_2\text{O}$  (it contains about 0.015 % of this heavy isotope of hydrogen in the form of heavy water  $\text{D}_2\text{O}$  [1, 25]). As for tritium T, it is planned to obtain it with the help of the  ${}^6_3\text{Li}$  lithium isotope introduced into the composition of the blanket of the TNR chamber – the massive shell surrounding the hot plasma [1, 27]. The  ${}^6_3\text{Li}$  lithium isotope, entering according to the above fifth exothermic (releasing energy and heat accordingly) nuclear reaction with fast high-

energy neutrons  ${}_0^1n$  (with their kinetic energy up to 14.1 MeV [1, 14]), will produce as a result of its nuclear decay ions of helium  ${}_2^4\text{He}$  and tritium T. The hydrogen isotope under consideration, after its separation from the products of the indicated nuclear interaction, is fed into a fusion fuel mixer, from which deuterium D and tritium T are discretely fed in a frozen state directly to the TNR camera. The  ${}_2^4\text{He}$  helium nuclei (alpha particles) formed in the core of the reactor are removed from the working chamber of the TNR, deionized, cleaned from thermonuclear fuel and pumped into the tanks for their further technical use (see Fig. 14). Therefore, it is possible to say that for the scheme of constructing a TNPP with a TNR shown in fig. 14, deuterium D and lithium isotope  ${}_3^6\text{Li}$  are used as fuel. Note that when obtaining tritium T, natural lithium  ${}_3^7\text{Li}$  can be used instead of lithium isotope  ${}_3^6\text{Li}$  in a TNR camera blanket. Here, as a result of its endothermic (with energy and, accordingly, heat absorption) nuclear interaction with fast high-energy neutrons  ${}_0^1n$ , nuclei of helium  ${}_2^4\text{He}$ , tritium T and one additional neutron  ${}_0^1n$  are formed [1, 18]. It should be noted that lithium isotopes  ${}_3^6\text{Li}$  и  ${}_3^7\text{Li}$ , capable of producing the required for the TNPP and its TNR tritium T, are quite widespread in the surrounding nature (at its percentage ratio as 7.5/92.5 [1, 4]). According to experts, one TNR with electrical power of 1000 MW will burn in its core about 100 kg of deuterium D and 300 kg of  ${}_3^6\text{Li}$  lithium isotope per year [1]. If we assume that in the 21st century, TNPPs around the world will produce approximately  $5 \cdot 10^{20}$  J/year (half of the future electricity needs of mankind), then the annual consumption of deuterium D and  ${}_3^6\text{Li}$  lithium isotope will be only 1,500 and 4,500 tons respectively [1]. With such a global annual consumption of deuterium D and lithium isotope  ${}_3^6\text{Li}$  on future TNPPs, these minerals on planet Earth will last for many millions of years [1, 5].

#### 6. Radiation safety of TNR and TNPP.

Maintaining a positive energy balance in the TOKAMAK type TNR requires constant and delicate control of the plasma «burning» process, as well as the strictly synchronized operation of all the main systems of such a reactor. In the TNR, built on the basis of the tokamak installation, the failure in the operation of any of its systems leads either to a loss of stability in the plasma cord, or to its contamination with impurities followed by cooling of the plasma and eventually to the breakdown of its «burning» [1]. In this regard, the difficulties in ensuring the sustainability of the CTS process in such TNR play a positive role for the safety of the TNR itself. At the same time, in any type of TNR structures, the mode of uncontrolled growth of its power is excluded. The retreat in the TNR from the mode of the steady flow of light nuclei in its mixture of the TCS to any direction immediately leads to the breakdown of the «burning» of the plasma cord and the cessation of nuclear reactions in it. Therefore, the TNR with magnetic plasma confinement is characterized by internal safety [1]. In the course of the operation of the TNR, radioactive elements accumulate in its active zone, which can pose a certain radiation hazard to the personnel serving it, the population of the surrounding areas of the TNPP and the environment. It should be noted that the fuel used in the TNR in the form of deuterium D and lithium isotope  ${}_3^6\text{Li}$  is not radioactive.

Not radioactive and the final product from the CTS in the TNR – helium  ${}_2^4\text{He}$ . In the TNR using D – T nuclear reactions, the main sources of radioactivity are: first, tritium T, which is involved in the fuel cycle of the reactor; secondly, induced by fast high-energy neutrons, radioactivity in the process of the CTS in its chamber, radioactivity in the structural materials of the reactor (especially in the wall of the blanket of the chamber in contact with the plasma through a magnetic field) [1, 5]. To reduce the artificial radioactivity of the blanket wall, it is required to choose for it special materials resistant to neutron radiation. The results of the research show that in the case of manufacturing the specified wall of a blanket from a vanadium-titanium alloy or silicon carbide, it (the wall) after stopping the reactor loses its radioactivity to the level of ore of natural uranium  ${}_{92}^{238}\text{U}$  in about 30 years [1]. We should not forget about the radioactive corrosion products present in the heat-transfer fluid of the primary cooling circuit of the reactor vessel. Compared to the NR of fission of heavy nuclei, which are currently used at powerful nuclear power plants, the TNR has a much greater radiation safety [1, 5].

#### 7. Development and creation of an international thermonuclear experimental reactor of the ITER type.

In 1985, a number of leading countries of the world (USSR, USA, France, Great Britain, Japan, etc.) launched a project to develop the largest International Thermonuclear Experimental Reactor (ITER) with electrical power of up to 1500 MW [1, 25-27]. For the basis of such ITER, the leading nuclear scientists of the world and the scientific and administrative leaders of this international project adopted a deeply improved design of a powerful thermonuclear installation of the type TOKAMAK [1, 27]. The TNR of the ITER type is planned to be put into trial operation in 2025 [1, 25-27]. Fig. 15 shows a general schematic view of this world's largest TNR using the construction scheme described in subsection 2.1 of a deeply refined classical tokamak [14, 27].

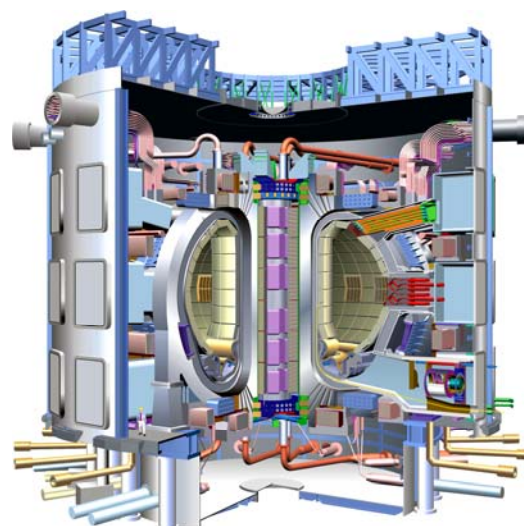


Fig. 15. Schematic 3D view in section of the International Thermonuclear Experimental Reactor of ITER type (International Thermonuclear Experimental Reactor – ITER), currently under construction in the framework of the largest international scientific and technical project of modernity (costing approximately EUR 15 billion in 2017) in the south of France (Provence) in the nuclear research center of Cadarache (60 km from Marseille) [14, 27]

Fig. 16 shows a general view of the working toroidal chamber of this powerful experimental tokamak reactor [14, 27].

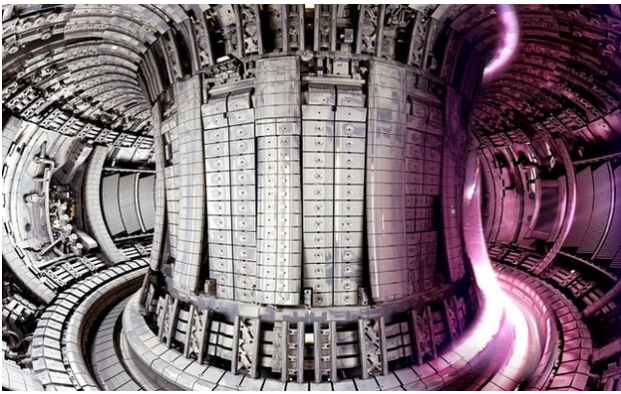


Fig. 16. General view from the inside of a layout of a toroidal vacuum chamber with a refractory massive blanket of a large-size TNR of the ITER type under construction in France [14, 27]

The following main systems and devices will be part of the ITER-type TNR [26, 27]:

- the reactor magnetic system containing 18 superconducting toroidal coils (conductors – Nb<sub>3</sub>Sn; current – 68 kA; magnetic flux density – 11.8 T; accumulated field energy – 41 GJ; weight – 6540 tons; cost – EUR 323 million), 6 superconducting poloidal field coils (conductors – NbTi; current – 52 kA; magnetic flux density – 6 T; accumulated field energy – 4 GJ; weight – 2163 tons; cost – EUR 122 million) and central solenoid (conductors – Nb<sub>3</sub>Sn; current – 46 kA; magnetic flux density – 13 T; accumulated field energy – 6.4 GJ; mass – 974 tons; cost – EUR 135 million);
- the vacuum toroidal chamber with a double wall (made of stainless steel 316LN in the American assortment and 03X16H15M3 in the Russian assortment; the large radius of the chamber is 6.2 m; the small radius of the chamber is 2 m; the height of the chamber is up to 11 m; the volume of the chamber cavities up to 1400 m<sup>3</sup>; mass up to 5000 tons; for trapping CTS products and cleaning the plasma from contamination, the chamber is equipped with a diverter from the bottom; distilled water circulates between the walls of the chamber to cool the chamber; the inner wall of the chamber is equipped with a blanket to protect against powerful thermal and neutron radiation);
- the blanket of the vacuum chamber which for ease of maintenance contains 440 cassettes (three cassettes contain <sup>6</sup>Li lithium isotope to produce <sup>3</sup>H tritium), each of which has a removable beryllium wall up to 10 mm thickness facing the plasma and a copper case reinforced with stainless steel (dimensions of each cassette amount to 1 × 1.5 m, and weight up to 4.6 t);
- the electron-cyclotron resonant plasma heater of the ECRH type (Electron Cyclotron Resonance Heating), designed for the initial heating of the gas mixture entering the chamber; 24 gyrotrons each with power of 1 MW, operating frequency of 170 GHz and pulse duration of up to 500 s are used as sources of electromagnetic energy; to enter energy from the gyrotrons into the chamber, there are special «windows» made of polycrystalline artificial

diamond (the diameter of each diamond disk is 1.1 mm thickness is 80 mm); the choice of diamond was due to the fact that it is transparent to microwave radiation, durable, radiation resistant and has thermal conductivity five times higher than that of copper; through each diamond «window» of the chamber power up to 500 MW/m<sup>2</sup> will pass;

- the ion-cyclotron resonant plasma heater of ICRH type (Ion Cyclotron Resonance Heating), designed to heat plasma ions; as a source of RF radiation (with frequency of up to 55 MHz), a powerful radio frequency generator on tetrodes is used, transmitting electromagnetic energy through waveguides and antennas to the TNR camera;

- the injector of neutral atoms, «firing» into the plasma cord of the reactor a powerful beam of deuterium D atoms, which were actually ionized to their nuclei and accelerated in a cyclotron to the kinetic energy of 1 MeV; before being fed into the TNR chamber, the accelerated deuterium nuclei D are deionized in cells filled with gas (here they capture electrons from the gas molecules and recombine; after these cells, the deuterium nuclei D that did not have time to recombine are deflected by the magnetic field and diverted to special braking targets); two powerful injectors of neutral atoms are planned to be installed at the ITER reactor (with a total power consumption of 55 MW), each of which is capable of introducing up to 16 MW of thermal energy into the hot plasma of the vacuum chamber of the reactor;

- the cryostat, which is the largest device of the reactor (has a stainless steel shell with volume of 16,000 m<sup>3</sup>, height of 29.3 m, diameter of 28.6 m and mass of 3850 tons); in addition to purely mechanical functions (the support for the reactor elements and their protection from damage) and the thermo-insulating function, the cryostat performs the role of a vacuum «thermos» and a barrier between the internal TNR cavity and the external environment; a cryostat to reduce the adverse effect on the environment of the intense neutron radiation of the reactor will be outside surrounded by a «blanket» of special concrete of 2 m thickness that plays the role of bioprotection (Bioshield) of the TNR;

- the fuel system supplying the reactor chamber core having the Lawson criterion  $n_p \tau_p > 10^{20} \text{ m}^{-3} \cdot \text{s}$ , a mixture of hydrogen isotopes – deuterium D and tritium T; at the beginning of the operation of the TNR, this mixture in a gaseous state through the injection system under low pressure enters the evacuated chamber, where it heats up, ionizes and turns into a plasma; then an «ice» gun is used to inject an additional deuterium-tritium fuel into the plasma cord, pulsing the frozen granules of the D – T mixture into this cord under pressure at speed of ~1000 m/s; at each current time, the reactor chamber should contain no more than 1 g of the specified fuel;

- the vacuum system designed to evacuate the cavity of the chamber (the pressure in it should not exceed 10<sup>-9</sup> from normal atmospheric pressure) and other elements of the TNR (for example, transmission lines into the chamber of microwave electromagnetic radiation, injection systems into the chamber of powerful flows of neutral atoms, etc.); it is planned that for vacuum

preparation of all subsystems of the reactor, a similar system will take about 48 hours;

- the cryogenic system that serves to cool the current-carrying parts of the magnetic system of the reactor to the superconducting state; it consists of nitrogen (provides thermal load of 1300 kW at temperature of boiling nitrogen of 80 K) and helium (provides thermal load of 65 kW with power consumption of refrigerating machines of 16 MW) contours; the helium supply in the system is 25 tons, which is stored in a liquid (at temperature of 4 K) and gaseous (at temperature of 80 K) state in special «tanks»; the total length of cryogenic lines is ~3 km;

- reactor power supply system, connected by a 1 km long power line to the 400 kV French industrial network; for internal needs of the TNR, the supplied mains voltage decreases to 22 and 66 kV; there are two internal power supply networks for the TNR equipment power supply: the first one of type SSEN (Steady State Electrical Network) - a network of constant power (its consumers do not need power «surges»; it has four transformers with weight of 90 t each); the second one of type PPEN (Pulsed Power Electrical Network) is a variable power network (its consumers require enormous power at the time of plasma «ignition» in the TNR toroidal chamber; its consumers include the central solenoid of the magnetic system of the reactor, the systems of cyclotron heating of the plasma, the TNR control systems; this network includes three transformers 240 tons each);

- the water cooling system of the reactor, designed to remove excess heat from the massive walls of the blanket and the chamber diverter; according to expert estimates, at the time of the ignition of the thermonuclear reaction in the chamber (with peak power of 1.1 GW), the blanket wall will heat up to 240 °C and the tungsten wall of the divertor up to 2000 °C; this system will also be used for cooling the ICRH-type plasma radiofrequency heater, the cryogenic system, etc.

Table 2 shows the main technical characteristics of the experimental ITER-type TNR selected in a long-term development process [26, 27].

Table 2

Corrected in the course of work the main technical characteristics of the world's largest ITER-type TNR being built in France in the framework of the international project [26, 27]

1	Total radius of the reactor structure, m	10.7
2	Reactor structure height, m	30
3	Vacuum chamber large radius, m	6.2
4	Vacuum chamber small radius, m	2
5	Hot plasma volume in the reactor, m <sup>3</sup>	837
6	Magnetic flux density in the chamber, T	5.3
7	Current in the plasma cord, MA	15
8	Power of the external plasma heating, MW	73
9	Average thermonuclear power in the pulse during one operating cycle, MW	500
10	Peak thermonuclear power in the pulse during one operating cycle, MW	1100
11	Power gain	10
12	Average hot plasma temperature, K	150·10 <sup>6</sup>
13	Pulse duration in the cycle, s	>400

The gigantism of the constructed ITER-type TNR is underlined by its total weight of about 23 thousand tons (for comparison, we point out that the weight of the Eiffel Tower in Paris is about 7.3 thousand tons) [27, 28]. This reactor is not the largest in terms of financial costs of an international project. Thus, the development, construction and maintenance of the International Space Station (the ISS project) cost donor countries one and a half times more expensive than work on the ITER project with an estimated cost of EUR 15 billion [27, 28]. It is planned that the first phase of experiments at the ITER reactor should be completed by retaining in its chamber the hot plasma heated to a temperature of 150·10<sup>6</sup> K for up to 17 min with the parameter  $Q \geq 10$  and the released thermonuclear power of at least 500 MW [27]. The second phase of experiments at the ITER should be completed with a continuous operation mode of this tokamak. The ITER project should demonstrate the capabilities of the CTS and help explore thermonuclear technologies for their further use for peaceful commercial purposes. The results of experimental work on the ITER-type TNR should lead specialists to develop an industrial TNR capable of operating at the TNPP.

**8. Possible prospects for the creation of industrial TNR, TNPP and in the development of global thermonuclear energy.** The currently available critical assessments by experts of the energy market indicate that the question of the profitability of the CTS in industrial conditions is still open [5]. In addition, there are more radical authoritative opinions about a possible future of the thermonuclear energy. For example, in 2006, Academician of Russian Academy of Sciences Yu.A.Trutnev (First Deputy Head of the RPhNC-VNIIEPh, Sarov), responding to a question about the prospects of the CTS problem, said the following [29]: «... I do not deal with this problem and do not believe in it. I believe that all these works are the satisfaction by the scientists of their curiosity at the expense of the state. Research in the field of thermonuclear energy is ongoing, but I do not believe that thermonuclear energy will become a source of energy even in a somewhat distant future». Nuclear power engineering, based on fission reactions of heavy nuclei by slow or fast neutrons, with all its disadvantages, is a serious alternative to thermonuclear power engineering [1, 2]. Supporters of the CTS believe that the final phase of experimental work at the ITER-type tokamak reactor should be the development of a prototype of the industrial reactor of the DEMO type, which will demonstrate the practical suitability of the solutions and structural materials used in it. The most optimistic forecasts for the time of completion of the phase of work on the TNR of the DEMO type are the year 2045 [5, 28]. Following the DEMO project, the design of the industrial TNR can begin. It is assumed that the world's first industrial TNPP can be created by 2055 [5, 27]. Experts believe that a TNPP with electrical power of 1000 MW in terms of radiation hazard would be equivalent to a fission reactor of heavy nuclei in natural uranium <sup>92</sup>238U, containing up to 0.71 % of the uranium isotope <sup>92</sup>235U fusing in a chain manner with a power of 1 kW [4] (this is a typical example of a University research NR) [5, 11]. With all

attractiveness of the TNPP, the question of their industrial application will become clearer in the world, probably only by the middle of the 21st century. By this time, still unresolved problems from the physics of high-temperature plasma of tokamaks will be studied and irrefutable experimental data will emerge about the possibility of creating an industrial design of the TNR, without which it is impossible to understand the prospects for CTS development, creation of TNPPs and thermonuclear energy in general.

### Conclusions.

1. From presented brief scientific and technical review of research in the leading countries of the world in the field of the CTS, actively conducted since the 1950s, and the thermonuclear energy of the distant future, it follows that the CTS of light nuclei (for example, hydrogen isotopes such as deuterium D and tritium  $T$ ) is fundamentally possible in terrestrial conditions. It can be stated that as of the end of 2017, the leading countries of the world conducted a huge complex of nuclear physics research in the field of the CTS. Various designs of TNR with magnetic and inertial confinement of hot plasma have been created and experimentally investigated. The record levels of temperature and retention time of hot plasma in D – T mixture in the experimental TNRs reached  $300 \cdot 10^6$  K and 6 min. Here, the main technical task all over the world for nuclear physicists and power engineers is the development and creation of an industrial design of the TNR that could economically compete with other powerful sources of energy known to mankind. At present, such a TNR design in the world does not yet exist. For its development, a complex of exploratory experimental work is being carried out, the apogee of which is to become the world's largest TNR tokamak of the type ITER, now being constructed in the framework of an international project in the south of France.

2. In the near future (possibly by 2030), specialists can obtain at the TNR (for example, on the same ITER-type tokamak) its energy indicator  $Q_f = 10$  (the thermonuclear energy obtained in the reactor is 10 times higher than the energy spent on hot plasma preparation and retention). Despite this achievement, the first industrial designs of the TNR will be much more expensive than uranium NRs of the same power (due to their more complex structure, large dimensions, the use of superconducting electromagnets and a shorter service life). Therefore, in the 21st century, they are unlikely to be able to win competition from NRs using neutron-fission reactions involving heavy nuclei of isotopes of uranium  $^{238}\text{U}$ , plutonium  $^{244}\text{Pu}$  and thorium  $^{232}\text{Th}$ .

3. In the author's opinion, as an electrical physicist scientist, despite such modest prospects for practical application of the CTS in this century, for the humanity taking into account its steady development in the third millennium and the mastery of new higher knowledge in basic science and technology, it is imperative to continue to work hard in the interest of progress in the field of peaceful development of thermonuclear energy.

### REFERENCES

1. <http://thermonuclear.narod.ru/rev.html> (Velikhov E.P., Putvinskiy S.V. Thermonuclear power engineering. Status and

role is in a long-term prospect. Lecture from 22.10.1999 y. in Energy Center of the World Federation of Scientists). (Rus).

2. Baranov M.I. An anthology of the distinguished achievements in science and technique. Part 44: Traditional power engineering. Nuclear power stations: retrospective view, state and prospects of their development. *Electrical engineering & electromechanics*, 2018, no.3, pp. 3-16. doi: **10.20998/2074-272X.2018.3.01**.

3. Baranov M.I. An anthology of the distinguished achievements in science and technique. Part 32: Alternative energy: state and prospects of development. *Electrical engineering & electromechanics*, 2016, no.3, pp. 3-16. doi: **10.20998/2074-272X.2016.3.01**.

4. Kuz'michev V.E. *Zakony i formuly fiziki* [Laws and formulas of physics]. Kiev, Naukova Dumka Publ., 1989. 864 p. (Rus).

5. Available at: [https://en.wikipedia.org/wiki/Fusion\\_power](https://en.wikipedia.org/wiki/Fusion_power) (accessed 15 April 2017).

6. Available at: <http://greensource.ru/vidy-jenergii/termojadernaja-jenergiya.html> (accessed 22 May 2017). (Rus).

7. Baranov M.I. *Antologija vydaishchikhsia dostizhenii v nauke i tekhnike: Monografiia v 3-h tomakh. Tom 1*. [An anthology of outstanding achievements in science and technology: Monographs in 3 vols. Vol.1]. Kharkov, NTMT Publ., 2011. 311 p. (Rus).

8. Artsimovich L.A. *Upravlyaemye termoyadernye reaktsii* [Guided thermonuclear reactions]. Moscow, Fizmatlit Publ., 1961. 467 p. (Rus).

9. Available at: <https://www.popmech.ru/science/12621-zvezdy-na-zemle-termoyad/#> (accessed 08 October 2016). (Rus).

10. Available at: [http://www.biblioatom.ru/founders/artsimovich\\_lev\\_andreevich](http://www.biblioatom.ru/founders/artsimovich_lev_andreevich) (accessed 25 March 2017). (Rus).

11. [http://reactors.narod.ru/pub/therm\\_nucl/therm\\_nucl.htm](http://reactors.narod.ru/pub/therm_nucl/therm_nucl.htm). (Rus).

12. Bondarenko B.D. Role played by O A Lavrent'ev in the formulation of the problem and the initiation of research into controlled nuclear fusion in the USSR. *Uspekhi Fizicheskikh Nauk*, 2001, vol.171, no.8, pp. 886-894. (Rus). doi: **10.3367/UFNr.0171.200108q.0886**.

13. Available at: <http://www.atomic-energy.ru/news/2016/12/02/70677> (accessed 06 February 2017). (Rus).

14. Available at: <http://lurkmore.to//Термоядерный синтез> (accessed 13 April 2017). (Rus).

15. Goncharov G.A. The 50th anniversary of the beginning of research in the USSR on the potential creation of a nuclear fusion reactor. *Uspekhi Fizicheskikh Nauk*, 2001, vol.171, no.8, pp. 894-901. (Rus). doi: **10.3367/ufnr.0171.200108r.0894**.

16. Artsimovich L.A., Mirnov S.V., Strelkov V.S. Research of the ohmic heating of plasma on the torus setting «ТОКАМАК-3». *Atomic energy*, 1964, vol.17, no.8, pp. 170-176. (Rus).

17. Khranov Yu.A. *Istoriia fiziki* [History of Physics]. Kiev, Feniks Publ., 2006. 1176 p. (Rus).

18. Available at: [https://www.google.com.ua/search?q=ua/search?q=termojadernaya\\_elektrostanciya](https://www.google.com.ua/search?q=ua/search?q=termojadernaya_elektrostanciya) (accessed 15 May 2017). (Rus).

19. Available at: <https://geektimes.ru/post/167523> (accessed 28 June 2017). (Rus).

20. Available at: <https://lenta.ru/articles/2015/12/11/wendelstein7x/> (accessed 04 May 2017). (Rus).

21. *Bol'shoj illjustrirovannyj slovar' inostrannyh slov* [Large illustrated dictionary of foreign words]. Moscow, Russkie slovari Publ., 2004. 957 p. (Rus).

22. Baranov M.I. *Antologija vydaishchikhsia dostizhenij v nauke i tekhnike: Monografiia v 3-h tomakh. Tom 3* [An anthology of the distinguished achievements in science and technique:

Monograph in 3 volumes. Volume 3]. Kharkiv, PhPB Panov A.N. Publ., 2016. 415 p. (Rus).

23. Available at: <http://www.kipt.kharkov.ua> (accessed 10 March 2017). (Rus).

24. Yuferov V.B., Druy O.S., Skibenko E.I., Kholod Yu.V., Chernyy O.V., Il'icheva V.O., Mufel' E.V., Rybalko A.N. Superconducting magnetic systems of difficult form and high-density of a transport current. *Electrical engineering & electromechanics*, 2003, no.2, pp.81-89. (Rus).

25. Available at: <http://foraenergy.ru/termovadernava-energetika> (accessed 09 September 2016). (Rus).

26. Available at: [https://www.gazeta.ru/science/2011/09/05\\_a\\_3756341.shtml](https://www.gazeta.ru/science/2011/09/05_a_3756341.shtml) (accessed 19 October 2016). (Rus).

27. Available at: <https://en.wikipedia.org/wiki/ITER> (accessed 22 January 2017).

28. Available at: <https://lenta.ru/articles/2014/05/28/iter/> (accessed 29 April 2017). (Rus).

29. Osadin B.A. Tokamafia: from Bringing Opponents into Discredit to a Global Monopoly. *History of Science and Engineering*, 2010, no.4, pp. 2-13. (Rus).

*Received 06.03.2018*

*M.I. Baranov, Doctor of Technical Science, Professor, Scientific-&-Research Planning-&-Design Institute «Molniya», National Technical University «Kharkiv Polytechnic Institute», 47, Shevchenko Str., Kharkiv, 61013, Ukraine, phone +380 57 7076841, e-mail: baranovmi@kpi.kharkov.ua*

*How to cite this article:*

Baranov M.I. An anthology of the distinguished achievements in science and technique. Part 46: Thermonuclear power engineering. Thermonuclear reactors and power plants: retrospective view of investigations of the controlled thermonuclear synthesis, their state-of-the-art and future. *Electrical engineering & electromechanics*, 2018, no.6, pp. 3-17. **doi: 10.20998/2074-272X.2018.6.01.**

V.F. Bolyukh, I.S. Schukin

## AN OPTIMIZATION APPROACH TO THE CHOICE OF PARAMETERS OF LINEAR PULSE INDUCTION ELECTROMECHANICAL CONVERTER

*Purpose. The purpose of the paper is to select the main parameters of the linear pulse induction electromechanical converters (LPIEC) for high-speed and power use with the use of the optimization approach, which provides an increase in speed and power indicators with limited electric, thermal and mass-dimensions. Methodology. A technique for finding the maximum of the integral efficiency criterion of LPIEC in the search space using a global optimization method that randomly searches for parameters, preventing entry into a local maximum, and a local method ensuring the contraction of the range of parameters with a global maximum to minimum dimensions is developed. As a global optimization method, genetic algorithms are used, and the Nelder-Mead method is used as the local method. Results. The LPIEC inductor should have a maximum external and minimum internal diameter, and its height should be less than that of the LPIEC of the basic design. The armature should have a maximum outer diameter, and the thickness of its wire should be minimal. The armature should be made with a significantly higher height, a greater number of turns and a wider wire. The height of the LPIEC inductor for power purposes should be almost the same as that of the LPIEC of the basic design. In this case, the number of turns of the inductor and the cross section of its wire should be approximately the same. The armature should be made with a slightly larger inner diameter and a significantly higher height. This armature should have a larger number of turns of wire, which must be stacked in 4 layers, and a large width of the wire. The average energy value and voltage of the capacitive energy storage for the LPIEC for high-speed and power applications should be higher than for the LPIEC of the basic design. Originality. An optimization approach to the choice of LPIEC parameters with a multi-turn squirrel arm is developed, which consists in finding the maximum of an integral efficiency criterion that takes into account the maximum speed and efficiency in a high-speed converter, the amplitude and magnitude of the electrodynamic force pulse in a power converter, with minimum temperature excesses, the mass of active elements and current of the inductor. The optimization uses a chain mathematical model that takes into account the interconnected electrical, magnetic, thermal and mechanical processes of the LPIEC. Practical value. The electric parameters of the capacitive energy storage device and the geometric parameters of the LPIEC are determined, which ensure the largest values of the integral efficiency criterion depending on the adopted version of the efficiency evaluation strategy. In optimized speed and power transfer converters, the integral efficiency criteria are 2.2 times higher on average than in the basic performance of the LPIEC. References 14, tables 6, figures 2.*

*Key words:* linear pulse induction electromechanical converter, chain mathematical model, integral efficiency criterion, optimization approach, genetic algorithms, Nelder-Mead method.

*Разработан оптимизационный подход к выбору параметров линейного импульсного индукционного электромеханического преобразователя (ЛИИЭП) с многовитковым короткозамкнутым якорем. Он состоит в нахождении максимума интегрального критерия эффективности, учитывающего максимальную скорость и КПД преобразователя скоростного назначения, амплитуду и величину импульса электродинамических усилий в преобразователе силового назначения при минимальных превышениях температур, массе активных элементов и токе индуктора. При этом используется цепная математическая модель, которая учитывает взаимосвязанные электрические, магнитные, тепловые и механические процессы ЛИИЭП. Разработана методика поиска максимума интегрального критерия эффективности ЛИИЭП в поисковом пространстве с использованием глобального и локального методов оптимизации. В качестве глобального метода используются генетические алгоритмы, а в качестве локального – метод Нелдера-Мида. Установлены электрические параметры емкостного накопителя энергии и геометрические параметры ЛИИЭП, обеспечивающие наибольшие значения интегрального критерия эффективности в зависимости от принятого варианта стратегии оценки эффективности. В оптимизированных преобразователях скоростного и силового назначения интегральные критерии эффективности в среднем в 2,2 раза выше, чем в ЛИИЭП основного исполнения. Библ. 14, табл. 6, рис. 2.*

*Ключевые слова:* линейный импульсный индукционный электромеханический преобразователь, цепная математическая модель, интегральный критерий эффективности, оптимизационный подход, генетические алгоритмы, метод Нелдера-Мида.

**Introduction.** Linear pulse electromechanical converters are widely used to accelerate the actuator (A) to high speed in a short active area and/or to create powerful power pulses on the object of action with a slight movement of A, made, for example, as a striker [1-4]. Such converters of high-speed and power purposes are used in many branches of science and technology as electromechanical accelerators and shock-power devices [5].

The most widely used converters are of induction type, which have a coaxial disk configuration. Such

linear pulsed induction electromechanical converters (LPIEC) contain an accelerated electrically conductive armature that magnetically interacts with a fixed inductor [6-8]. When the inductor is excited, a current is induced from a capacitive energy storage (CES) in an electrically conductive armature. The interaction of the inductor's magnetic field with induced current leads to the occurrence of electrodynamic forces (EDF), causing axial displacement of the armature with A. In this case, it is considered expedient to excite the inductor by a

© V.F. Bolyukh, I.S. Schukin

polar aperiodic pulse, which allows the use of electrolytic capacitors with an increased specific energy index for the CES [5].

However, at operation with a rapid change in the electromagnetic, mechanical and thermal parameters, the efficiency of the power and speed indicators of LPIEC is not high enough. One of the ways to improve these indicators is to use an optimization approach to the choice of the main parameters of LPIEC. With this choice, it is advisable to use the integral efficiency criterion, which should include the main speed or power indicators of LPIEC, taking into account its electrical, thermal and mass-dimensional indicators.

**The goal of the paper** is the choice of the basic parameters of LPIEC for speed and power purposes using an optimization approach that provides an increase in speed and power indicators with limited electrical, thermal and mass-dimensional indicators.

To increase the speed of the computational algorithm we use the chain mathematical model of LIIEP, which uses lumped parameters of the inductor and armature [9, 10]. This model takes into account interconnected electrical, magnetic, thermal and mechanical processes. To eliminate the influence of the skin effect, we consider an armature made as a short-circuited multi-turn winding tightly wound with a relatively thin copper wire.

**Parameters and indicators of LPIEC.** The optimization process consists in finding a set of parameters that provide the maximum values of velocity and kinetic energy in LPIEC for high-speed assignment and maximum values of amplitude and value of the impulse of EDF in LPIEC for power purposes. These indicators should be provided with the minimum temperature increases and mass of the  $n$ -th active elements ( $n = 1, 2$  are the indices of the inductor and armature, respectively) and the minimum current of the inductor, which is important for the control system.

#### Main LPIEC parameters

##### *CES electrical parameters:*

- $U_0, W_0$  – CES voltage and energy, respectively.

*LPIEC geometrical parameters* for the  $n$ -th active element:

- $w_n$  – number of turns of the wire;
- $d_{0n}$  – diameter of round wire;
- $h_{zn}, h_{rn}$  – height and width of rectangular wire;
- $D_{ex n}, D_{in n}$  – outer and inner diameters;
- $H_n$  – axial height.

##### LPIEC additional parameters:

- $m_2, m_e$  – mass of the armature and A, respectively;
- $\Delta z_0 = 0.5 \cdot (H_1 + H_2) + \Delta_0$  – initial axial

displacement between the centers of the  $n$ -th active elements, where  $\Delta_0$  – initial gap between active elements;

• converter shape: disk or cylindrical feedthrough (armature inside the inductor or vice versa);

- type of armature (multiturn, massive, combined);

• circuit of the formation of a current pulse in the inductor when excited from the CES;

- initial temperature  $T_{0n}$  of the  $n$ -th active element;
- mechanical factors: the forces of resistance to the movement of the armature, friction, etc.;
- parameters of lead wires and connecting elements.

These parameters are subject to parametric and functional limitations:

##### for energy source

$U_0 \leq U_{0\max}$  – on CES voltage;

$W_{0\min} \leq 0.5 \cdot C \cdot U_0^2 \leq W_{0\max}$  – on CES energy,

where  $C = 2W_0U_0^{-2}$  – CES capacitance;

##### for load

$0 \leq m_e \leq m_{e\max}$  – on mass of the accelerated A;

$f_{c\min} \leq f_c \leq f_{c\max}$  – on braking and opposing forces;

##### for electronic control system

$i_1 \leq i_{1\max}$  – limitation on the amplitude of the inductor excitation current;

##### for geometrical parameters

$1 \leq w_n \leq Ent \left( 0.5 \frac{D_{ex n} - D_{in n}}{h_{rn} + 2h_s} \right) \cdot Ent \left( \frac{H_n}{h_{zn} + 2h_s} \right)$  – for the

number of turns of rectangular wire, where  $Ent(f)$  – the largest integer not exceeding  $f$ ;  $h_s$  – winding conductor insulation thickness;

$1 \leq Ent \left( 0.5 \frac{D_{ex n} - D_{in n}}{h_{rn} + 2h_s} \right) \leq K_{wn\max}$  – for the number of

layers of rectangular wire;

$0 \leq \Delta z_0 \leq 0.5 \cdot (H_1 + H_2)$ ;  $0 \leq D_{in 2} \leq D_{in 2\max}$ ;

$D_{in 2} + 2 \cdot (h_{r2} + 2 \cdot h_s) \leq D_{ex 2} \leq D_{in 1} - \Delta_0$  – for cylindrical feedthrough converter, there  $D_{in 2\max}$  – maximum value of the armature inner diameter;

When using a round wire in parametric constraints, instead of  $h_{rn}$  and  $h_{zn}$  it is necessary to use its diameter  $d_{0n}$ ;

$i_1(t)i_2(t) \frac{dM_{12}}{dz}(z) \leq f_{z\max}$  – on the amplitude of EDF

active along the  $z$ -axis; where  $i_n(t)$  – current of the  $n$ -th active element,  $M_{12}$  – mutual inductance between active

elements;  $F_{z\min} \geq \int_0^{t_p} f_z dt \geq F_{z\max}$  – on the EDF impulse

value, where  $t_p$  is the duration of the EDF action;

$W_{kin\min} \geq 0.5 \cdot (m_2 + m_e) V_p^2 \geq W_{kin\max}$  – on the kinetic

energy, where  $V_p$  is the armature velocity at the end of the

operation process;  $V_{\min} \geq v \geq V_{\max}$  – on the velocity of

displacement of the armature with A;  $\theta_n \leq \theta_{n\max}$  – on

the maximum permissible temperature rise of the  $n$ -th active element.

**LPIEC of basic design.** As the basic design, we consider LPIEC with following parameters: [11]:

**Inductor:** outer diameter  $D_{ex1}=100$  mm, inner diameter  $D_{in1}=10$  mm, height  $H_1=10$  mm. The inductor is made as a two-layer winding with external electrical leads; rectangular wire cross section  $h_{z1} \times h_{r1}=1.8 \times 4.8$  mm<sup>2</sup>, number of turns of the wire  $w_1=46$ .

**Armature:** outer diameter  $D_{ex2}=100$  mm, inner diameter  $D_{in2}=6$  mm, height  $H_2=2.5$  mm. The armature is made as a multilayer short-circuited winding, the cross section of a rectangular copper wire  $h_{z2} \times h_{r2}=1.0 \times 1.2$  mm<sup>2</sup>, number of turns of the wire  $w_2=80$ .

**CES:** capacitance  $C_0=3$  mF, voltage  $U_0=0.4$  kV.

Initial distance between inductor and armature  $\Delta_0=1$  mm.

In LPIEC for speed purposes, the return spring's coefficient of elasticity is  $K_p=50$  kN/m. Mass of A  $m_e=0.5$  kg. We believe that in LPIEC of power designation the counteracting force is significant and there is no movement of A.

In LPIEC of the basic design of speed purpose, the following indicators are implemented: the amplitude of the inductor current  $i_{1m}=2.57$  kA, the maximum current density in the inductor's conductor  $j_{1m}=297.5$  A/mm<sup>2</sup>, the maximum current density in the armature  $j_{2m}=764.56$  A/mm<sup>2</sup>, the amplitude of EDF  $f_{zm}=13.983$  kN, the value of the impulse of EDF  $F_z=5.674$  Ns, the maximum speed of the armature with the inductor  $V_m=8.43$  m/s, the efficiency  $\eta=10.32$  %, the temperature rise of the inductor  $\theta_1=0.37$  °C, the temperature rise of the armature  $\theta_2=0.97$  °C. The mass of copper in the inductor is  $m_1=0.69$  kg, the mass of copper in the armature is  $m_2=0.17$  kg.

The following indicators are implemented in the LPIEC of the basic design of power purpose: the amplitude of the inductor current  $i_{1m}=2.953$  kA, the maximum current density in the inductor's conductor  $j_{1m}=341.78$  A/mm<sup>2</sup>, the maximum current density in the armature  $j_{2m}=893.51$  A/mm<sup>2</sup>, the amplitude of EDF  $f_{zm}=20.171$  kN, the magnitude of the impulse of EDF  $F_z=9.076$  Ns, the temperature rise of the inductor  $\theta_1=0.4$  °C, the temperature rise of the armature  $\theta_2=1.45$  °C.

**Integral efficiency criterion.** Since the efficiency of LPIEC of speed or power purpose is characterized by a number of versatile indicators, we introduce an integral efficiency criterion, which takes into account the maximum speed or power indicators with minimum values of the inductor current amplitude, temperature rises and the total mass of copper wire of active elements. In a dimensionless form, it can be written as follows.

$$K^* = \frac{\beta_1}{i_{1m}^*} + \beta_2 A^* + \beta_3 B^* + \frac{\beta_4}{\theta_1^*} + \frac{\beta_5}{\theta_2^*} + \frac{\beta_6}{m_\Sigma^*}; \quad \sum_{j=1}^J \beta_j = 1,$$

where  $\beta_j$  are the weights of the corresponding indicator;  $J=6$  is the number of functional indicators, normalized relative to LPIEC of the basic design (marked with asterisks);

$m_\Sigma = 0.5\pi\gamma_{Cu} \sum_{n=1}^2 (D_{exn} + D_{inn}) h_{rn} h_{zn} w_n$  is the total mass

of the copper wire in the  $n$ -th active elements,

where  $\gamma_{Cu}$  is the copper wire's density;

$A=f_{zm}$ ,  $B=F_z$  – for LPIEC of power purpose;

$A=V_m$ ,  $B=\eta$  – for LPIEC of speed purpose;

$f_{zm}$  is the EDF amplitude;

$V_m$  is the maximum speed of the armature with A;

$$\eta = 100 \frac{(m_2 + m_e) v_z^2 + K_p \Delta z^2}{C_0 U_0^2}, \% \quad \text{is the LPIEC}$$

efficiency.

Note that LPIEC of a basic design of speed or power designation has  $K^*=1$ . The best will be the converter with the maximum value of  $K^*$  showing how many times it is more efficient than LPIEC of the basic design.

**A technique of finding the maximum of the target function.** The integral efficiency criterion of LPIEC  $K^*$  is a target function of the optimization process. The strategy for finding the maximum of the target function of  $m$  variables in the search space is to share the global optimization method that performs a random search for LPIEC parameters in a given space, preventing it from falling into a local extremum, and a local method that provides tightening the parameter area with a global extremum to the minimum sizes.

As a global optimization method, we use genetic algorithms based on the mechanisms of population genetics [12, 13]. According to this method, each attribute of an object in the phenotype corresponds to one gene in the genotype, which is a bit string of fixed length. The sign is divided into tetrads, converted by the Gray code. When encoding a binary string of  $l$  bits of the variable  $x_k$ , which belongs to the segment  $[x_{\min}, x_{\max}]$ , each string  $s_k$  expresses the value of the variable  $x_k$ :

$$x_k = x_{\min} + s_k(x_{\max} - x_{\min})/2^l,$$

where  $s_k$  is the value of the binary number encoded by this string.

Operating on a set (population) of possible solutions  $P = (x_1, \dots, x_m)$ , the set of parameters  $x_i$ , of structured in a certain way in the form of a chain of finite length is processed, and subsequent generations of the solution population are generated using genetic operators. Thus, a randomized search with centralized control is implemented, using selection and genetic mechanisms of reproduction, with an arbitrary choice of points of application of operators.

Genetic algorithms can be represented as follows:

$$GA = (P^0, m, l, S, Q, \iota, \xi),$$

where  $P^0 = (a_1^0, \dots, a_m^0)$  is the initial population;  $a_i^0$  is the problem solution in the form of a chromosome,  $i=1, m$ ;  $m$  is the population dimension;  $l$  is the length of each chromosome of the population;  $S$  is the selection operator;  $Q$  is the recombination mapping recombination (crossover, mutation);  $\iota$  is the optimality function;  $\xi$  is the break criterion.

The work of genetic algorithms is an iterative process that continues until a given condition is met, for example, slowing down the growth of the efficiency criterion  $K^*=1$  to a given value.  $P^0$  is a randomly generated initial population. At each iteration cycle, selection, crossover, and mutation operators are implemented. The selection operator  $S$  generates an intermediate population  $R^t$  from the population  $P^t$  by

selecting and generating new copies of the elements  $\mathbf{P}^t$ :  $\mathbf{R}^t = S(\mathbf{P}^t)$ . The optimality function  $\iota$ , which provides feedback on the results of optimization during generation  $t$ , is used to select individuals in the population. The selection is made based on the probabilities  $p_S(a_i^t)$  calculated for each individual:

$$p_S(a_i^t) = \frac{\iota(a_i^t)}{\sum_{j=1}^m \iota(a_j^t)}.$$

After the selection is completed, for the element  $a_i^t \in \mathbf{R}^t$  a partner is selected from  $\mathbf{R}^t$  for recombination and a new chromosome is built.

The crossover with probability  $p_C$  is performed as follows:

- random selection of crossbreeding partners  
 $a_1 = (a_{1,1} \dots a_{1,l}) \in \mathbf{R}^t$ ,  $a_2 = (a_{2,1} \dots a_{2,l}) \in \mathbf{R}^t$ ;
- random crossover point selection  $x \in \{1, \dots, l-1\}$ ;
- formation of two new individuals  
 $a_1' = (a_{1,1} \dots a_{1,x} \ a_{2,x+1} \dots a_{2,l})$ ,  
 $a_2' = (a_{2,1} \dots a_{2,x} \ a_{1,x+1} \dots a_{1,l})$ .

A mutation is a random change in the chromosome bit:

- random selection with probability  $p_M$  of positions  $\{x_1, \dots, x_k\} \subseteq \{1, \dots, l\}$  inside the bit string  
 $a = (a_1 \dots a_l) \in \mathbf{R}^t$ , prone to mutation;
- formation of a new individual  
 $a = (a_1 \dots a_{x_1-1} \ \overline{a_{x_1}} \ a_{x_1+1} \dots a_{x_i-1} \ \overline{a_{x_i}} \ a_{x_i+1} \dots a_l)$ , ( $i = \overline{1, k}$ ).

As a local optimization method for finding the maximum of the optimality criterion  $K^*(X)$  in the  $n$ -dimensional Euclidean space  $R^n$

$$\max K^*(X) = K^*(X^*), \quad X \in R^n$$

the Nelder-Mead method is used changing the current simplex [14].

As a result of reflection of the  $k$ -th vertex of the simplex with the coordinates of the vertices  $X_i^r, i \in [1, n+1]$ , a simplex is formed with the coordinates of the vertices

$$X_i^{r+1} = X_i^r, \quad i \in [1, n+1], \quad i \neq k, \quad X_k^{r+1} = 2X_C^r - X_k^r,$$

where  $X_C^r = \frac{1}{n} \sum_{i=1, i \neq k}^{n+1} X_i^r$  is the vector of coordinates of the

center of gravity of the remaining vertices of the simplex.

As a result of the reduction of the vertices of the simplex  $X_i^r$  to the vertex  $X_k$ , we obtain the simplex with the coordinates of the vertices

$$X_i^{r+1} = X_k^r + \gamma(X_i^r - X_k^r), \quad i \in [1, n+1], \quad i \neq k, \quad X_k^{r+1} = X_k^r,$$

where  $\gamma \in (0.1)$ ,  $\gamma \approx 0.5$  is the reduction factor.

After the operation of compressing the simplex  $X_i^r$  in the direction  $(X_k^r - X_C^r)$ , we obtain a simplex with the coordinates of the vertices

$$X_i^{r+1} = X_k^r, \quad i \in [1, n+1], \quad i \neq k, \quad X_k^{r+1} = X_C^r + \beta(X_k^r - X_C^r),$$

where  $\beta \in (0.1)$ ,  $\beta \approx 0.4-0.6$  is the compression factor.

As a result of extension of the simplex  $X_i^r$  in the direction  $(X_k^r - X_C^r)$ , we obtain a simplex with the coordinates of the vertices

$$X_i^{r+1} = X_i^r, \quad i \in [1, n+1], \quad i \neq k, \quad X_k^{r+1} = X_C^r + \alpha(X_k^r - X_C^r),$$

where  $\alpha \approx 2.8-3.0$  is the extension factor.

Since the deformation procedure is repeated many times, the polyhedron adapts to the local relief of the target function and shrinks, ensuring the convergence of the algorithm in the local maximum, allowing by the size of the polyhedron  $\sigma_i$  to judge the stage of the search for the converter parameters.

**Realization of the task of choosing the parameters of LPIEC.** Consider a LPIEC of a disk configuration with a multiturn armature that is excited by a polar aperiodic pulse (CES is shunted by a reverse diode). The following are used as independent variables that are included in the LPIEC design variables vector: outer  $D_{\text{ext}}$  and inner  $D_{\text{int}}$  diameters, height  $H_n$ , number of turns  $w_n$ , height  $h_{zn}$ , and width  $h_{rn}$  of a rectangular wire of the  $n$ -th active element; voltage  $U_0$  and energy  $W_0$  of CES. Restrictions on these parameters impose the boundaries of the search space (Table 1).

Table 1  
Functional and parametric limitations of LPIEC parameters

Parameter	Value
CES energy $W_0$ , J	150...500
CES voltage $U_0$ , V	150...500
Outer diameter of the $n$ -th active elements $D_{\text{ext}}$ , mm	50...100
Inner diameter of the inductor $D_{\text{in1}}$ , mm	10...20
Inner diameter of the armature $D_{\text{in2}}$ , mm	2...20
Inductor height $H_1$ , mm	5...22
Armature height $H_2$ , mm	1...10
Number of inductor layers $K_{w1}$	2
Number of turns of inductor $w_1$	30...75
Inductor wire height $h_{z1}$ , mm	1...2
Inductor wire width $h_{r1}$ , mm	2...10
Number of armature layers $K_{w2}$	1...8
Number of turns of armature $w_2$	20...200
Armature wire height $h_{z2}$ , mm	0.5...1.5
Armature wire width $h_{r2}$ , mm	1.0...3.0
Wire insulation thickness $h_s$ , mm	0.1
Initial gap between the $n$ -th active elements $\Delta_0$ , mm	1.0

For optimization calculations, a computational algorithm was applied, which includes the following steps [7].

1. A genetic representation of the polyhedron is specified by a set of  $N+1$  parameters – vectors of design variables  $P^0 = (x_1^0, \dots, x_{N+1}^0)$ ,  $x(x_1, \dots, x_N) \in \mathfrak{R}^N$ .

2. From  $K$  source polyhedra  $P_i^0 = (\mathbf{x}_{i,1}^0, \dots, \mathbf{x}_{i,N+1}^0)$ ,  $i = 1, \dots, K$  the population  $D_i(P_i^0)$  is randomly formed.

3. The operators of reflection, extension, compression, and reduction are applied to each polyhedron  $P_i^0$  to perform a specified number of steps  $s$  in the search space.

4. The value of the target function  $F^t(\mathbf{x}_{i,j}^t), i = 1, \dots, K, j = 1, \dots, N+1$  is determined in each vertex of the polyhedron as well as its the «best» vertex  $\mathbf{x}_{i,b}^t, i = 1, \dots, K$ .

5. The polyhedra are ranked relative to the value of the target function of their best vertexes.  $F_b^t(\mathbf{x}_{i,b}^t), i = 1, \dots, K$ .

6. The polyhedron with the worst parameters is eliminated.

7. A new polyhedron  $P_K^t$  is formed by applying genetic operators of the crossover and mutation, acting with probability  $\rho_{mut}$ , to two randomly selected polyhedra from the remaining  $(K-1)$ .

8. The value of the target function  $F(\mathbf{x}_{K,j}^t), j = 1, \dots, N+1$  and the «best» vertex of the polyhedron  $P_K^t$  are determined.

9. Polyhedrons  $P_i^t$  are ranked by size  $\sigma(P_i^t), i = 1, \dots, K$ .

10. Threshold  $\sigma^t$  is determined for getting into the search group by size of the  $h$ -th population  $\sigma(P_h^t)$ .

11. To  $(K-h)$  populations operators of reflection, extension, compression and reduction are applied.

12. Return to step 4.

**The results of the choice of parameters of LPIEC of speed purpose.** The choice of parameters is largely determined by the adopted version of the strategy for assessing the effectiveness of LPIEC. Consider four options for the strategy (Table 2).

Table 2

The weights of the options for the evaluation strategy for the LPIEC efficiency, p.u.

Strategy options	$\beta_1$	$\beta_2$	$\beta_3$	$\beta_4$	$\beta_5$	$\beta_6$
I	0.2	0.2	0.2	0.1	0.1	0.2
II	0.1	<b>0.3</b>	<b>0.3</b>	0.1	0.1	0.1
III	0.05	<b>0.5</b>	0.2	0.1	0.1	0.05
IV	0.05	0.2	<b>0.5</b>	0.1	0.1	0.05

In option I, all LPIEC indicators are estimated equally (the total value of the temperature rise indicator is 0.2). In option II, the maximum speed  $V_m$  and the efficiency  $\eta$  of the converter are estimated to be the highest and equivalent. In option III, the maximum speed  $V_m$  is most highly estimated, and in option IV – efficiency  $\eta$ .

As a result of calculations for each of the options of the strategy for evaluating the effectiveness, the relative parameters of LPIEC for speed purpose were obtained: energy  $W_0^*$ , voltage  $U_0^*$ , and capacitance  $C^*$  of CES; outer  $D_{ex1}$  and inner  $D_{in1}$  diameters, height  $H_1^*$ , number of turns  $w_1^*$ , thickness  $h_{z1}$  and width  $h_{r1}$  of the wire of the

inductor; outer  $D_{ex2}$  and inner  $D_{in2}$  diameters, height  $H_2^*$ , number of turns  $w_2^*$  and number of layers  $K_{w2}$ , thickness  $h_{z2}$  and width  $h_{r2}$  of the wire of the armature (Table 3).

Table 3

Relative parameters of LPIEC of speed purpose

Parameter	Strategy options for estimation of LPIEC efficiency				Average value
	I	II	III	IV	
$D_{ex1}^*$	1.0	1.0	1.0	1.0	<b>1.0</b>
$D_{in1}^*$	1.1	1.0	1.0	1.0	<b>1.0</b>
$H_1^*$	0.62	0.62	0.82	0.66	<b>0.68</b>
$w_1^*$	1.63	1.39	0.87	0.95	<b>1.21</b>
$h_{z1}^*$	0.55	0.67	1.11	1.11	<b>0.86</b>
$h_{r1}^*$	0.625	0.625	0.830	0.662	<b>0.686</b>
$D_{ex2}^*$	1.0	1.0	1.0	1.0	<b>1.0</b>
$D_{in2}^*$	1.2	1.3	1.1	1.0	<b>1.15</b>
$H_2^*$	4.8	6.8	1.6	2.52	<b>3.93</b>
$w_2^*$	2.2	2.1	1.2	1.5	<b>1.75</b>
$K_{w2}^*$	2.0	2.0	1.0	1.5	<b>1.63</b>
$h_{z2}^*$	1.0	1.0	1.0	1.0	<b>1.0</b>
$h_{r2}^*$	2.08	3.33	1.5	1.66	<b>2.14</b>

The operation of LPIEC is estimated by the following relative indicators: inductor current amplitude  $i_{1m}^*$ , maximum current density in conductors of inductor  $j_{1m}^*$  and armature  $j_{2m}^*$ , maximum speed  $V_m^*$  and efficiency  $\eta^*$ , temperature rise of the inductor  $\theta_1^*$  and armature  $\theta_2^*$  at the end of the working process, total mass of the wire  $m_\Sigma^*$  and the criterion of efficiency  $K^*$  (Table 4).

Table 3, 4 also show the average values of the parameters and indicators of LPIEC for speed purpose.

Table 4

Relative indicators of LPIEC of speed purpose

Indicator	Strategy options for estimation of LPIEC efficiency				Average value
	I	II	III	IV	
$W_0^*$	0.729	0.937	2.08	1.458	<b>1.301</b>
$U_0^*$	0.437	0.562	1.25	1.25	<b>0.875</b>
$C^*$	3.8	2.96	1.33	0.933	<b>2.256</b>
$i_{1m}^*$	0.345	0.565	1.553	1.3	<b>0.941</b>
$j_{1m}^*$	0.992	1.268	1.677	1.754	<b>1.423</b>
$j_{2m}^*$	0.141	0.12	0.958	0.568	<b>0.447</b>
$V_m^*$	0.449	0.516	1.592	1.257	<b>0.965</b>
$\eta^*$	0.537	0.727	1.403	1.573	<b>1.061</b>
$\theta_1^*$	1.953	2.834	4.1	3.712	<b>3.15</b>
$\theta_2^*$	0.053	0.037	0.86	0.34	<b>0.323</b>
$m_\Sigma^*$	1.456	1.856	0.976	1.03	<b>1.33</b>
$K^*$	2.858	3.331	1.3	1.376	<b>2.216</b>

Based on the results obtained, the following conclusions can be drawn. Inductor of LPIEC must have the maximum outer  $D_{ex1}=0.1$  m and minimum inner  $D_{in1}=0.01$  m diameters. The armature should have the maximum outer diameter  $D_{ex2}=0.1$  m, and the

thickness of its wire should be minimum  $h_{z2}=1$  mm. These parameters accept the limiting functional limitations (Table 1) and correspond to the parameters of LPIEC of basic design in all options of the effectiveness evaluation strategy.

The height of the inductor should be less than that of LPIEC of the basic design and, depending on the strategy options, averages  $H_1=6.8$  mm. Here, the number of turns of the inductor in options I and II should be greater, and in options III and IV less than of the basic design of LPIEC, averaging  $w_1=56$  turns of the wire with cross section  $h_{z1} \times h_{r1}=1.5 \times 3.3$  mm<sup>2</sup>. The armature of the optimized converter should be made with large inner diameter  $D_{in2}=7$  mm and significantly larger height  $H_2=9.8$  mm, with large number of turns  $w_2=140$  and wire width  $h_{r2}=2.6$  mm.

CES of optimal LPIEC should have less energy in options I and II, while its average value should be higher than that of LPIEC of basic design and be  $W_0=312$  J. Voltage of CES in options I and II is low and averages  $U_0=200$  V, and in options III and IV – the maximum  $U_0=500$  V. The average values of maximum current densities as compared to LPIEC of the basic design in the inductor conductors are increased to  $j_{1m}=423$  A/mm<sup>2</sup>, and in the armature conductors are reduced to  $j_{12m}=342$  A/mm<sup>2</sup>.

Maximum speed and efficiency are reduced in strategy options I and II and increased in options III and IV. For example, in option III of the strategy, maximum speed is  $V_m=13.4$  m/s, and the efficiency in option IV is  $\eta = 16.2$  %.

Compared to LPIEC of the basic design, in optimized converters, the temperature rise of the inductor increases, and the armature temperature rise decreases, averaging  $\theta_1=1.17$  °C and  $\theta_2=0.31$  °C. The weight of copper wire increases on average to  $m_\Sigma=1.14$  kg. Compared to the basic design of LPIEC, the integral efficiency criteria of optimized converters increase on average to a value  $K^*=2.2$ .

Fig. 1 shows the electromechanical characteristics of LPIEC of speed purpose, optimal in strategy option IV. A feature of these characteristics is that the maximum values of current densities in the windings of the inductor and the armature occur almost simultaneously, which causes the nature of the change in EDF  $f_z$ . Movement of the armature with A begins in 0.2 ms after the start of the working process.

**The results of the choice of parameters of LPIEC of power purpose.** Let us consider four options of the strategy for evaluating the effectiveness of LPIEC for power purpose (Table 2). In option II, the amplitude  $f_{zm}$  and the value of the impulse  $F_z$  of EDF are estimated most highly and equally. In option III, the amplitude of EDU  $f_{zm}$  is most evaluated. In option IV, the value of the impulse of EDU  $F_z$  is most evaluated.

Table 5, 6 show the average values of parameters and indicators of LPIEC for power purpose.

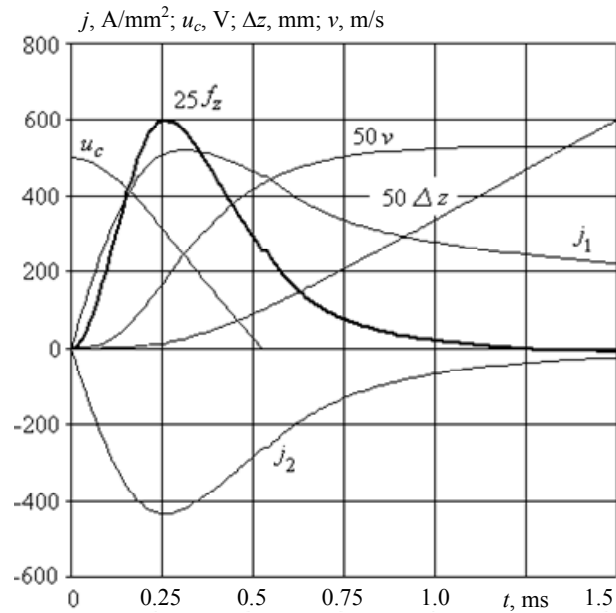


Fig. 1. Electromechanical characteristics of the optimal LPIEC of speed purpose (option of strategy IV)

Table 5  
Relative parameters of LPIEC of power purpose

Parameter	Strategy options for estimation of LPIEC efficiency				Average value
	I	II	III	IV	
$D_{ex1}^*$	1.0	1.0	1.0	1.0	<b>1.0</b>
$D_{in1}^*$	1.1	1.0	1.0	1.0	<b>1.0</b>
$H_1^*$	1.04	1.04	1.06	0.86	<b>1.0</b>
$w_1^*$	0.87	1.39	1.09	0.91	<b>1.07</b>
$h_{z1}^*$	1.11	0.66	0.89	1.11	<b>0.94</b>
$h_{r1}^*$	1.04	1.04	1.06	0.88	<b>1.01</b>
$D_{ex2}^*$	1.0	1.0	1.0	1.0	<b>1.0</b>
$D_{in2}^*$	1.2	1.2	1.3	1.4	<b>1.275</b>
$H_2^*$	5.0	5.0	6.0	3.84	<b>4.96</b>
$w_2^*$	2.1	2.3	2.2	2.2	<b>2.2</b>
$K_{w2}^*$	2	2	2	2	<b>2</b>
$h_{z2}^*$	1.0	1.0	1.0	1.0	<b>1.0</b>
$h_{r2}^*$	2.5	2.5	2.9	1.92	<b>2.46</b>

Table 6  
Relative indicators of LPIEC of power purpose

Indicator	Strategy options for estimation of LPIEC efficiency				Average value
	I	II	III	IV	
$W_0^*$	0.625	2.08	1.875	2.08	<b>1.665</b>
$U_0^*$	0.375	1.25	1.125	1.2	<b>0.988</b>
$C^*$	4.444	1.333	1.481	1.45	<b>2.177</b>
$i_{1m}^*$	0.818	0.993	1.234	1.616	<b>1.165</b>
$j_{1m}^*$	0.703	1.43	1.333	1.662	<b>1.282</b>
$j_{2m}^*$	0.146	0.288	0.243	0.428	<b>0.276</b>
$f_{zm}^*$	0.382	1.47	2.018	1.361	<b>1.308</b>
$F_z^*$	0.891	3.147	2.918	3.318	<b>2.568</b>
$\theta_1^*$	1.062	3.382	3.181	4.198	<b>2.956</b>
$\theta_2^*$	0.051	0.19	0.125	0.291	<b>0.164</b>
$m_\Sigma^*$	1.832	1.832	2.032	1.456	<b>1.788</b>
$K^*$	2.664	2.147	2.159	2.047	<b>2.254</b>

The height of the inductor of this converter should be almost the same as that of LPIEC of the basic design, and should be on average  $H_1=10$  mm. At the same time, the number of inductor turns in strategy options I and IV should be less, and in strategy options II and III more than in the basic design of LPIEC, averaging  $w_1=50$  turns. The cross section of the inductor wire  $h_{z1} \times h_{r1}=1.7 \times 4.8$  mm<sup>2</sup> should be almost the same. The armature should be made with slightly larger inner diameter  $D_{in2}=7.6$  mm and significantly larger height  $H_2=12.4$  mm. This armature should have greater number of turns of wire  $w_2=176$ , which should be laid in 4 layers, and large wire width  $h_{r2}=3.0$  mm.

CES of LPIEC for power purpose should have less energy only in option I of strategy, in which all indicators are evaluated equally. The average value of the energy of CES should be higher than that of LPIEC of the basic design and be  $W_0=400$  J. The voltage of CES in the option of strategy I is low and is  $U_0=150$  V, and in other variants it is increased and is  $U_0=450-500$  V. The capacitance of CES increases in all variants of the strategy, averaging  $C=6530$   $\mu$ F.

The average values of the maximum current densities compared with LPIEC of the main design in inductor conductors are on average increased to  $j_{1m}=438$  A/mm<sup>2</sup>, and in armature conductors reduced to  $j_{2m}=246$  A/mm<sup>2</sup>. The amplitude and value of the impulse of EDF are increased except for option of strategy I. Thus, in the option of strategy III, the amplitude of EDF is  $f_z=40.7$  kN, and in the option of strategy IV, the value of the impulse of EDF is  $F_z=30.11$  N·s. In all options of the strategy, compared to LPIEC of the basic design, the temperature rise of the inductor increases, and the armature temperature rise decreases, averaging  $\theta_1=1.18$  °C and  $\theta_2=0.24$  °C, respectively. The mass of copper wire increases on average to  $m_2=1.54$  kg. Compared to the basic design of LPIEC, the integral efficiency criteria of optimized converters of power purpose increase on average to the value  $K^*=2.25$ .

Fig. 2 shows the electrodynamic characteristics of LPIEC for power purpose, optimal in strategy option IV. Compared with LPIEC speed purpose, in this converter the electrodynamic processes proceed with large delay in time, with large amplitudes of the current densities in the inductor and armature, and also EDF.

### Conclusions

1. An optimization approach has been developed for choice parameters of LPIEC with a multi-turn short-circuited armature, which consists in finding the maximum of the integral efficiency criterion that takes into account the maximum speed and efficiency of the converter of speed purpose, amplitude and value of the impulse of EDF of the converter of power purpose with minimum temperature rises, mass of active elements and current in inductor. The optimization uses a chain mathematical model that takes into account the interconnected electrical, magnetic, thermal, and mechanical processes of LPIEC.

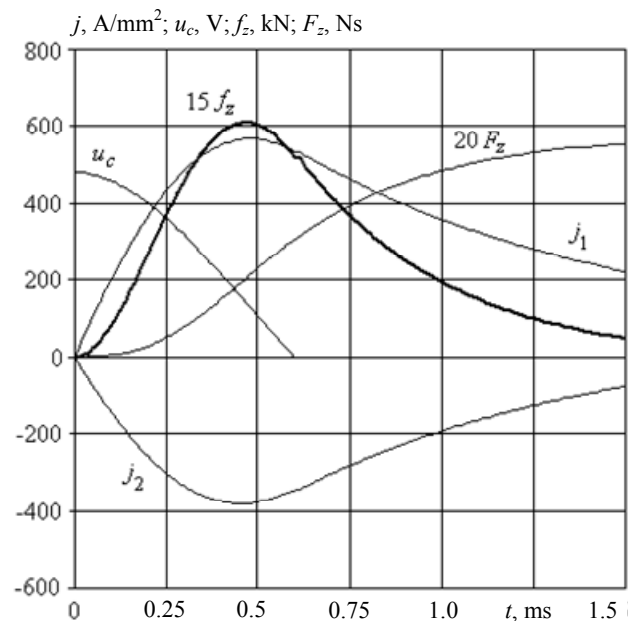


Fig. 2. Electrodynamic characteristics of the optimal LPIEC of power purpose (option of strategy IV)

2. A technique has been developed for finding the maximum of the integral criterion of LPIEC efficiency in the search space using a global optimization method that performs a random search for parameters, preventing it from falling into a local maximum, and a local method that provides a parameter region tightening with a global maximum to the minimum size. Genetic algorithms are used as a global optimization method, and the Nelder-Mead method is used as a local optimization method.

3. The values of the electrical parameters of the capacitive energy storage and the geometrical parameters of LPIEC are determined, which provide the highest values of the integral efficiency criterion depending on the adopted option of the effectiveness evaluation strategy. In optimized converters for speed and power purposes, the integral efficiency criteria are on average 2.2 times higher than in LPIEC of basic design.

### REFERENCES

- Balikci A., Zabar Z., Birenbaum L., Czarkowski D. Improved performance of linear induction launchers. *IEEE Transactions on Magnetics*, 2005, vol.41, no.1, pp. 171-175. doi: 10.1109/tmag.2004.839283.
- Tomashevsky D.N., Koshkin A.N. Modeling of linear impulse electric motors. *Russian Electrical Engineering*, 2006, no.1, pp. 24-27. (Rus).
- Chemerys V.T., Bolyukh V.F. Prospectives of new coilgun design development. *Artillery and small arms*, 2008, no.3, pp. 44-52.
- D.-K. Lim, D.-K. Woo, I.-W. Kim, D.-K. Shin, J.-S. Ro, T.-K. Chung, H.-K. Jung. Characteristic Analysis and Design of a Thomson Coil Actuator Using an Analytic Method and a Numerical Method. *IEEE Transactions on Magnetics*, 2013, vol.49, no.12, pp. 5749-5755. doi: 10.1109/tmag.2013.2272561.
- Bolyukh V.F., Shchukin I.S. *Lineinye induktsionno-dinamicheskie preobrazovately* [Linear induction-dynamic converters]. Saarbrücken, Germany, LAP Lambert Academic Publ., 2014. 496 p. (Rus).
- Bolyukh V.F., Oleksenko S.V., Shchukin I.S. Comparative analysis of linear pulse electromechanical converters

electromagnetic and induction types. *Technical Electrodynamics*, 2016, no.5, pp. 46-48. (Rus).

7. Bissal A., Magnusson J., Engdahl G. Comparison of two ultra-fast actuator concept. *IEEE Transactions on Magnetics*, 2012, vol.48, no.11, pp. 3315-3318. doi: **10.1109/tmag.2012.2198447**.

8. J. Young-woo, L. Hyun-wook, L. Seok-won. High-speed AC circuit breaker and high-speed OCD. *Proceeding of the conf. «22-th international conference on electricity distribution»*. 2013, 10-13 June, Stockholm. - Paper 608.

9. Li W., Koh C.S. Parametric analysis of Thomson-coil actuator using adaptive equivalent circuit method. *Digests of the 2010 14th Biennial IEEE Conference on Electromagnetic Field Computation*, May 2010, pp. 1-9. doi: **10.1109/cefc.2010.5481673**.

10. Bolyukh V.F., Kocherga A.I., Schukin I.S. Investigation of a linear pulse-induction electromechanical converter with different inductor power supply circuits. *Electrical engineering & electromechanics*, 2018, no.1, pp. 21-28. (Rus). doi: **10.20998/2074-272X.2018.1.03**.

11. Bolyukh V.F., Schukin I.S. Investigation of thermal processes in a linear pulse-induction electromechanical converter of cyclic action. *Electrical engineering & electromechanics*, 2017, no.5, pp. 14-22. doi: **10.20998/2074-272X.2017.5.02**.

12. Nolan R., Pillay P., Haque T. Application of genetic algorithms to motor parameter determination. *Proceedings of*

*1994 IEEE Industry Applications Society Annual Meeting*, Baltimore, USA, 1994, pp. 42-54. doi: **10.1109/ias.1994.345500**.

13. Bolyukh V.F., Lysenko L.I., Bolyukh E.G. Parameters of high-efficiency pulsed inductive electromechanical converters. *Russian Electrical Engineering*, 2004, vol.75, no.12, pp. 1-11.

14. Nelder J.A., Mead R. A Simplex Method for Function Minimization. *The Computer Journal*, 1965, vol.7, no.4, pp. 308-313. doi: **10.1093/comjnl/7.4.308**.

Received 04.09.2018

V.F. Bolyukh<sup>1</sup>, Doctor of Technical Science, Professor,  
I.S. Schukin<sup>2</sup>, Candidate of Technical Science, Associate Professor,

<sup>1</sup> National Technical University «Kharkiv Polytechnic Institute»,  
2, Kyrpychova Str., Kharkiv, 61002, Ukraine,  
phone +380 57 7076427,  
e-mail: vfbolyukh@gmail.com

<sup>2</sup> Firm Tetra, LTD,  
2, Kyrpychova Str., Kharkiv, 61002, Ukraine,  
phone +380 57 7076427,  
e-mail: tech@tetra.kharkiv.com.ua

How to cite this article:

Bolyukh V.F., Schukin I.S. An optimization approach to the choice of parameters of linear pulse induction electromechanical converter. *Electrical engineering & electromechanics*, 2018, no.6, pp. 18-25. doi: **10.20998/2074-272X.2018.6.02**.

G.G. Zhemerov, D.S. Krylov

## CONCEPT OF CONSTRUCTION OF POWER CIRCUITS OF A MULTILEVEL MODULAR CONVERTER AND ITS TRANSISTOR MODULES

**Goal.** The goal of the paper is to study the peculiarities of building power circuits of a modular multilevel converter (MMC) of electrical energy for DC transmission lines, to investigate its operating principles and basic characteristics. **Methodology.** We have applied the theory of electrical circuits and mathematical simulation in Matlab package. **Results.** A Matlab-model of the MMC power circuit was constructed with shunting of all the shoulders by current sources, which made it possible to check the correctness of the formulas for the characteristics of the proposed circuits. **Originality.** Variants of power circuits of MMC with shunting of all shoulders of the converter by current sources are offered. The tables of states of HB and FB modules for forward and backward direction of the current of the shoulders are made. **Practical value.** The use of the proposed structure of the converter power circuit and the algorithms of operation of the power transistor modules will help to determine the scope of their application, will help in the synthesis of the control system and analysis of possible emergency modes of the MMC. References 8, tables 8, figures 9.

**Key words:** power supply system, multilevel modular converter, transistor module, shoulder currents, Matlab model of three-phase MMC, state of valves.

**Цель.** Целью статьи является исследование особенностей построения силовых цепей многоуровневого модульного преобразователя (MMC) электроэнергии для линий электропередачи постоянного тока, исследование его принципов работы и основных характеристик. **Методика.** Для проведения исследований использовалась теория электрических цепей, математическое моделирование в пакете Matlab. **Результаты.** Построена Matlab-модель силовой схемы MMC с шунтированием всех плеч источниками тока, позволившая проверить корректность формул для характеристик предложенных схем. **Научная новизна.** Предложены варианты силовых схем MMC с шунтированием всех плеч преобразователя источниками тока. Составлены таблицы состояний HB и FB модулей при прямом и обратном направлении токов плеч. **Практическое значение.** Использование предложенной структуры силовой схемы преобразователя и алгоритмов работы силовых транзисторных модулей позволит определить сферу их применения, поможет в синтезе системы управления и анализе возможных аварийных режимов MMC. Библ. 8, табл. 8, рис. 9.

**Ключевые слова:** система электроснабжения, многоуровневый модульный преобразователь, транзисторный модуль, токи плеч, Matlab-модель трехфазного MMC, состояние вентиляей.

**Introduction.** In recent years, powerful industrial semiconductor converters of a new type – *modular multilevel converters*, first proposed in [1, 2] by R. Marquarratt and A. Lesnicar in 2001, 2003, have gained wide industrial application. In numerous publications [3-8], the steady abbreviation MMC is used for these converters. It should be noted the speed with which the MMS was developed, manufactured and put into commercial operation in DC power lines (HVDC). The first HVDC system with MMC, developed by Siemens, connected the cities of Pittsburgh and San Francisco in California, USA [7] in November 2010. A DC cable is designed for 400 MW,  $\pm 200$  kV.

Tennet Off-Shore Wind Farm Complex, located in the North Sea near the coast of Germany, implements several HVDC projects for wind power plants using MMC. Table 1 shows the characteristics of these projects [8].

In [7] information on the implementation of several other projects using MMC, located in Europe and China by Siemens, is presented.

However, despite the active introduction in the world energy sector, in the domestic literature there is practically no information about this type of converter, the principles of its construction, the scope of application.

**The goal of the work** is to study the peculiarities of building power circuits of a modular multilevel converter (MMC) of electrical energy for DC transmission lines, to investigate its operating principles and basic characteristics.

Table 1  
Off-shore wind power plants using MMC

Wind Power plant	Power (MW)	Voltage (kV)	Cable length (km)	Performer	State of works
Helwin 1	576	$\pm 250$	130	Siemens	Operating since 2013
Dolwin 1	800	$\pm 640$	165	ABB	Testing in 2013
Borwin 2	800	$\pm 300$	200	Siemens	Testing in 2013
Sylwin 1	864	$\pm 320$	205	Siemens	Operating since 2014
Dolwin 2	900	$\pm 640$	135	ABB	Operating since 2015
Dolwin 3	900	$\pm 320$	162	ABB	No data

**The power circuit and the principle of operation of MMC.** Fig. 1 shows the power circuits, respectively, of single-phase and three-phase MMC. As can be seen from Fig. 1, the power circuit of the converter is powered by two constant voltage sources. Three-phase MMC consists of three single-phase MMC, operating independently of each other. Common points of voltage sources and load,  $Z_L$ , are combined. The shoulders of the MMC power circuit, – two shoulders in a single phase and six shoulders in a three phase, – are a series connection of  $N$  half-bridge HB modules or full-bridge FB modules, shown in Fig. 1.

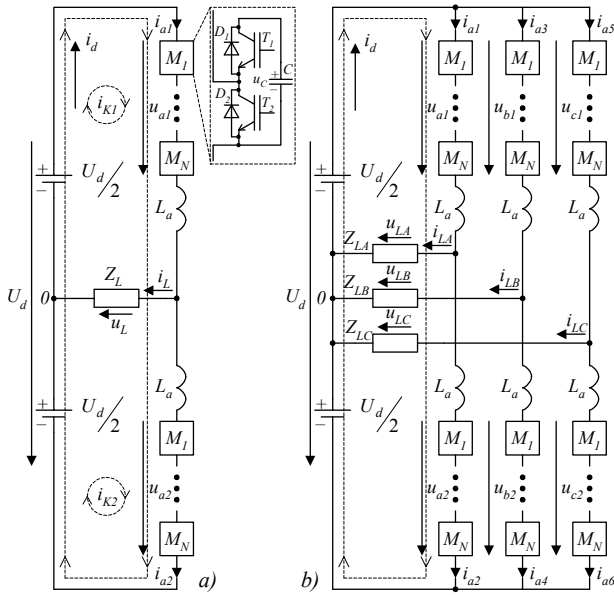


Fig. 1. Power circuits of MMC

An equalization reactor  $L_a$  is included in each shoulder of the circuit. Voltage regulation on the load is carried out by switching on a specified number of modules and a predetermined algorithm of their operation. In the steady-state operation mode of MMC, all six keys conduct current at any time, and the total voltage in the closed circuits shown in Fig. 1, a by the dotted line, at zero equalizing current should be zero. Graphs of shoulder voltages are shown in Fig. 2, they correspond to the relations:

$$u_{a1} = \frac{U_d}{2} - v \cdot \frac{U_d}{2} \cdot \sin \vartheta, \quad (1)$$

$$u_{a2} = \frac{U_d}{2} + v \cdot \frac{U_d}{2} \cdot \sin \vartheta, \quad (2)$$

where  $\vartheta = 2\pi ft$  is the dimensionless time;  $f$  is the voltage frequency on the converter output;  $v$  is the relative load voltage

$$v = \frac{U_{1\max}}{U_d/2}. \quad (3)$$

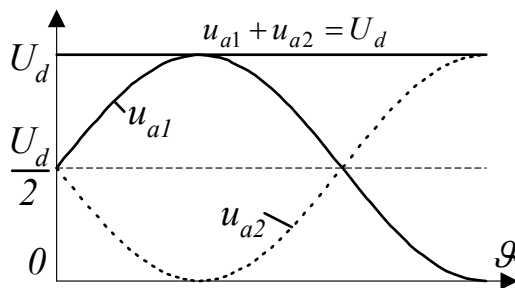


Fig. 2. Voltages of the MMC shoulders

For three-phase MMC, the shoulder voltages are determined from the relations:

$$u_{b1} = \frac{U_d}{2} - v \cdot \frac{U_d}{2} \cdot \sin\left(\vartheta - \frac{2\pi}{3}\right), \quad (4)$$

$$u_{b2} = \frac{U_d}{2} + v \cdot \frac{U_d}{2} \cdot \sin\left(\vartheta - \frac{2\pi}{3}\right), \quad (5)$$

$$u_{c1} = \frac{U_d}{2} - v \cdot \frac{U_d}{2} \cdot \sin\left(\vartheta - \frac{4\pi}{3}\right), \quad (6)$$

$$u_{c2} = \frac{U_d}{2} + v \cdot \frac{U_d}{2} \cdot \sin\left(\vartheta - \frac{4\pi}{3}\right). \quad (7)$$

Consider the dependence of the voltage on the load  $u_L$  on the voltage of the shoulders  $u_{a1}$  and  $u_{a2}$ .

For the two closed circuits shown in Fig. 1, a by the dotted line, the following relations are true:

$$i_{LOAD} = i_{a1} - i_{a2}. \quad (8)$$

For the first circuit:

$$\frac{U_d}{2} - u_{a1} - L_a \frac{di_{a1}}{dt} - u_L = 0, \quad (9)$$

or

$$u_L = -u_{a1} - L_a \frac{di_{a1}}{dt} + \frac{U_d}{2}. \quad (10)$$

For the second circuit:

$$\frac{U_d}{2} - u_{a2} - L_a \frac{di_{a2}}{dt} + u_L = 0, \quad (11)$$

or

$$u_L = u_{a2} + L_a \frac{di_{a2}}{dt} - \frac{U_d}{2}. \quad (12)$$

Summing up the left and right sides of equations (10) and (12), we get

$$2u_L = u_{a2} - u_{a1} - L_a \frac{d(i_{a1} - i_{a2})}{dt}. \quad (13)$$

Taking into account (8), we convert (13):

$$u_L = \frac{u_{a2} - u_{a1}}{2} + \frac{L_a}{2} \cdot \frac{di_{LOAD}}{dt}, \quad (14)$$

or

$$u_L = \frac{u_{a2} - u_{a1}}{2} + \frac{\omega L_a}{2} \cdot \frac{di_{LOAD}}{d\vartheta}, \quad (15)$$

In relations (14), (15) there is an inequality

$$I_{LOAD} \cdot \omega \cdot L_a \ll U_{L\max}, \quad (16)$$

which, under certain conditions, allows us to simplify the relation (15)

$$u_L = \frac{u_{a2} - u_{a1}}{2}. \quad (17)$$

In the circuit of Fig. 1, a

$$U_{L\max} = v \frac{U_d}{2}. \quad (18)$$

Assuming that  $u_L$  is determined by (17), taking into account (1) and (2), we obtain:

$$u_L = \frac{\frac{U_d}{2} + v \frac{U_d}{2} \sin \vartheta - \frac{U_d}{2} + v \frac{U_d}{2} \sin \vartheta}{2} = v \frac{U_d}{2} \sin \vartheta. \quad (19)$$

Fig. 3 shows the relative position of the voltage curves of the shoulders and the load of phase  $a$ . The voltages of phases  $b$  and  $c$  are repeated in the form of the voltage of phase  $a$  and are behind it, respectively, at angles of  $2\pi/3$  and  $4\pi/3$ .

In single-phase MMC, shoulder currents have two components – a constant current  $I_d$  and an alternating sinusoidal current with an amplitude equal to half the

amplitude of the load current  $I_{L \max}$ . The dependencies for shoulder currents are:

$$i_{a1} = I_d + \frac{1}{2} I_{L \max} \cdot \sin(\vartheta - \varphi), \quad (20)$$

$$i_{a2} = I_d - \frac{1}{2} I_{L \max} \cdot \sin(\vartheta - \varphi), \quad (21)$$

where  $\varphi$  is the phase angle between voltage and load current.

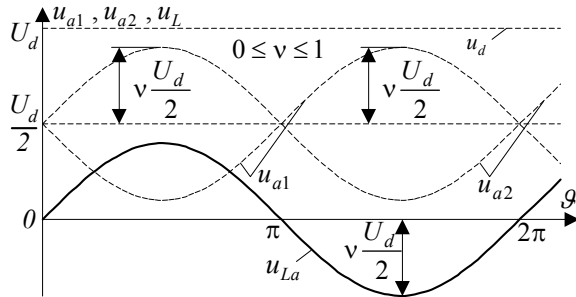


Fig. 3. Graphs of current and voltages of phase  $a$

In the three-phase *MMC*, the DC component of the shoulder current will be one third of the current  $I_d$ .

Note that the value of the current  $I_d$  at  $U_d = \text{const}$  uniquely determines the rate of energy transfer from the source to the load. At the same time, the average value of the total energy in the module capacitors for the period of repetition remains unchanged.

Fig. 4 shows the graphs of voltages and currents of the shoulders and load in the repetition period. From Fig. 4 it follows that the amplitude of the load current must be less than the current  $I_d$ :

$$I_{L \max} < I_d, \quad (22)$$

and the amplitude of the voltage on the load  $U_{L \max}$  must not exceed  $U_d/2$ :

$$U_{L \max} < \frac{U_d}{2}. \quad (23)$$

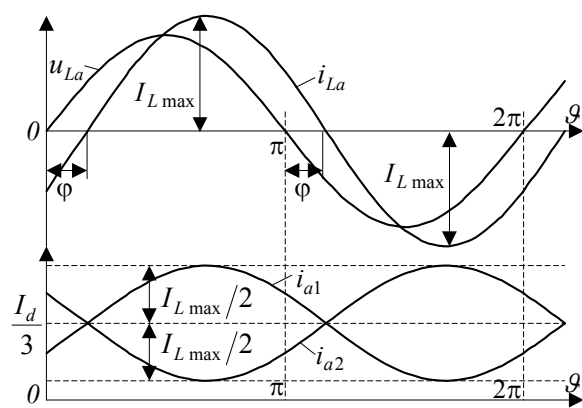


Fig. 4. Graphs of voltages and currents of shoulders and load in the repetition period

At further analysis it is convenient to go to the relative values of voltages and currents.

The basic values of voltages, currents and active power of a three-phase converter:

$$U_{base} = U_d/2, \quad (24)$$

$$I_{base} = \frac{2}{3} I_d, \quad (25)$$

$$P_{base} = U_d \cdot I_d. \quad (26)$$

From relations (3), (24) we find the relative value of the amplitude of the sinusoid voltage on the load:

$$U_{L \max}^* = \frac{U_{L \max}}{U_{base}} = \frac{2U_{L \max}}{U_d} = \nu, \quad (27)$$

and taking into account (25) – the relative value of the amplitude of the current phase of the load:

$$I_{L \max}^* = \frac{3}{2} \frac{I_{L \max}}{I_d} = m. \quad (28)$$

Assuming that there are no losses in the *MMC*, we can write a relation for the average active power at the input and output of the three-phase *MMC*:

$$U_d \cdot I_d = \frac{3}{2} I_{L \max} U_{L \max} \cos \varphi. \quad (29)$$

Substituting in (29)  $U_{L \max}$  from (27) and  $I_{L \max}$  from (28), we obtain:

$$2 = \nu \cdot m \cdot \cos \varphi. \quad (30)$$

Relation (30) connects the relative values of voltage  $\nu$  and the amplitude of the load current  $m$ .

In [3] it is recommended to set the range of change of  $\nu$  within

$$0 \leq |\nu| \leq 1, \quad (31)$$

at using the *HB*-modules and within

$$0 \leq \nu \leq \sqrt{2}, \quad (32)$$

at using the *FB*-modules.

This recommendation can be explained by the assumption of flattening of the output voltage curve in the amplitude region. The sign of the modulus of  $\nu$  in relations (31), (32) does not make sense, since, in accordance with (27), the quantity is always positive.

The recommended value of the parameter  $m$  [3]:

$$|m| \geq 2, \quad (33)$$

for both types of modules.

Possible theoretical values of the parameter  $m$ , calculated as a function of the parameters  $\nu$  and  $\cos \varphi_2$  and by expression (30), are given in Table 2.

**Mathematical modelling.** In order to verify the results obtained above, in the *MatLab/Simulink* software environment a mathematical model of a three-phase *MMC*, corresponding in its structure to Fig. 1,b, was created. The view of the model is shown in Fig. 5.

The model consists of a power source  $U_d$ , a capacitive divider  $C_{d1}-C_{d2}$ , to the midpoint of which a common output of a three-phase active-inductive load  $L_A, L_B, L_C$ , connected to a star, is connected. The shoulder voltages are set by adjustable AC voltage sources  $U_{a1}-U_{a2}, U_{b1}-U_{b2}, U_{c1}-U_{c2}$  for each of the three phases. The shoulder current shapes are set by adjustable sources  $I_{a1}-I_{a2}, I_{b1}-I_{b2}, I_{c1}-I_{c2}$  with elements connected in parallel with them that simulate the active and inductive resistances of the shoulders of *MMC*. The *Inverter* block generates the control task for the elements of the circuit. Numerous oscilloscopes and digital displays allow to control all the parameters of the model operation.

Parameter  $m$  values as a function of parameters  $\nu$ ,  $\cos\phi_2$

$\nu \backslash \cos\phi_2$	1.0	0.9	0.8	0.7	0.6	0.5	0.4	0.3	0.2	0.1
1.0	2.00	2.22	2.50	2.86	3.33	4.00	5.00	6.67	10.00	20.00
0.9	2.22	2.47	2.78	3.17	3.70	4.44	5.56	7.41	11.11	22.22
0.8	2.50	2.78	3.13	3.57	4.17	5.00	6.25	7.14	12.50	25.00
0.7	2.86	3.17	3.57	4.08	4.76	5.71	7.14	9.52	14.29	28.57
0.6	3.33	3.70	4.17	4.76	5.56	6.67	8.33	11.11	16.67	33.33
0.5	4.00	4.44	5.00	5.71	6.67	8.00	10.00	13.33	20.00	40.00
0.4	5.00	5.56	6.25	7.14	8.33	10.00	12.50	16.67	25.00	50.00
0.3	6.67	7.41	7.14	9.52	11.11	13.33	16.67	22.22	33.33	66.67
0.2	10.00	11.11	12.50	14.29	16.67	20.00	25.00	33.33	50.00	100.0
0.1	20.00	22.22	25.00	28.57	33.33	40.00	50.00	66.67	100.0	200.0

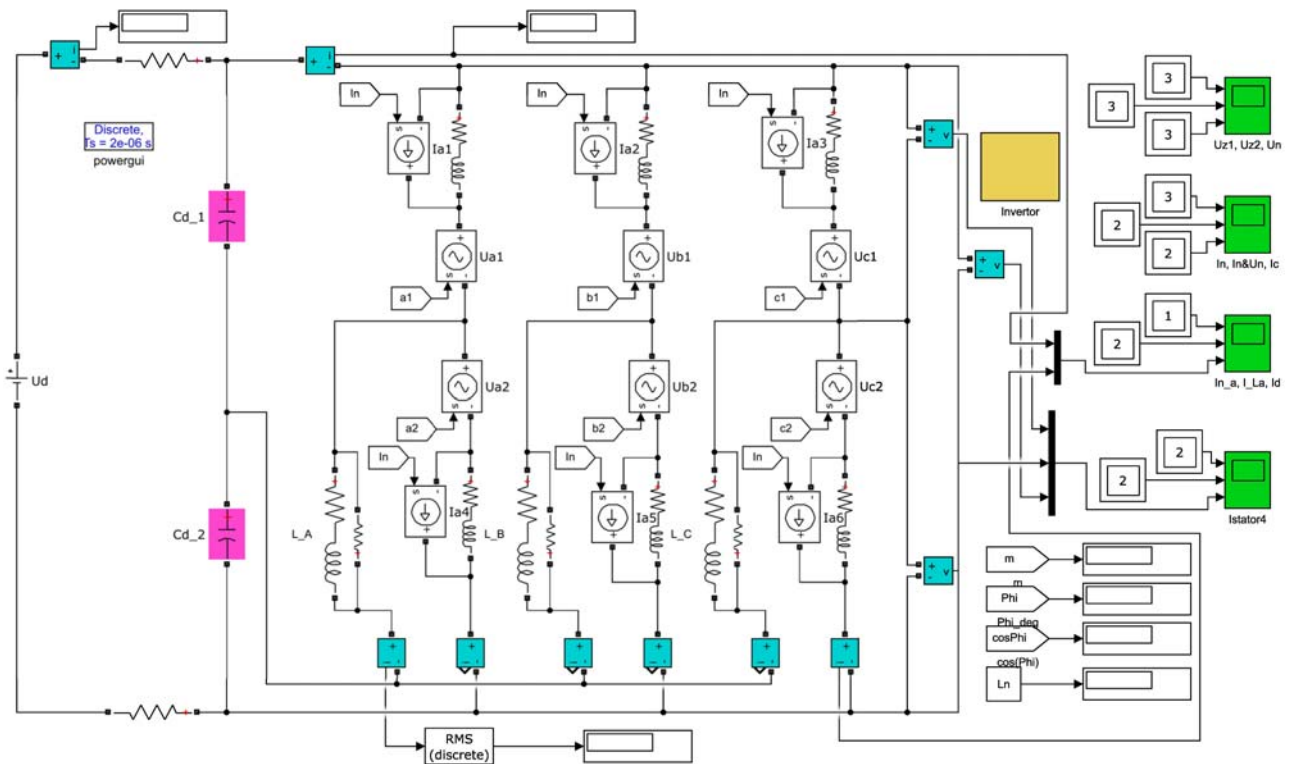


Fig. 5. MatLab model of the three-phase MMC

The current and voltage sources are controlled in the model in exact accordance with the MMC algorithm described above. This concept of building a model allows to check the validity of previously made assumptions about the relationship of the main parameters in the operation of the circuit without using models of specific power modules and building a complex system of their control and autoregulation.

During receipt of machine diagrams and dependencies, the following values were taken in the model: the average value of the supply voltage and input current, respectively,  $U_d = 1000\text{ V}$ ,  $I_d = 1000\text{ A}$ ; active and inductive resistance of the shoulder  $1\text{ m}\Omega$  and  $10\text{ }\mu\text{H}$ ; active load resistance  $0.632\text{ }\Omega$ , capacitance of the divider capacitor  $5\text{ mF}$ .

Fig. 6 shows machine diagrams of the voltage of the power source  $U_d$  and the voltage of the shoulders of the phase  $c$  for the operation mode  $\nu=1$ , which fully

corresponds to the theoretical graphs shown in Fig. 2.

Fig. 7 shows machine diagrams of the load voltage of phase  $c$  and the voltages forming it for the operation mode  $\nu = 0.8$ , which fully corresponds to the theoretical graphs shown in Fig. 3.

Figure 8 shows machine diagrams of the current of load and phase  $c$  shoulders for the operation mode  $\nu = 0.8$ . Comparison of Fig. 8 and Fig. 4 makes it possible to verify the validity of the previously accepted theoretical premises.

Also, the model of Fig. 5 allowed to check the MMC operation with various combinations of parameters  $m$ ,  $\nu$  and  $\cos\phi_2$ , confirming the validity of the values given in Table 2 with an accuracy of two decimal places.

**Characteristics of power modules.** The use of a concrete type of power transistor module does not affect the overall concept of MMC operation, however, it affects the features of building the control system and

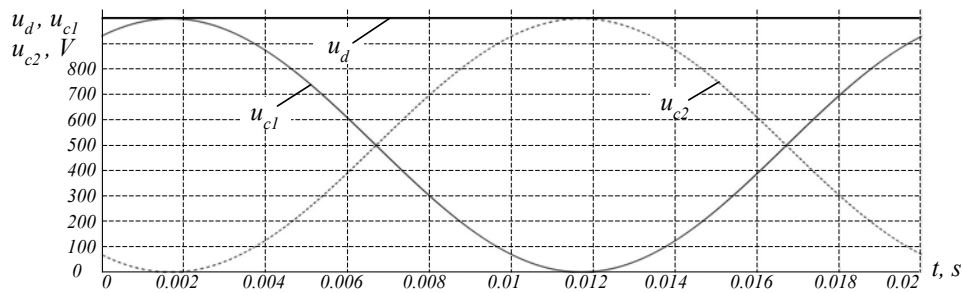


Fig. 6. Voltage of the phase *c* shoulders

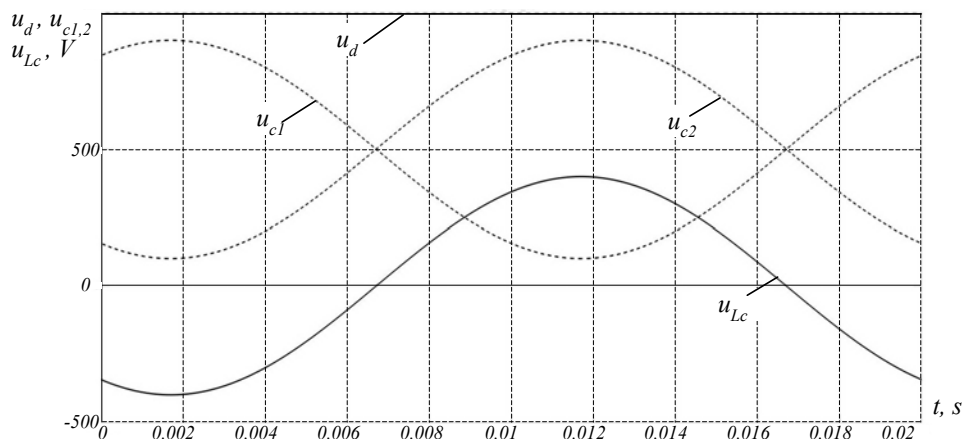


Fig. 7. Voltage of the phase *c* load

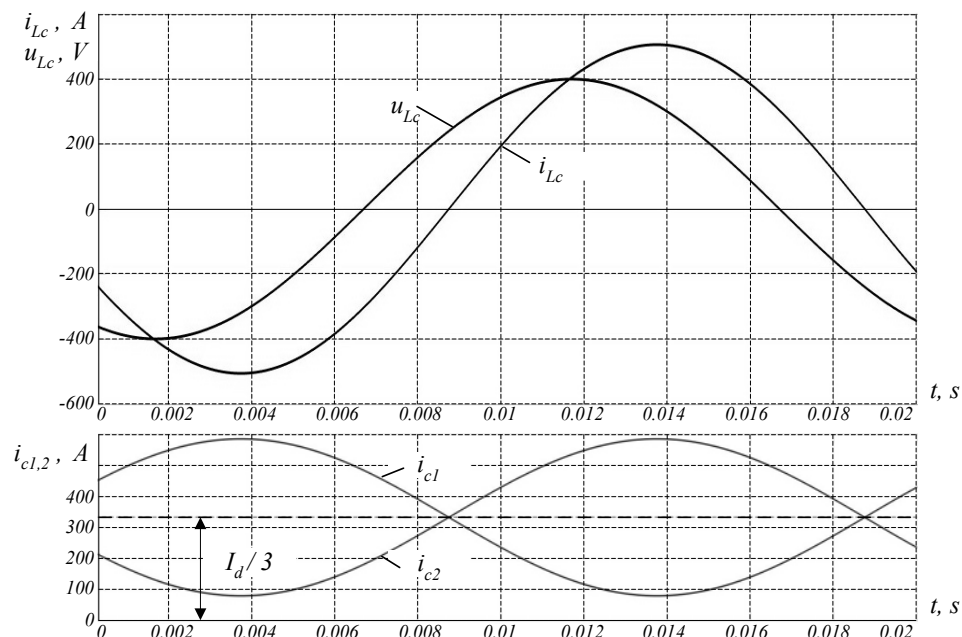


Fig. 8. Current of the phase *c* load and shoulders

autoregulation and also determines the possible emergency modes in the operation of the circuit. Therefore, we consider their operation in more detail.

a) *Half-bridge HB module.* The diagram of the half-bridge *HB* module is shown in Fig.9,a. The current through the module from the power supply can be either positive (the direction of the positive current is shown in Fig. 9,a) or negative. The voltage on the capacitor *C* is always positive, so when the module is operating, the transistors *T1* and *T2* cannot be opened at the same time.

With this in mind, there are three possible combinations of open state transistors for each direction of current *i*:

- both transistors are closed;
- transistor *T1* is on, transistor *T2* is locked;
- transistor *T2* is on, transistor *T1* is locked.

Consider the path of current flow, the voltage on the capacitor and the value of the voltage at the input of the module corresponding to the above combinations for positive and negative currents, summarizing the result in Table 3, 4.

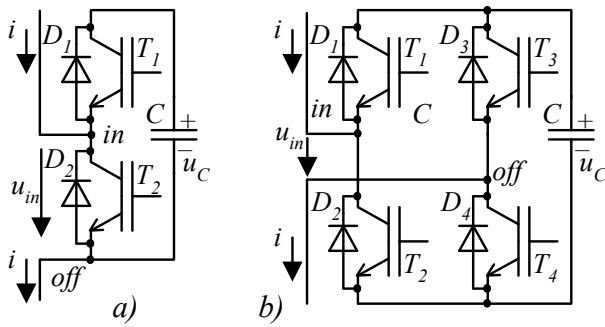


Fig. 9. Circuits of MMC power modules

Table 3  
Voltage at the input and at the capacitor of the HB module at positive current  $i > 0$

Combination No.	Transistors on	Current path	Capacitor voltage	Voltage at the module input
1.1	–	$in, D1, C, off$	charge	$u_{in}=u_C$
1.2	$T1$	$in, D1, C, off$	charge	$u_{in}=u_C$
1.3	$T2$	$in, T1, off$	does not change	$u_{in}=0$

Table 4  
Voltage at the input and at the capacitor of the HB module at negative current  $i < 0$

Combination No.	Transistors on	Current path	Capacitor voltage	Voltage at the module input
2.1	–	$off, D2, in$	does not change	$u_{in}=u_C$
2.2	$T1$	$off, C, T1, in$	discharge	$u_{in}=u_C$
2.3	$T2$	$off, D2, in$	does not change	$u_{in}=0$

From the analysis of Table 3, 4 it follows that the capacitor can be charged only with positive current of the module, and it can be discharged only with negative current of the module. Moreover, there are two combinations that ensure the charge of the capacitor and only one combination corresponding to the discharge.

*b) Full-bridge FB module.*

In the circuit of the bridge module shown in Fig. 9,b, pairs of transistors  $T1, T2$  and  $T3, T4$  cannot be simultaneously on. Therefore, there are nine possible combinations of on transistors for each of the two directions of current  $i$ .

- all transistors are locked;
- a pair of transistors  $T1, T2$  is on;
- a pair of transistors  $T2, T3$  is on;
- transistors  $T1, T3$  are on;
- transistors  $T2, T4$  are on;
- transistor  $T1$  is on, the rest are closed;
- transistor  $T2$  is on, the rest are closed;
- transistor  $T3$  is on, the rest are closed;
- transistor  $T4$  is on, the rest are closed.

Consider the operation of the circuit at a positive current ( $i > 0$ ). The result of the analysis is summarized in Table 5.

In accordance with Table 5, in the case of  $i > 0$ , only one combination of switching on transistors ensures the discharge of a capacitor at  $u_{in} = -u_C$ . Four combinations provide the charge of the capacitor, another four – the constant voltage on the capacitor.

Table 5  
Voltage at the input and at the capacitor of the FB module at positive current  $i > 0$

Combination No.	Transistors on	Current path	Capacitor voltage	Voltage at the module input
3.1	–	$in, D1, C, D4, off$	charge	$u_{in}=u_C$
3.2	$T1, T4$	$in, D1, C, D4, off$	charge	$u_{in}=u_C$
3.3	$T2, T3$	$in, T2, C, T3, off$	discharge	$u_{in} = -u_C$
3.4	$T1, T3$	$in, D1, T3, off$	does not change	$u_{in}=0$
3.5	$T2, T4$	$in, T2, D4, off$	does not change	$u_{in}=0$
3.6	$T1$	$in, D1, C, D4, off$	charge	$u_{in}=u_C$
3.7	$T2$	$in, T2, D4, off$	does not change	$u_{in}=0$
3.8	$T3$	$in, D1, T3, off$	does not change	$u_{in}=0$
3.9	$T4$	$in, D1, C, D4, off$	charge	$u_{in}=u_C$

Consider the case when  $i < 0$ . From Table 6 it follows that at  $i < 0$ , only one combination ensures the discharge of the capacitor at  $u_{in} = +u_C$ , four combinations ensure the charge of the capacitor at  $u_{in} = -u_C$ , four more combinations ensure that the voltage on the capacitor remains constant at  $u_{in} = 0$ . The analysis data are given in Table 7, 8.

Table 6  
Voltage at the input and at the capacitor of the FB module at negative current  $i < 0$

Combination No.	Transistors on	Current path	Capacitor voltage	Voltage at the module input
4.1	–	$off, D3, C, D2, in$	charge	$u_{in} = -u_C$
4.2	$T1, T4$	$off, T4, C, T1, in$	discharge	$u_{in}=u_C$
4.3	$T2, T3$	$off, D3, C, T2, in$	charge	$u_{in} = -u_C$
4.4	$T1, T3$	$off, D3, T1, in$	does not change	$u_{in}=0$
4.5	$T2, T4$	$off, T4, D2, in$	does not change	$u_{in}=0$
4.6	$T1$	$off, D3, T1, in$	does not change	$u_{in}=0$
4.7	$T2$	$off, D3, C, D2, in$	charge	$u_{in} = -u_C$
4.8	$T3$	$off, D3, C, D2, in$	charge	$u_{in} = -u_C$
4.9	$T4$	$off, T4, D2, in$	does not change	$u_{in}=0$

The data of Table 3-8 can be used in the synthesis of the control system and for the analysis of possible emergency conditions in the *MMC* modules.

Since the current  $i$  is generated by the current source, the open circuit inside the module is most dangerous. In the *HB* modules (Fig. 9,a), when the  $T2$  transistor is closed, an open circuit in the current  $i$  flow circuit will cause an arc, overvoltage on the  $T2$  transistor and the  $D2$  diode with subsequent breakdown of one of them.

Table 7  
Numbers of options for the operation mode of the *FB* module at  $i > 0$

Voltage sign at the output $u_m$		+	-	0
Voltage on the capacitor	charge (increased)	3.1, 3.2, 3.6, 3.9	no	no
	discharge (decreases)	no	3.3	no
	does not change	no	no	3.4, 3.5, 3.7, 3.8

Table 8  
Numbers of options for the operation mode of the *FB* module at  $i < 0$

Voltage sign at the output $u_m$		+	-	0
Voltage on the capacitor	charge (increased)	no	4.1, 4.3, 4.7, 4.8	No
	discharge (decreases)	4.2	no	no
	does not change	no	no	4.4, 4.5, 4.6, 4.9

When transistors  $T1$ ,  $T2$  are simultaneously on, capacitor  $C$  is discharged to them. The discharge current can lead to burnout of the conductors (tracks) inside the transistors, the occurrence of an arc and the emission of plasma.

### Conclusions.

1. The concept of construction of a multi-level modular converter (*MMC*) for DC transmission lines in power engineering and powerful frequency-controlled electric drive is considered.

2. Mathematical modeling in *MatLab/Simulink* software environment confirmed the validity of the considered *MMC* operation algorithm and the correctness

of mathematical relationships describing the processes in the steady state operation.

3. The characteristics of the full set of combinations of states of transistors of half-bridge *HB* (six states) and full-bridge *FB* (eighteen states) power modules are given, which should be considered when synthesizing a control system and analyzing emergency modes.

### REFERENCES

1. Marquardt R. *Stramrichterhaltungen mit verteilten energiespeichern*. Patent German, DE20 122923V1, 2001. (Ger).
2. Lesnicar A., Marquardt R. An innovative modular multilevel converter topology suitable for a wide power range. *2003 IEEE Bologna Power Tech Conference Proceedings*, 2003, vol.3, p. 6. doi: 10.1109/PTC.2003.1304403.
3. Hagiwara M., Akagi H. PWM control and experiment of modular multilevel converters. *2008 IEEE Power Electronics Specialists Conference*, 2008, pp. 154-161. doi: 10.1109/PESC.2008.4591917.
4. Alstom. *HVDC MaxSine*. Available at: <http://www.alstom.com/grid/products-and-services/engineeredenergy-solutions/hvdc-transmission-systems/HVDC-MaxSine> (accessed 22 August 2013).
5. ABB. *HVDC Light Gen. 4*. Available at: [www.new.abb.com/systems/hvdc](http://www.new.abb.com/systems/hvdc) (accessed 12 August 2013).
6. EPRI. *HVDC Flexible*. Available at: [www.epri.sgcc.com.cn/prgc/english/Product\\_Solution/HVDC\\_Flexible](http://www.epri.sgcc.com.cn/prgc/english/Product_Solution/HVDC_Flexible) (accessed 20 July 2013).
7. SIEMENS. *SINAMICSSM120*. Available at: [http://www.industry.siemens.com/drives/global/en/converter/my\\_drives/sinamics-sm120-cm](http://www.industry.siemens.com/drives/global/en/converter/my_drives/sinamics-sm120-cm) (accessed 20 June 2013).
8. Perez M.A., Bernet S., Rodriguez J., Kouro S., Lizana R. Circuit Topologies, Modeling, Control Schemes, and Applications of Modular Multilevel Converters. *IEEE Transactions on Power Electronics*, 2015, vol.30, no.1, pp. 4-17. doi: 10.1109/tpel.2014.2310127.

Received 03.09.2018

G.G. Zhemerov<sup>1</sup>, Doctor of Technical Science, Professor,  
D.S. Krylov<sup>1</sup>, Candidate of Technical Science, Associate Professor,

<sup>1</sup>National Technical University «Kharkiv Polytechnic Institute»,  
2, Kyrpychova Str., Kharkiv, 61002, Ukraine,  
phone +380 57 7076312,  
e-mail: zhemerov@gmail.com

### How to cite this article:

Zhemerov G.G., Krylov D.S. Concept of construction of power circuits of a multilevel modular converter and its transistor modules. *Electrical engineering & electromechanics*, 2018, no.6, pp. 26-32. doi: 10.20998/2074-272X.2018.6.03.

B.I. Kuznetsov, T.B. Nikitina, V.V. Kolomiets, I.V. Bovdvi

## IMPROVING OF ELECTROMECHANICAL SERVO SYSTEMS ACCURACY

*Aim. Improving of accuracy parameters and reducing of sensitivity to changes of plant parameters of nonlinear robust electromechanical servo systems of guidance and stabilization of lightly armored vehicle weapons based on multiobjective synthesis. Methodology. The method of multicriterion synthesis of nonlinear robust controllers for controlling by nonlinear multimass electromechanical servo systems with parametric uncertainty based on the choice of the target vector of robust control by solving the corresponding multicriterion nonlinear programming problem in which the calculation of the vectors of the objective function and constraints is algorithmic and associated with synthesis of nonlinear robust controllers and modeling of the synthesized system for various modes of operation of the system, with different input signals and for various values of the plant parameters. Synthesis of nonlinear robust controllers and non-linear robust observers reduces to solving the system of Hamilton-Jacobi-Isaacs equations. Results. The results of the synthesis of a nonlinear robust electromechanical servo system for the guidance and stabilization of lightly armored vehicle weapons are presented. Comparison of the dynamic characteristics of the synthesized servo electromechanical system showed that the use of synthesized nonlinear robust controllers allowed to improve the accuracy parameters and reduce the sensitivity of the system to changes of plant parameters in comparison with the existing system. Originality. For the first time carried out the multiobjective synthesis of nonlinear robust electromechanical servo systems of guidance and stabilization of lightly armored vehicle weapons. Practical value. Practical recommendations are given on reasonable choice of the gain matrix for the nonlinear feedbacks of the regulator and the nonlinear observer of the servo electromechanical system, which allows improving the dynamic characteristics and reducing the sensitivity of the system to plant parameters changing in comparison with the existing system. References 12, figures 1.*

*Key words: electromechanical servo systems of guidance and stabilization of lightly armored vehicle weapon, nonlinear robust system, multiobjective synthesis, dynamic characteristics.*

*Цель. Повышение параметров точности и уменьшение чувствительности системы к изменениям параметров объекта управления нелинейной робастной электромеханической следящей системы наведения и стабилизации вооружения легкобронированной машины на основе многокритериального синтеза. Методология. Метод многокритериального синтеза нелинейных робастных регуляторов для управления нелинейными многомассовыми электромеханическими следящими системами с параметрической неопределенностью основан на выборе вектора цели робастного управления путем решения соответствующей задачи многокритериального нелинейного программирования, в которой вычисление векторов целевой функции и ограничений носит алгоритмический характер и связано с синтезом нелинейных робастных регуляторов и моделированием синтезированной системы для различных режимов работы системы, при различных входных сигналах и для различных значений параметров объекта управления. Синтез нелинейных робастных регуляторов и нелинейных робастных наблюдателей сводится к решению системы уравнений Гамильтона – Якоби – Айзекса. Результаты. Приводятся результаты синтеза нелинейной робастной электромеханической следящей системы наведения и стабилизации вооружения легкобронированной машины. Сравнение динамических характеристик синтезированной следящей электромеханической системы показало, что применение синтезированных нелинейных робастных регуляторов позволяет повысить параметры точности и снизить чувствительность системы к изменению параметров объекта управления по сравнению с существующей системой. Оригинальность. Впервые проведен многокритериальный синтез нелинейной робастной электромеханической следящей системы наведения и стабилизации вооружения легкобронированной машины. Практическая ценность. Приводятся практические рекомендации по обоснованному выбору матриц коэффициентов усиления нелинейных обратных связей регулятора и нелинейного наблюдателя следящей электромеханической системы, что позволяет улучшить динамические характеристики и снизить чувствительность системы к изменению параметров объекта управления по сравнению с существующей системой. Библ. 12, рис. 1.*

*Ключевые слова: электромеханическая следящая система наведения и стабилизации вооружения легкобронированной машины, нелинейная робастная система, многокритериальный синтез, динамические характеристики.*

**Introduction.** Lightly armored wheeled and tracked vehicles produced in Ukraine have high tactical and technical characteristics and successfully compete with foreign weapons [1]. The basis of combat in modern conditions is firing off at a high speed and maneuvering movement of the machine, so all modern lightly armored vehicles in the world equipped with weapons stabilizers, allowing to guide the target fire on the move. The probability of fire engagement of the target at maximum speeds, high maneuverability and effective evasion of the machine against the enemy's fire damage is largely determined by the accuracy of maintaining the specified direction of the combat module on the target with intense perturbations on the machine's side. Increasing the

accuracy has an important economic component. For example, the practice of using the Protector combat module in Kongsberg's Crows II version based on actual operation data in 2007 made it possible to reduce the consumption of 12.7-mm cartridges by 70 % due to a sharp increase in the accuracy of the hit from the first shot. Therefore, the issues of further improving the accuracy of weapons stabilization are an urgent problem, both in the development of new weapons systems and in the modernization of existing systems in service.

To systems of guidance and stabilization of lightly armored vehicles weapons, sufficiently stringent requirements are set for the performance indicators in

© B.I. Kuznetsov, T.B. Nikitina, V.V. Kolomiets, I.V. Bovdvi

various modes. We bring a part of such requirements for the light-armored vehicle presented to the guidance and stabilization system [1]: time of working out of a given angle of error; acceleration time to rated speed and deceleration time to full stop; an error in working out a harmonic signal of a specified amplitude and frequency; stabilization error when moving along a normalized path with a random profile change with a given speed; maximum speed of guidance; minimum speed of guidance; failure of guidance at minimum speed. Naturally, this should take into account the voltage and current limitations of the anchor chain of the drive motor, as well as the speed of rotation of the drive motor.

**The goal of this work** is to improve of the accuracy parameters and reduce of sensitivity to changes of plant parameters for electromechanical servo system guidance and stabilization of lightly armored vehicle weapons based on multiobjective synthesis of nonlinear robust control.

**Problem statement.** Stabilizers of armored vehicles weapons in a vertical and horizontal plane are built according to the same type of scheme [1-4]. With the help of an optical sight, the sight mirror is mounted in the direction of the target, respectively in the horizontal and vertical planes. The specified direction is compared with the actual direction of the armament block and the voltages proportional to the discrepancy signals between the specified directions of the shot lines and the axis of the bore channel are fed to the inputs of the turret drives in the horizontal guidance channel and the arming unit in the vertical guidance channel. In addition, the absolute speed of rotation of the turret in the horizontal plane and the combat module in the vertical plane are measured with the aid of gyroscopic angular velocity sensors mounted on the arms block and used to develop control.

The turret in the horizontal plane and the combat module in the vertical plane are driven by DC motors driven from permanent magnets, whose armature circuits are powered by pulse-width converters. The rotational speed of the motors that drive the turret and the combat module is measured using tachogenerators. The currents of the motor armature anchors are measured by shunts included in the motor armature circuits, converted and also used for control purposes

The presence in the electromechanical servo systems of elastic elements between the drive motor and the operating element, the uncertainty of the parameters of the control objects, the change in mass-inertial characteristics, complex cinematic schemes, unknown external and internal disturbances do not allow to obtain potentially high dynamic characteristics inherent in modern electromechanical systems with standard regulators [2, 3]. The use of state control by complex electromechanical systems containing nonlinear and elastic elements allows obtaining acceptable quality indicators. To reduce the sensitivity of synthesized systems to changing the parameters and structure of the control object and external influences, robust control is used as the state control. Consider the design of such system.

Let us consider the nonlinear model of a discrete plant of robust control of a multimass system with a state

vector  $x_k$  in the form of a difference state equation in the standard form

$$x_{k+1} = f(x_k, u_k, \omega_k, \eta_k), \quad (1)$$

where  $u_k$  is the control vector,  $\omega_k$  and  $\eta_k$  are the vectors of the external signal and parametric perturbations [5, 6],  $f$  is a nonlinear function.

The mathematical model (1) takes into account the nonlinear frictional dependencies on the shafts of the drive motor, the rotating parts of the reducer and the operating element, the play between the teeth of the driving and driven gears, the control constraints, current, torque and engine speed, as well as the moment of inertia of the plant.

**Method of synthesis.** The task of synthesis is the determination of such a regulator [7, 8] which, based on the measured output of the initial system

$$y_k = Y(x_k, \omega_k, u_k) \quad (2)$$

forming control  $u_k$  using a dynamic system described by the difference state equation and output

$$\xi_{k+1} = f(\xi_k, u_k, \omega_k, \eta_k) + \sum_{i=1}^3 G_i (y_k - \dots - Y(\xi_k, \omega_k, u_k)); \quad (3)$$

$$u_k = \sum_{i=1}^3 U_i(\xi_k, y_k), \quad (4)$$

where  $i$  is the order of the forms  $G_i$  and  $U_i$ .

The synthesis of the regulator (4) is reduced to determining the matrix of the forms of the regulator gain  $U_i$  by minimizing the norm of the target vector

$$z(x_k, u_k, \eta_k) = \sum_{i=2}^4 Z_i(x_k, u_k, \eta_k) \quad (5)$$

on control vector of  $u_k$  and maximization of the same norm on a of plant uncertain vector  $\eta_k$  for the worst case disturbance.

The synthesis of the observer (3) is reduced to determining the observer gain coefficients  $G_i$  by minimization of the error vector of the recovery of the state vector  $x_k$  of the initial system and maximization of the same norm of the error vector along the plant uncertainty vector  $\eta_k$  and the vector of external signal influences  $\omega_k$ , which also corresponds to the worst case disturbance.

Matrices of the regulator  $U_i$  and observer  $G_i$  gain coefficients are found from approximate solutions of the Hamilton-Jacobi-Isaacs equations [7, 8], in which the matrices of linear forms being found from the four Riccati equations solutions. This approach corresponds to the standard 4-Riccati approach to the synthesis of linear robust or anisotropic regulators [9].

To determine the regulator (4) for plant (1) with target vector (5) consider Hamiltonian function

$$H(x_k, u_k, \eta_k) = z(x_k, u_k, \eta_k) + V_x^T(x_k, u_k, \eta_k) f(x_k, u_k, \eta_k), \quad (6)$$

where  $V_x$  are partial derivatives with respect to the state vector  $x_k$  of the infinite-horizon performance functional (Lyapunov function)

$$V(x_k, u_k, \eta_k) = \sum_{i=k}^{\infty} z(x_i, u_i, \eta_i). \quad (7)$$

To determine the robust regulator (4) it is necessary to find the minimum norm of the target vector (5) along the control vector  $u_k$  and the maximum of this norm in the external perturbations vector  $\eta_k$ , which reduces to solving the minimax extremal problem of Hamiltonian function [7]

$$H^*(x_k) = \min_{u_k} \max_{d_k} \{H(x_k, u_k, \eta_k)\}. \quad (8)$$

The necessary conditions for the extremum of the Hamiltonian function (8) both in the control vector  $u_k$  and in the external perturbation vector  $\eta_k$  are these equations

$$H_u(x_k, u^*(x_k), \eta^*(x_k)) = 0; \quad (9)$$

$$H_\eta(x_k, u^*(x_k), \eta^*(x_k)) = 0, \quad (10)$$

which are Hamilton-Jacobi-Isaacs equations. Here  $H_u$  and  $H_\eta$  are the partial derivatives of the Hamiltonian function with respect to the control vector  $u_k$  and with respect to the external perturbations vector  $\eta_k$ .

Note that these equations (9) – (10) are also necessary conditions for optimizing a dynamic game, in which the first player – the regulator which minimizes the target vector, and the second player – external disturbances which maximizes the same target vector.

The difficulty of obtaining a nonlinear discrete control law is due to the fact that the difference Hamilton-Jacobi-Isaacs equations (9) – (10) is a nonlinear algebraic equation, while the Hamilton-Jacobi-Isaacs equations for a continuous system is a partial differential equation. Therefore, the difference Hamilton-Jacobi-Isaacs equations is not a quadratic equations in the control and perturbation.

In this paper we use an approximate solution of the Hamilton-Jacobi-Isaacs equation (9) – (10) assuming the analytical dependences of the nonlinearities of the original system (1), (2), (5) in the form of the corresponding series [8]. Then the linear approximation of the Hamilton-Jacobi-Isaac equation (9), (10) are the algebraic Riccati equations

$$P = A^T P A + R - \begin{bmatrix} A^T P B & A^T P E \end{bmatrix} \dots \begin{bmatrix} I + B^T P B & B^T P E \\ E^T P A & E^T P E - \gamma^2 I \end{bmatrix}^{-1} \begin{bmatrix} B^T P A \\ E^T P A \end{bmatrix}. \quad (11)$$

Here, the matrices A and B in (11) are the corresponding matrices of the linear system obtained by linearizing the original nonlinear system (1), (2), (5).

Similarly matrices of the observer  $G_i$  gain coefficients (3) are found from approximate solutions of the Hamilton-Jacobi-Isaacs equations type (9) – (10).

With this approach the strategy that is best for one of the players is at the same time the worst for the other player. This is the so-called saddle point principle, which corresponds to the condition of equilibrium: the minimum guaranteed loss of the first player is equal to the maximum guaranteed win of the second, so that none of the players is interested in changing the optimal strategy of behavior.

According to the modern concept of guaranteed result, a mathematical model of uncertainty is constructed on the basis of the hypothesis of the «worst» behavior of perturbing factors. The essence of this hypothesis, overcoming the uncertainty in the control problem, consists in interpreting uncontrolled perturbing factors as some hypothetical deterministic perturbation, of which only the ranges of its change are known. This perturbation is introduced into the model of the dynamics of the control object with the assumption of its most unfavorable (extreme) effect on the control process. In other words, it is considered that in the a priori a given range of perturbation change, those values are realized that ensure the lowest quality of the control process.

It should be noted that the perturbation introduced into the study admits a very broad interpretation and does not appear as a physical, but as an abstract mathematical concept, symbolizing the influence of disturbing factors. Thus, not only the «external» perturbations applied to the object from the side of the environment, but also all sorts of «internal» disturbances (for example, noise and measurement errors) can be attributed to it. It is also possible to include here also uncertain factors related to the inaccuracy of the mathematical description of the object: unknown parameters of the object, unaccounted inertial and nonlinear links, errors in linearization and discretization of the object model.

**Robust control target vector choice.** A synthesized system including a nonlinear plant (1) that is closed by a robust controller (3) – (4) has certain dynamic characteristics that are determined by the control system model of the system (1), the parameters of the measuring devices (2), the target vector (5).

The most important stage in the formalization of the problem of optimal control is the choice of the quality criterion, determined both by the functional purpose of the control object and by the capabilities of the mathematical apparatus used.

The problem of a reasonable choice of the quality criterion, despite its relevance, is still unresolved. The choice of the quality criterion is a very complex, ambiguous and, often, contradictory task. It is known [7] that any asymptotically stable control system even with unsatisfactory quality of transient processes is optimal in the sense of some criterion of this type.

From the engineering point of view, it seems natural to construct optimal criteria that directly take into account the direct indicators of the quality of the management process, such as steady errors, regulation time, overshoot, magnitude of oscillations, etc., which are physically most clear and have clear limits of permissible values, based on a rich experience in the design of systems. However, in methods of designing control systems, indirect quality indicators are more widely used, which, as a rule, are easier to calculate and more convenient in analytical research.

For the correct definition of the target vector (7), we introduce the vector of the unknown parameters  $\chi = \{Z_i(x_k, u_k, \eta_k)\}$ , the components of which are the required weight matrices of the norm  $Z_i(x_k, u_k, \eta_k)$ . We introduce the vector target function

$$F(x) = [F_1(x), F_2(x) \dots F_m(x)]^T \quad (10)$$

in which the components of the vector target function  $F_i(x)$  are direct quality indicators that are presented to the system in various modes of its operation such as the time of the first matching, the time of regulation, overshooting, etc. To calculate the vectors objective function (10) and constraints on state variables and control, the initial nonlinear system (1), (2) is modeled by a closed synthesized nonlinear regulator (3), (4) in various modes of operation, with different input signals and for various values of the plant parameters [10, 11]. This multiobjective nonlinear programming problem is solved on the basis of multi-swarm stochastic multi-agent optimization algorithms [12].

**Computer simulation results.** We present the results of research of dynamic characteristics and sensitivity to the plant parameters change of a nonlinear two-mass electromechanical servo system of lightly armored vehicle weapons [1] with synthesized nonlinear robust regulators. In the existing system, PD regulators are used, which are realized with the aid of a gyroscopic angle sensor and a gyroscopic angular velocity sensor. The introduction of the integral control law leads to the emergence of undamped oscillations in the mode of working out the given angles of the combat module position, due to the presence of dry friction on the shafts of the drive motor and the working member. With the help of robust controllers it was possible to ensure a stable operation of the system taking into account all the essential nonlinearities inherent in the elements of this system when two integrating links are introduced into the control loop.

As an example, Fig.1 shows the transient processes of state variables: *a)* the combat module angle; *b)* the combat module speed; *c)* the elasticity moment and *d)* motor speed in the guidance mode with a low speed 0.5 grad/s in the synthesized system. As can be seen from Fig.1,*b* and Fig.1,*d*, the drive motor and the combat module are moving in a «stick-slip» mode. As can be seen from Fig.1,*a*, the established error in the processing of the linearly changing driving force of the gun barrel angle of the combat module of a lightly armored machine is practically zero.

Such system with second-order astatism, taking into account all the non-linearities and the moment of inertia of the working element that changes during operation, made it possible to improve the smoothness of the motion of the control object by more than 3.7 times when hovering at low speeds. We note that this indicator largely determines the potential accuracy of the operation of the electromechanical servo system in one of the most important modes of its operation.

The use of synthesized nonlinear robust controllers has also made it possible to reduce the time of transient processes in the regime of working out small angles by more than 5.3 times in comparison with the existing system. Moreover, when the moment of inertia of the working mechanism changes within the given limits, the transient processes change insignificantly and satisfy the technical requirements imposed on the system.

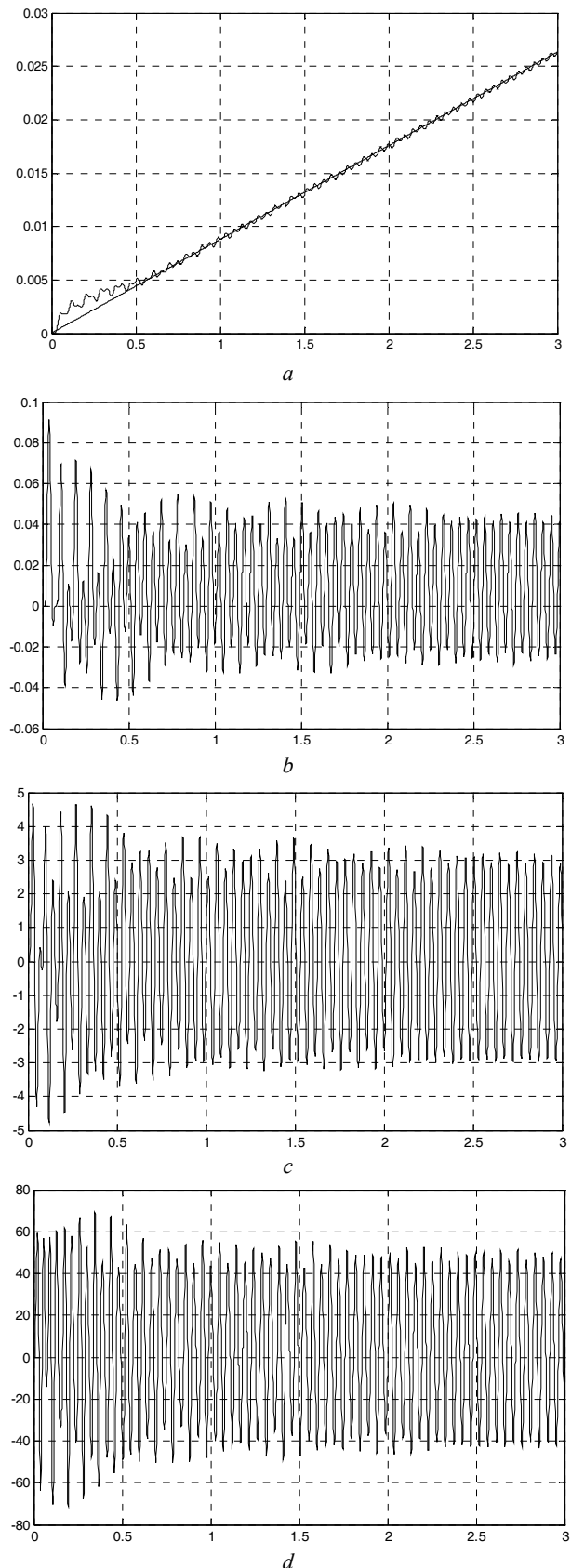


Fig. 1. Transient processes of state variables: *a)* the combat module angle and *b)* combat module speed; *c)* elasticity moment and *d)* the motor rotation speed in the guidance mode at a rate of 0.5 grad/s

The synthesized system also allowed to increase the accuracy of working out harmonic influences of a given

range of frequencies in 2.7 – 3.3 times, which increased the efficiency of the system installed on a mobile base moving along an uneven road at a given speed and given parameters of road irregularities.

**Experimental researches results.** For carrying out of experimental researches the model of a two-mass electromechanical system is developed. The layout consists of two electric machines, the shafts of which are connected by an elastic element whose parameters are chosen so that the natural frequencies of the mechanical elastic vibrations of the layout coincide with the experimentally obtained oscillations of the real system. Experimental research of model of electromechanical servo system confirmed the correctness of computer simulation results and experimental research.

#### Conclusions.

1. For the first time the multiobjective synthesis of nonlinear robust regulators for controlling by non-linear multi-mass electromechanical servo systems of lightly armored vehicles weapons with parametric uncertainty based on the choice of the target vector of robust control by solving the corresponding multiobjective nonlinear programming problem. Calculation of the vectors of the objective function and constraints of nonlinear programming problem are algorithmic character and are connected with synthesis of nonlinear robust controllers and modeling of the synthesized system for various operating modes of the system, with different input signals and for different values of the plant parameters is given.

2. Synthesis of nonlinear robust regulators and nonlinear robust observers reduces to solving the system of Hamilton-Jacobi-Isaacs equations.

3. Based on the analysis of the dynamic characteristics of the synthesized servo electromechanical system of lightly armored vehicles weapons have shown that the use of synthesized nonlinear robust controllers has allowed to improve the accuracy parameters and to reduce the sensitivity to plant parameters changes in comparison with the existing system.

4. Further increase of accuracy can be obtained by restoring, with the observer of plant parametric uncertainty vector and of external signal disturbances vector and basis on their design of feed forward control system. In addition, to further improve accuracy, it is expedient to replace the DC drive motor with a high-torque motor and realize a gearless drive with separate stabilization of the aiming and aiming lines.

#### REFERENCES

1. Bezvesilna O.M., Kvasnikov V.P., Klymenko O.I., Maliarov S.P., Ponomarenko A.I., Sibruk L.V., Tsiрук V.H., Chikovani V.V. *Naukovi, tekhnolohichni, orhanizatsiini ta vprovadzhuvalni osnovy stvorennia novoho pryladovoho kompleksu stabilizatora ozbroiennia lehkyykh bronovanykh mashyn* [Scientific, technological, organizational and implementing bases for the creation of a new instrumentation complex of lightly armored vehicles weapons stabilizer]. Kyiv, 2015. (Ukr).

2. Binroth W., Cornell G.A., Presley R.W. *Closed-loop optimization program for the M60A1 tank gun stabilization system*. Rock Island Arsenal, 1975. 251 p.

3. Aleksandrov E.E., Bogaenok I.N., Kuznetsov B.I. *Parametricheskii sintez sistem stabilizatsii tankovogo vooruzheniia* [Parametric synthesis of tank weapon stabilization systems]. Kyiv, Technika Publ., 1997. 112 p. (Rus).

4. Kuznetsov B.I., Vasilets T.E., Varfolomiyeв O.O. Synthesis of neural network Model Reference Controller for aiming and stabilizing system. *Electrical Engineering & Electromechanics*, 2015, no.5, pp. 47-54. doi: 10.20998/2074-272x.2015.5.06.

5. Buriakovskiy S.G., Maslii A.S., Panchenko V.V., Pomazan D.P., Denis I.V. The research of the operation modes of the diesel locomotive CHME3 on the imitation model. *Electrical Engineering & Electromechanics*, 2018, no.2, pp. 59-62. doi: 10.20998/2074-272x.2018.2.10.

6. Rozov V.Yu., Tkachenko O.O., Erisov A.V., Grinchenko V.S. Analytical calculation of magnetic field of three-phase cable lines with two-point bonded shields. *Technical Electrodynamics*, 2017, no.2, pp. 13-18 (Rus). doi: 10.15407/teched2017.02.013.

7. William M. McEneaney. *Max-plus methods for nonlinear control and estimation*. Birkhauser Boston, 2006. 256 p. doi: 10.1007/0-8176-4453-9.

8. Wilson J. Rugh. *Nonlinear system theory. The Volterra/Wiener Approach*. The Johns Hopkins University Press, 2002. 330 p.

9. Kuznetsov B.I., Nikitina T.B., Tatarchenko M.O., Khomenko V.V. Multicriterion anisotropic regulators synthesis by multimass electromechanical systems. *Technical electrodynamics*, 2014, no.4, pp. 105-107. (Rus).

10. Ray S., Lowther D.A. Multi-objective optimization applied to the matching of a specified torque-speed curve for an internal permanent magnet motor. *IEEE Transactions on Magnetics*, 2009, vol.45, no.3, pp. 1518-1521. doi: 10.1109/TMAG.2009.2012694.

11. Ren Z., Pham M.-T., Koh C.S. Robust global optimization of electromagnetic devices with uncertain design parameters: comparison of the worst case optimization methods and multiobjective optimization approach using gradient index. *IEEE Transactions on Magnetics*, 2013, vol.49, no.2, pp. 851-859. doi: 10.1109/TMAG.2012.2212713.

12. Shoham Y., Leyton-Brown K. *Multiagent Systems: Algorithmic, Game-Theoretic, and Logical Foundations*. Cambridge University Press, 2009. 504 p.

Received 14.07.2018

B.I. Kuznetsov<sup>1</sup>, Doctor of Technical Science, Professor,  
T.B. Nikitina<sup>2</sup>, Doctor of Technical Science, Professor,  
V.V. Kolomiets<sup>2</sup>, Candidate of Technical Science,  
I.V. Bovdui<sup>1</sup>, Candidate of Technical Science,  
<sup>1</sup> State Institution «Institute of Technical Problems  
of Magnetism of the NAS of Ukraine»,  
19, Industrialna Str., Kharkiv, 61106, Ukraine,  
phone +380 50 5766900,  
e-mail: kuznetsov.boris.i@gmail.com

<sup>2</sup> Kharkov National Automobile and Highway University,  
25, Yaroslava Mudroho Str., Kharkov, 61002, Ukraine,  
e-mail: tatjana55555@gmail.com

#### How to cite this article:

Kuznetsov B.I., Nikitina T.B., Kolomiets V.V., Bovdui I.V. Improving of electromechanical servo systems accuracy. *Electrical engineering & electromechanics*, 2018, no.6, pp. 33-37. doi: 10.20998/2074-272X.2018.6.04.

## OPTIMAL CONTROL OF THE ELECTRIC SHIPS' PROPULSION MOTORS DURING REVERSAL

*Introduction. Reliability and safety of electric ships' maneuverability depends on the maneuvering characteristics of their propulsion motors (PM). Therefore, the issues of improving the process of controlling propulsion motors at maneuvers are topical. The aim of this paper is to find the optimal laws of control. The indicators estimating electric ships' maneuvering properties are chosen as criteria of optimality. Methodology. A proportional control law is traditionally used in electrical propelling plants with frequency-controlled PM. However, it does not provide the necessary maneuvering characteristics to the electric ships, since it does not take into account the process of the vessel's movement. To search for the optimal control laws of propulsion motors at maneuvers, the electrical propulsion plant is considered in unity with all the components of the ship's propulsion complex. The dimensionless parameters of the complex are revealed from the mathematical model of the transient modes of its operation. They determine the numerical values of the optimality criteria. Control signals are formed by frequency and voltage. A method for the formation of optimal control laws is proposed. The nature of the target functions is revealed and a special optimization method is developed. A minimum of the braking distance and a minimum of energy spent on maneuvering are taken as criteria of optimality. Results. The parameters of the complexes that significantly affect the optimality criteria are revealed. For various combinations of the values of these parameters, optimization calculations have been carried out and the optimal control laws of the propulsion motors during electric ships' reversal have been found. Optimization is carried out by the criterion of the minimum of the braking distance and by the criterion of minimum energy consumption. The results are presented in an analytical form and in a graphical form. The effectiveness of the proposed control laws is illustrated. Scientific novelty. The method of searching for the optimal control laws of the propulsion motors is constructed according to the system principle. This allows us to find the control laws of the propulsion motors on the final result – on the indicators of electric ships' maneuverability. The proposed recommendations cover a wide class of vessels with electric motion. Practical value. The proposed optimal control laws for propulsion motors can be used both in the design of propulsion power plants and in their operation. The best control law can be selected and incorporated into the control system for any particular electric ship of the considered class, depending on the quality of maneuvering. In particular, the optimal control law for propulsion motors during reversal providing electric ship's minimum braking distance or minimum energy consumption for maneuvering can be chosen. References 9, tables 4, figures 3.*

*Key words:* control of propulsion motors during electric ships' maneuvers, optimization method, optimal control laws.

*Целью работы является поиск оптимальных законов управления гребными электродвигателями (ГЭД) судов с электродвижением. Критериями оптимальности выбраны показатели, характеризующие маневренные свойства электроходов. Методика. Пропорциональный закон управления ГЭД не обеспечивает нужные маневренные свойства электроходов. Оптимальные законы управления ГЭД, обеспечивающие наилучшие маневренные характеристики электроходов могут быть найдены при совместном рассмотрении гребной электроэнергетической установки, гребных винтов и корпуса судна. Результаты. Предложен новый способ формирования оптимальных законов управления. Выявлен характер целевых функций и разработан метод оптимизации. Проведены оптимизационные расчеты и найдены оптимальные законы управления гребными электродвигателями при реверсе электроходов. Оптимизация проведена по критериям минимума тормозного пути и минимума расхода энергии. Проиллюстрирована эффективность использования предлагаемых законов управления. Научная новизна. Метод поиска оптимальных законов управления построен по системному принципу. Это позволяет находить законы управления гребными электродвигателями по конечному результату – по показателям судна. Практическая значимость. Предложенные рекомендации могут использоваться как при проектировании гребных электроэнергетических установок, так и при их эксплуатации. Для конкретного электрохода, в зависимости от показателей качества маневрирования, может быть выбран (из предложенных) и заложен в систему регулирования наилучший закон управления гребными электродвигателями. Библ. 9, табл. 4, рис. 3.*

*Ключевые слова:* управление гребными электродвигателями электроходов на маневрах, метод оптимизации, оптимальные законы управления.

**Relevance of the problem.** A distinctive feature of vessels with electric propulsion is that maneuverable modes – acceleration, braking, reverse, exit to circulation – are for them the main operational modes of operation. The high maneuverability of electric ships is one of the main qualities that determined the reason for such a high interest in the use of modern electric propulsion systems on ships and warships. Not surprisingly, special attention is paid to the reliability and safety of maneuverable operations.

The results of a comparative analysis show that electrically-powered vessels have significantly better maneuverability characteristics than vessels with

traditional types of power plants. The most important maneuver for electric ships is the reverse of propulsion electric motors. In particular, for the majority of vessels with power plants with direct transfer of torque of primary engines to propellers, the reversal process is protracted and lasts 1-2 minutes. The duration of the reverse of the propulsion motors (PMs) rarely exceeds 15-20 s (for example, for the «Arktika» atomic electric ship, the reverse time from «full forward» to «full back», when the power limiter is 100 %, is about 30 s). The procedure for reversing internal combustion engines is incomparably more complicated compared to the reverse

of the PM. In addition, not every reverse can be successful. Namely, due to the late maneuvering leading to an additional run-down of the vessel, up to 40 % of ship collisions occur. Thus, even such a brief comparison shows that propulsion power plants (PPPs) provide higher reliability and safety of maneuvering operations.

One of the promising options for the construction of a PPP is an electromotive system based on induction frequency-controlled propulsion motors. In this regard, the issues of improving the control of propulsion electric motors for PPP during maneuvers are highly relevant. Moreover, the need to evaluate the maneuvering properties of electric ships and to search for the best laws for controlling the propulsion electric motors during maneuvers arises both at the initial stages of their design and during the operation of ships.

When searching for the best PM control laws, the criteria for evaluating them should, first of all, be indicators that evaluate the performance of the vessel itself, as the «older» system. This is the only way to ensure a systematic approach to the selection of optimal control laws for propulsion electric motors during maneuvers.

**The state of the issue considered.** In relation to the propulsion electric power plants with frequency-regulated PMs, the optimal control law, borrowed from the theory of frequency control of general industrial electric drives ( $\gamma/\alpha = \text{const}$ ), has traditionally been proposed. Here  $\gamma$  is the relative voltage  $\gamma = U/U_n$ ,  $\alpha$  is the relative frequency  $\alpha = f/f_n$ . However, it should be remembered that the recommended proportional optimal control law was obtained in relation to the «electrical» performance indicators of electric motors. At a systematic approach, these indicators fade into the background. There is a need to search for the laws of control that will provide the best values of the quality indicators of an electric ship's maneuvering, with controlled (with specified tolerances) performance of propulsion electrical installation, too.

In accordance with the defined task, the analysis of the operation of PPPs on maneuvers should be carried out in conjunction with all the components of the propulsion complex of the electric ship, including the ship electric power installation (primary engines, electric current generators, electric power converters, PMs), propellers, steering wheel and ship hull. Only in this formulation we can carry out a thorough analysis of the maneuverable modes of operation, assess the maneuverability properties of the electric ship and find the optimal PM control laws that provide the best maneuverability of the vessel.

In [1], attempts were made to find the optimal laws of control of the propulsion motors of electric ships when performing maneuverable operations. For this purpose, a mathematical model of the transient operating modes of the propulsion electrical installation was developed as part of a single ship propulsion complex. Based on the model, algorithms for calculating transient modes are developed and a method for finding optimal control laws is proposed. But:

- when describing the processes occurring in heat engines of the propulsion electric power plant, a number

of assumptions were adopted that do not allow controlling the dynamic indicators of their operating modes;

- a mathematical description of the processes occurring in synchronous generators was built on the basis of a vector diagram of the generator, which also made it impossible to fully evaluate their dynamics, and led to certain errors in assessing the dynamic performance of the PPP;

- the proposed type of voltage control laws, as shown by the results of the analysis, does not fully satisfy the tasks set.

In order to search for control laws for propulsion electric motors that, on the one hand, provide the best values of quality indicators for maneuvering, and, on the other hand, allowable dynamic loads on the propulsion electrical installation and heat engines of the ship power plant, it is necessary to improve the mathematical model and clarify the type and procedure for finding optimal control laws. It is proposed to accept as the main indicators of the quality of maneuvering (as an example of solving such problems) the minimum stopping distance of the vessel or the minimum energy (fuel consumption costs) to perform the maneuver. The choice of the indicator is determined by the goals and conditions of the maneuver.

**The goal of the paper** is to find the optimal laws of control of the propulsion electric motors, ensuring high maneuverability properties of the electric ships.

**The method of solving the problem.** In [2], a refined mathematical model of the transient modes of the propulsion electric power installations of electric ships as part of ship propulsion complexes was proposed. In it:

- isodromic all-mode regulators of indirect action were considered as regulators of the speed of rotation of heat engines; as voltage regulators of synchronous generators, combined (by the control action and by the deviation of the controlled variable) regulators are considered;

- transients in the speed regulators of rotation of heat engines are described taking into account rigid and flexible feedbacks, and taking into account the operation of the active power distribution system (with parallel generating units);

- transients in synchronous generators are represented by the Park-Gorev equations;

- the composition of the combined system of automatic voltage regulation of synchronous generators includes a circuit for regulating the distribution of reactive power (with parallel generating units).

To give generality to the results of calculations, the model is reduced to relative units. As a result, the criteria of dynamic similarity (dimensionless parameters) of the propulsion complexes «heat engines – propulsion electric installation – propulsions – steering – ship hull» were revealed. Possible ranges of variation of their values are found. It is these parameters that determine the current, in the course of the execution of the maneuver, the values of performance indicators of all components of the complex and directly affect the numerical values of the indicators of the quality of maneuver. For the calculation of maneuvering modes a package of application programs is

developed. Basic is a program that allows to calculate the current values of the relative performance indicators.

This approach allows to give generality to the obtained results – electric ships with equal values of dimensionless parameters will have respectively the same values (in relative units) of the quality indicators of maneuvering.

The composition of the power plant includes several power circuits (by the number of propulsion motors). Usually there are two-three of them. Each circuit (each PM) is controlled independently of the others from the control station (CS) located on the bridge. In this case, two control signals are formed on the frequency converter: by the relative frequency  $\alpha$  and by the relative voltage  $\gamma$ .

It is proposed to generate control signals by the relative frequency  $\alpha = \alpha(T)$  and by the relative voltage  $\gamma = \gamma(\alpha)$  in the form:

$$\alpha = \alpha_{prim} + K_1 (1 - \exp(-K_5 T)); \quad (1)$$

$$\gamma = K_2 \alpha + K_3 \alpha^2 + K_4 \alpha^3 + (1 - K_2 - K_3 - K_4) \alpha^4, \quad (2)$$

where  $\alpha_{prim}$  is the initial value of the relative frequency of the PM supply voltage;  $T = \frac{v_0 t}{L}$  is the dimensionless

time;  $v_0$  is the steady state speed of the vessel;  $L$  is the vessel length;  $t$  is the current time;  $K_1, K_2, K_3, K_4, K_5$  are the optimized factors.

The need for an initial non-zero  $\alpha_{prim}$  becomes apparent from a comparison (Fig. 1) of the reverse characteristics of the propeller (curve 2) with the mechanical characteristics of the induction PM with the opposite direction of rotation of the magnetic field (curves 1).

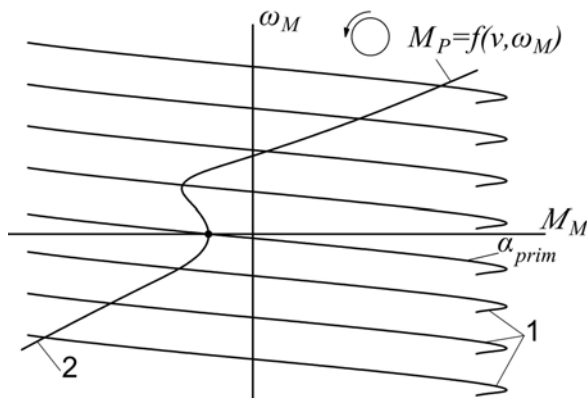


Fig. 1. Reversible propeller characteristic and mechanical characteristics of PM

Optimization of the control laws should be carried out according to the rate of change of the relative frequency (depending on the shift of the CS handle) and according to the relative voltage  $\gamma = \gamma(\alpha)$ .

The following criteria were selected as optimality criteria:

- minimum stopping distance –  $L_{Tmin}$ ;
- minimum energy losses to perform the maneuver –  $L_{Tmin}$ .

The problems to be solved belong to the field of nonlinear programming and consist in finding the extrema of the target function  $f(x)$  under given constraints  $g_j(x)$  in

the form of inequalities. In other words, it is necessary to minimize some objective function.

$$f(x), x \in E^n \quad (3)$$

with  $p$  linear constraints in the form of inequalities

$$g_j(x) \geq 0, j = 1, \dots, p, \quad (4)$$

where  $E^n$  is the admissible domain of the  $n$ -dimensional space.

The optimal solution is a pair  $x^*$  and  $f(x^*)$  consisting of the optimal point  $x^* = [x_1^*, x_2^*, \dots, x_n^*]$  and the corresponding value of the target function  $f(x^*)$ .

The objective choice of the optimal solution variant requires the use of a quantitative complex criterion that takes into account, for each version of the ship electric power installation, a set of heterogeneous indicators of the quality of operation and the corresponding costs.

In the course of optimization calculations, problems of both single-criterion and multi-criteria optimization can be solved. In the first case, one of the quality indicators serves as the target function. In the second case, the objective function is constructed as

$$f(x) = \sum m_j f_j(x),$$

where  $m_j$  is the weight coefficient of the  $j$ -th quality indicator.

In accordance with the goals set in the paper, either the minimum stopping distance of the vessel  $L_{Tmin}$ , or the minimum energy losses on the execution of the maneuver  $W_{min}$  are taken as the criteria for optimality. All other criteria fade into the background and are taken into account in the form of restrictions (4). Thus, in this paper, single-objective optimization problems were solved. There is no need to estimate weight coefficients.

Procedures for finding optimal solutions were based on the identified nature of the target functions. As shown by numerous calculations, they are multi-extremal, with an unknown number of points of local minima. Therefore, global optimization methods were used as the basis for algorithms for finding optimal solutions.

It is known that the existing classical optimization methods [4-6], as a rule, are not suitable for solving real practical optimization problems. We need special methods that take into account the specifics and nature of the target functions.

The values of  $f(x)$  are found as a result of calculations of the maneuvers described by a complex system of algebraic and differential equations with numerous restrictions in the form of inequalities. It is just unrealistic to set the task of searching for the first and, moreover, the second derivative of the target functions.

A large number of preliminary calculations and their analysis showed that the target functions have the form of steep and elongated ravines. The analysis of existing methods of searching for global optima of such target functions gave grounds to lay the well-known, well-proven method of global random search – the random multi-start, as the basis for the developed global optimization algorithms.

In its pure form, a random multi-start is ineffective due to possible repeated descents to points of local minima. Therefore, a combination of one of the passive coating methods, the random grid method, with the modified tunnel algorithm method [1] was incorporated into the global optimization algorithm.

When developing methods for searching for local minima (internal procedures of global optimization), it was again taken into account that the target functions have an implicitly gully character. On this basis, local optimum search algorithms were created based on a combination of local descent methods and ravine search methods. The methods of Powell and Nelder-Mead [7] turned out to be the most effective for solving such problems.

The ravine search for a local optimum was carried out as follows. Two local descents from nearby starting points were organized. We searched from each point for intermediate local minima  $f_1^*(x_1^*)$  and  $f_2^*(x_2^*)$ . Then we found a new direction  $s_0^*$  drawn from  $x_1^*$  to  $x_2^*$  (or vice versa, depending on which of the found intermediate minima  $f_1^*(x_1^*)$  or  $f_2^*(x_2^*)$  is more), and along it we searched the minimum value of the function  $f_{opt.loc}(x^*)$  which was the local optimum.

To solve the minimization problems, the optimization methods used were combined with the method of penalty functions [8], which made it possible to reduce the nonlinear programming problem with constraints to an equivalent sequence of problems without constraints.

The search for optimal control laws is carried out as follows. Each time, after setting a random starting point, the investigated maneuver is calculated and the corresponding values of the optimality criteria (in particular, the stopping distance or the energy losses for the maneuver) are found. Then, in accordance with the described procedure of movement to the optimum, new initial data (new values of optimized parameters) are calculated, the maneuver is calculated again and the corresponding values of the optimality criteria are found. The calculation ends when the global optimum is reached.

The developed mathematical apparatus allows to find the optimal laws of control of the propulsion electric motors during maneuvers.

Below we consider the search for the optimal control laws for the propulsion electric motors of electric ships during reverse. It was noted that the choice of quality indicators and, accordingly, the type of the target function of the optimization process is determined by the goals set and conditions of the maneuver. When operating in cramped conditions, the reverse (the quality of the reversal) directly affects the safety of maneuvering operations. In this case, the main criterion for optimality is the minimum stopping distance of the electric ship  $L_{Tmin}$ . If maneuvering is carried out in «calm» conditions, there are no other vessels or other objects nearby, the stopping distance of the electric ship fades into the background. In this case, as an optimality criterion, it makes sense to take the minimum energy losses on the execution of the maneuver  $W_{min}$ . And in one, and in another case, it will be about single-criteria optimization tasks. The remaining indicators of the quality of maneuvering are taken into account in the form of restrictions (together with the settings of protection systems and restrictions ensuring the normal functioning of the propulsion complex). This is fully consistent with the principles of the systems approach [3].

For electric ships, the frequency-controlled stage of reversal of propulsion electric motors starts from the moment of time when the angular velocity of rotation of the PM passes through a zero value. This stage is characterized by intensive braking of an electric ship. It should be borne in mind that the propulsion motors at the same time operate in a very heavy mode, experiencing a large moment of resistance from the propellers, thereby significantly increasing the load on all the component parts of the propulsion electric power plant.

For each particular electric ship when performing maneuver operations, the optimal control laws will be different. At the same time, the proposed mathematical apparatus makes it possible to find the optimal control laws for a sufficiently large class of vessels. To do this, it is necessary to identify those dimensionless parameters of the complex that most significantly affect the control laws, find ranges of changes in their values (covering as much as possible the class of ships) and, after carrying out the necessary optimization procedures, find the optimal control laws for different combinations of these parameters. In other words – to find control laws for a whole class of vessels.

The results of the analysis of the influence of the initial conditions for the fulfillment of the maneuver and dimensionless parameters of the complex on the criteria  $L_{Tmin}$ , and  $W_{min}$  carried out by methods of active planning of experiments [9], give grounds to consider the following as significant influencing parameters:

- $v_{prim}$  – initial vessel velocity;
- $N_X$  – power ratio of the electric ship

$$N_X = \frac{L \sum K_{Pj} P_{ej0}}{(m + \lambda_{11}) v_0^2}; \quad (5)$$

- $C_{M18}$ ,  $C_{M20}$  – dimensionless parameters of frequency-controlled PM

$$C_{M18} = \frac{c_M^2}{r_{2M}^2} \alpha_0^2; \quad (6)$$

$$C_{M20} = \frac{\omega_M \alpha_0}{\omega_{1Mn}}, \quad (7)$$

where  $P_{ej}$  and  $K_{Pj}$  are the useful stop of the propeller and its share in the total stop, respectively;  $m$  is the vessel mass;  $\lambda_{11}$  are the attached to the vessel the masses of water along its longitudinal axis;  $\omega_M$  is the angular frequency of the PM rotation;  $\omega_{1Mn}$  is the angular speed of rotation of the PM stator magnetic field;  $r'_{2M}$  is the reduced PM rotor resistance;  $c_M = x_{0M} \tau_M$  is the constant design factor of frequency-controlled induction PM.

**The results of the work.** Table 1 presents the results of the search for optimal control laws for propulsion electric motors, providing the minimum braking distance of the electric ship  $L_{Tmin}$  (the minimum stopping distance contributes to the safety of maneuver operations).

A series of optimization calculations were carried out for various combinations of values of significant dimensionless parameters. Different combinations of parameters are, in fact, nothing more than different electrical ships.

Table 1

Combinations of significant parameters and found optimal solutions by criterion  $L_{Tmin}$  (at  $v_{prim} = 0.3$ )

Variant	Values of significant parameters			$L_{Tclassic}$ p.u.	Optimal solutions					$L_{Tmin}$ p.u.	Efficiency, %
	$N_X$	$C_{M18}$	$C_{M20}$		equations $\alpha = \alpha(T)$		equations $\gamma = \gamma(\alpha)$				
					$K_1$	$K_5$	$K_2$	$K_3$	$K_4$		
1	0.12	15.7	0.88	0.43	0.57	7.03	0.99	0.26	1.35	0.36	16.3
2	0.165	15.7	0.88	0.403	0.57	7.59	1.17	0.22	1.28	0.33	18.1
3	0.21	15.7	0.88	0.365	0.56	6.75	1.02	0.27	1.32	0.31	15.1
4	0.12	43.9	0.88	0.437	0.57	6.98	1.32	-0.19	1.33	0.35	19.9
5	0.165	43.9	0.88	0.406	-	-	-	-	-	-	-
6	0.21	43.9	0.88	0.369	0.57	6.22	1.34	-0.19	1.3	0.31	16
7	0.12	72	0.88	0.444	0.6	6.89	1.19	0.2	0.89	0.35	21.2
8	0.165	72	0.88	0.412	0.57	7.14	1.35	0.106	1.3	0.33	19.9
9	0.21	72	0.88	0.373	0.6	6.2	1.2	0.2	0.87	0.3	19.6
10	0.12	15.7	0.925	0.403	0.6	6.28	1.2	0.2	0.99	0.32	20.6
11	0.165	15.7	0.925	0.378	0.6	6.12	1.85	0.24	1.33	0.3	20.6
12	0.21	15.7	0.925	0.345	0.6	6.6	1.17	0.26	1.35	0.28	18.8
13	0.12	43.9	0.925	0.407	0.62	6.14	1.2	0.19	0.74	0.32	21.4
14	0.165	43.9	0.925	0.381	0.619	6.56	1.28	0.2	1.38	0.3	21.3
15	0.21	43.9	0.925	0.348	0.61	6.6	1.18	0.22	1.05	0.28	19.5
16	0.12	72	0.925	0.412	0.63	7.54	1.19	0.21	0.95	0.31	24.8
17	0.165	72	0.925	0.385	0.63	6.49	1.2	0.2	0.93	0.3	22.1
18	0.21	72	0.925	0.351	0.63	6.43	1.2	0.2	0.93	0.28	20.2
19	0.12	15.7	0.97	0.38	0.64	6.46	1.19	0.2	0.86	0.28	26.3
20	0.165	15.7	0.97	0.358	0.63	6.48	0.96	0.26	1.33	0.26	27.4
21	0.21	15.7	0.97	0.328	0.639	6.487	0.968	0.263	1.332	0.261	20.4
22	0.12	43.9	0.97	0.382	0.64	6.57	1.18	0.22	1.05	0.28	26.7
23	0.165	43.9	0.97	0.361	0.65	6.47	1.2	0.2	0.86	0.27	25.2
24	0.21	43.9	0.97	0.33	0.65	6.17	1.19	0.2	0.85	0.26	21.2
25	0.12	72	0.97	0.386	0.65	5.82	1.36	0.2	0.76	0.29	24.9
26	0.165	72	0.97	0.364	0.65	5.81	1.36	0.195	0.74	0.28	23.1
27	0.21	72	0.97	0.332	0.656	5.886	1.365	0.192	0.745	0.258	22.3

Table 1 shows a small part (as an example) of possible combinations of parameters. The variation in each parameter was carried out at three (minimum, medium and maximum) levels. For all combinations, the optimal control laws were found using the algorithm described above. (Similar tables were compiled for other initial values of vessel velocity  $v_{prim}$ . Optimal solutions were also found for them).

Also, in Table 1, for evaluating the effectiveness of the carried out optimization calculations, the values of the criterion  $L_{Tmin}$  are given, obtained by controlling PM using the «classical» law  $\gamma / \alpha = \text{const}$  traditionally recommended for propulsion electric drives. This is the  $L_{Tclassic}$  column. Comparison of the results obtained (see the last column of Table 1) clearly demonstrates the efficiency of using the calculated laws of optimal control.

Optimization results are conveniently presented graphically. As an example, in Fig. 2 the dependencies

$\alpha = \alpha(T)$ ,  $\gamma = \gamma(T)$  and  $\gamma = \gamma(\alpha)$  are presented for the first three variants of the combination of parameters (for three electric ships). Analysis of the calculation results shows that the transition to the optimal (by  $L_{Tmin}$ ) control of the propulsion electric motors can significantly reduce the braking distance of the electric ship. Depending on the specific vessel (specific combinations of parameters of the complex), this reduction is in the range from 15 % to 27 %.

The results obtained (in analytical form – the coefficients of optimal control laws  $\alpha = \alpha(T)$  and  $\gamma = \gamma(\alpha)$  in Table 1 and in graphic interpretation in Fig. 2) allow for any electric ship of the considered class to assign PM control laws that ensure the implementation of the «reverse» maneuver with a minimum stopping distance. If the dimensionless parameters of the electric ship differ from those given in the Tables, you can use any interpolation method.

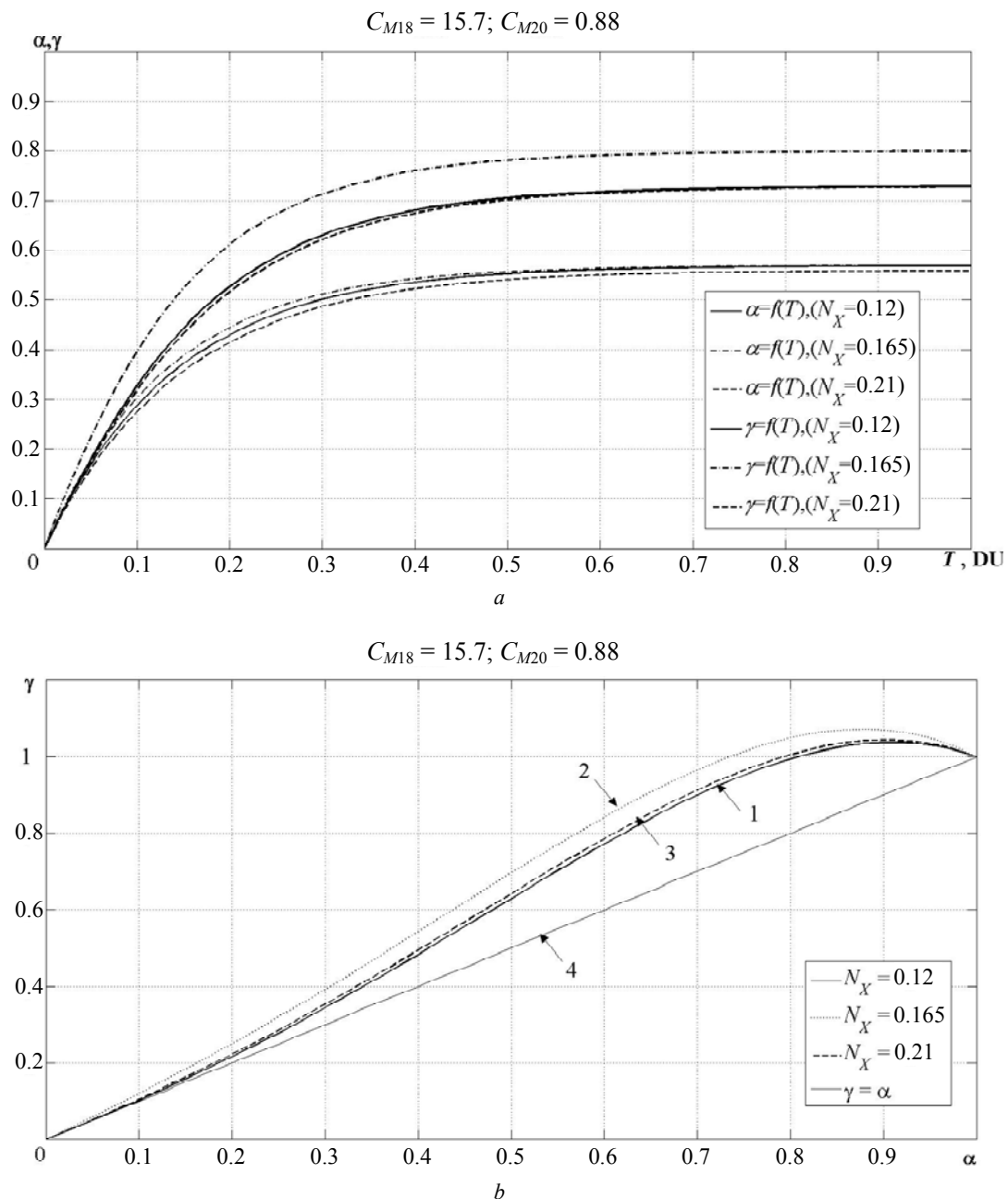


Fig. 2. Optimal control laws by criterion  $L_{Tmin}$  ( $v_{prim} = 0.3$ )  
 $a - \alpha, \gamma = f(T), b - \gamma = f(\alpha)$

If maneuvering is carried out in an unrestricted water area, in the absence of other vessels nearby, it makes sense to take the minimum energy losses for the maneuver  $W_{min}$  as the optimality criterion. Most likely, the laws of control will be different. We tried to find them.

In accordance with the conducted studies, the results of which are given in [9], the significantly influencing parameters and by this criterion of optimality (with a contribution level of at least 10 %) are  $v_{prim}$ ,  $N_X$ ,  $C_{M18}$ ,  $C_{M20}$ . Some variants of combinations of these parameters and the optimal solutions found (and  $W_{classic}$  values obtained with the classical  $\gamma / \alpha = const$  control law – for evaluating the efficiency of optimization) are given in Table 2.

These control laws can also be graphically illustrated

in the same way as was done for optimal control by the criterion of minimum stopping distance. The efficiency (in terms of energy losses) of the proposed control is in the range of 14–34 %.

The obtained results can be useful in the very initial stages of the design of propulsion electric power plants. It is already possible at these stages to evaluate the maneuverability characteristics of future electric ships. They can also be useful for vessels in service. For a particular electric ship, in accordance with the goals set, the best control law for propulsion electric motors can be selected and incorporated into the control system.

As an example, consider the project of a particular electric ship. Its main characteristics, necessary for the calculation of the significantly affecting dimensionless parameters  $N_X$ ,  $C_{M18}$ ,  $C_{M20}$  are given in Table 3.

Table 2

Combinations of significant parameters and found optimal solutions by criterion  $W_{\min}$  ( $v_{prim} = 0.3$ )

Variant	Values of significant parameters, p.u.			$W_{classics}$ p.u.	Optimal solutions					$W_{\min}$ p.u.	Efficiency, %
	$N_X$	$C_{M18}$	$C_{M20}$		equations $\alpha = \alpha(T)$		equations $\gamma = \gamma(\alpha)$				
					$K_1$	$K_5$	$K_2$	$K_3$	$K_4$		
1	0.12	15.7	0.88	4.235	0.601	4.745	1.245	-0.075	0.092	3.583	15.4
2	0.165	15.7	0.88	3.527	0.590	1.052	1.117	0.092	0.721	2.993	15.1
3	0.21	15.7	0.88	2.92	0.576	6.149	1.231	0.014	1.351	2.522	13.6
4	0.12	43.9	0.88	4.41	0.591	1.432	1.363	0.147	1.451	3.549	19.5
5	0.165	43.9	0.88	3.573	0.526	4	1.31	0.378	2.07	2.774	22.4
6	0.21	43.9	0.88	3.063	0.526	4.33	1.31	0.378	2.07	2.36	23
7	0.12	72	0.88	4.59	0.569	4.5	1.397	0.199	1.106	3.492	23.9
8	0.165	72	0.88	3.74	0.575	4.507	1.367	0.193	1.092	2.937	21.5
9	0.21	72	0.88	3.1	0.53	5.1	1.31	0.38	2.07	2.36	23.9
10	0.12	15.7	0.925	4.083	0.615	5.97	1.239	-0.0007	0.738	3.372	17.4
11	0.165	15.7	0.925	3.416	0.662	1.421	1.304	0.154	1.468	2.824	17.3
12	0.21	15.7	0.925	2.836	0.5	5.31	1.216	0.4	2.9	2.29	19.3
13	0.12	43.9	0.925	4.247	0.631	1.433	1.375	0.159	1.448	3.335	21.5
14	0.165	43.9	0.925	3.458	0.53	3.98	1.31	0.328	2.17	2.3	33.5
15	0.21	43.9	0.925	2.97	0.53	4.43	1.31	0.38	2.07	2.3	22.6
16	0.12	72	0.925	4.417	0.635	6.181	1.334	0.131	1.251	3.273	25.9
17	0.165	72	0.925	3.62	0.633	6.74	1.249	0.005	1.323	2.764	23.6
18	0.21	72	0.925	3.00	0.636	6.669	1.36	0.131	1.161	2.354	21.5
19	0.12	15.7	0.97	3.93	0.633	3.976	1.276	0.058	1.529	3.199	18.6
20	0.165	15.7	0.97	3.31	0.642	2.696	1.224	0.011	1.251	2.696	18.5
21	0.21	15.7	0.97	2.843	0.62	4.87	1.22	0.28	1.56	2.27	20.2
22	0.12	43.9	0.97	4.08	0.658	8.523	1.053	-0.006	1.48	3.189	21.8
23	0.165	43.9	0.97	3.35	0.666	5.426	1.285	0.036	0.56	2.677	20.1
24	0.21	43.9	0.97	2.873	0.57	4.45	1.3	0.586	1.03	2.24	22
25	0.12	72	0.97	4.235	0.666	4.546	1.417	-0.028	0.775	3.16	25.4
26	0.165	72	0.97	3.492	0.56	4	1.31	0.33	2.17	2.61	25.3
27	0.21	72	0.97	2.91	0.47	3.16	1.38	0.46	2.48	2.16	25.8

Table 3

Main characteristics of the electric ship

The length of the vessel at the waterline, $L$	160 m
Ship velocity in steady state, $v_0$	22 knots
Vessel mass, $m$	33540 t
Total stop of propellers, $\sum K_{pj} P_{ej0}$	6250 t·m/s <sup>2</sup>
Attached to the vessel the masses of water along its longitudinal axis, $\lambda_{11}$	0.11 t
Angular velocity of the PM rotation, $\omega_M$	120 rpm
Angular velocity of the PM stator magnetic field rotation, $\omega_{1Mn}$	124 rpm
Constant design factor, $c_M$	0.423 $\Omega$
Reduced resistance of the PM rotor, $r'_{2M}$	0.0639 $\Omega$

The numerical values of significant parameters calculated from the above relations are given in Table 4.

Table 4

Values of the dimensionless electric ship parameters

Parameter	Numerical values of the parameters
$N_X$	0.21
$C_{M18}$	43.9
$C_{M20}$	0.97

For this combination of parameters – for this electric ship – the optimal law of control of the propulsion electric motors providing the minimum stopping distance  $L_{Tmin}$  will be option 24 of the Table 1. Namely:

$$\alpha = 0.1 + 0.65 (1 - \exp(-6.17 T));$$

$$\gamma = 1.19 \alpha + 0.2 \alpha^2 + 0.85 \alpha^3 - 1.24 \alpha^4.$$

It is these laws of control of the relative frequency  $\alpha$  and relative voltage  $\gamma$  that are recommended to be inserted into the control system of the propulsion electric motors, if it is necessary to ensure the minimum stopping distance of the electric ship when reversed. Here, it will be 0.26 of the vessel length, or in absolute units – 41.6 m.

If we apply the traditional proportional control law, the stopping distance will be 0.33 vessel length, or in absolute units – 52.8 m. Thus, the effectiveness of applying the recommended optimal control law is 21.2 %.

The results obtained can be illustrated graphically. Fig. 3 shows the curves of the time variation of the relative frequency  $\alpha = f(T)$  and the relative voltage  $\gamma = f(T)$  (Fig. 3,a), as well as the dependencies (Fig. 3,b)

of the optimal control law  $\gamma = f(\alpha)$  when reversing PM of an electric ship moving at a low speed (at initial speed  $v_{prim} = 0.3$ ) and proportional (for comparison with the optimal) control law  $\gamma_0 = f(\alpha)$ .

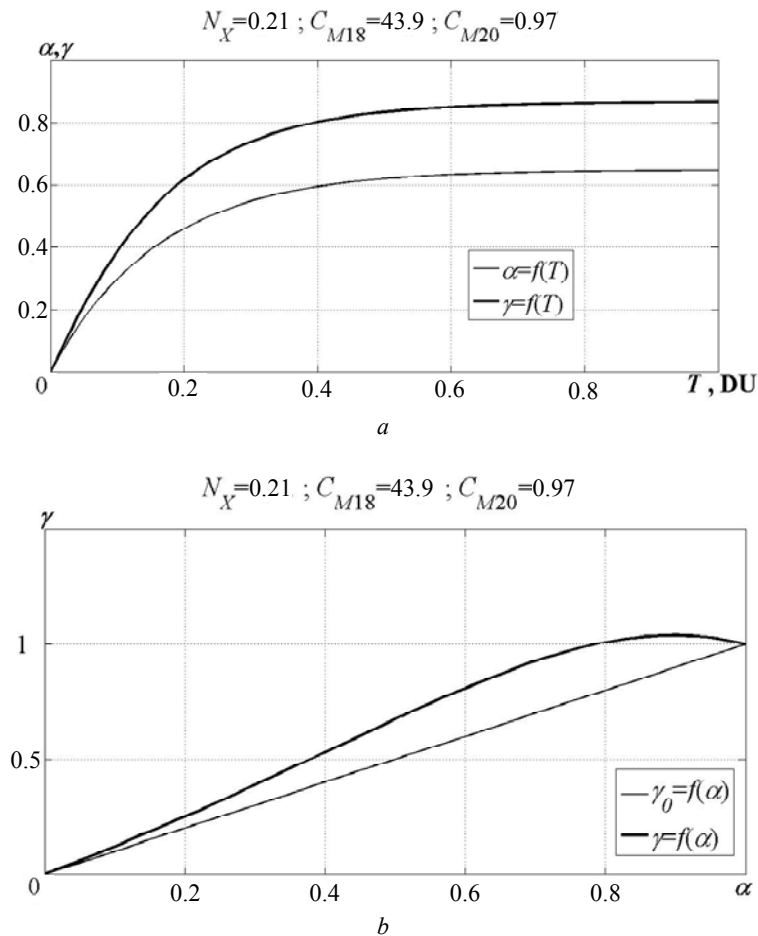


Fig. 3. Optimal control laws (for the project of an electric ship) by criterion  $L_{Tmin}$  (at  $v_{prim} = 0.3$ ):  
 $a - \alpha, \gamma = f(T)$ ,  $b - \gamma = f(\alpha)$

If the reversal is carried out in unfilled conditions and it is advisable to ensure a minimum of energy consumption, then the optimal control law of this electric ship will be the same option 24, but from Table 2. The control laws in this case:

$$\alpha = 0.1 + 0.57 (1 - \exp(-4.45 T));$$

$$\gamma = 1.3 \alpha + 0.586 \alpha^2 + 1.03 \alpha^3 - 1.916 \alpha^4.$$

When controlled by these laws, energy consumption is reduced compared to the classic version from 2.873 to 2.24 relative units.

If necessary, laws can be clarified. To do this, it is necessary to substitute the numerical values of the dimensionless parameters of the complex into the mathematical model and calculate, using the developed method, the optimal control law (now refined) with the appropriate optimality criterion. However, it is advisable to do this already at the later design stages, in the presence of more complete information about the designed ship.

#### Conclusions.

1. It has been established that the traditional principles of constructing optimal control laws for frequency-controlled induction electric motors of electric ships do

not allow to obtain the maximum return from the propulsion electric power plant. A new method of forming optimal laws, based on a systematic principle, is proposed.

2. The nature of the target functions is identified, a technique of optimization is developed. The procedure of optimization calculations is proposed.

3. Optimization calculations were carried out and optimal control laws for propulsion electric motors were found at the reverse of electric ships. Optimization was carried out according to the criteria of minimum stopping distance and minimum power consumption.

4. The effectiveness of using the proposed control laws is illustrated.

#### REFERENCES

1. Yarovenko V.A. *Raschet i optimizatsiia perekhodnykh rezhimov propul'sivnykh kompleksov elektrokhodov* [Calculation and optimization of transient regimes of propulsion complexes of electric vessels]. Odessa, Mayak Publ., 1999. 188 p. (Rus).
2. Yarovenko V.A., Chernikov P.S. A calculation method of transient modes of electric ships' propelling electric plants. *Electrical engineering & electromechanics*, 2017, no.6, pp. 32-41. doi: 10.20998/2074-272X.2017.6.05. (Rus).

3. Sukharev A.G., Timokhov A.V., Fedorov V.V. *Kurs metodov optimizatsii* [Course of optimization methods]. Moscow, Fizmatlit Publ., 2005. 368 p. (Rus).
4. Bonnans J.-F., Gilbert J.C., Lemarechal C., Sagastizábal C.A. *Numerical optimization: theoretical and practical aspects*. Berlin, Heidelberg: Springer-Verlag, 2006. 494 p. **doi: 10.1007/978-3-662-05078-1**.
5. Fletcher R. *Practical Methods of Optimization*. Wiley, 2000. 450 p. **doi: 10.1002/9781118723203**.
6. Antoniou A., Lu W.-S. *Practical optimization. Algorithms and engineering applications*. Springer, 2007. 675 p.
7. Floudas C.A., Pardalos P.M. *Encyclopedia of optimization*. Springer, 2009. 4646 p. **doi: 10.1007/978-0-387-74759-0**.
8. Panteleev A.V., Letova T.A. *Metody optimizatsii v primerakh i zadachakh* [Optimization methods in examples and problems]. Moscow, High school Publ., 2008. 544 p. (Rus).
9. Chernikov P.S., Yarovenko V.A., Zaritskaya E.I. Influence of electric ships' parameters on quality indices of electric power

plants' performance at maneuvers. *Bulletin of the National Technical University «KhPI» Series: «Electric machines and electromechanical energy conversion»*, 2018, no.5(1281), pp. 46-54. (Rus).

*Received 31.07.2018*

*V.A. Yarovenko*<sup>1</sup>, *Doctor of Technical Science, Professor,*  
*P.S. Chernikov*<sup>1</sup>, *Senior Instructor,*  
*R.A. Varbanets*<sup>1</sup>, *Doctor of Technical Science, Professor,*  
*E.I. Zaritskaya*<sup>1</sup>, *Candidate of Technical Science, Associate Professor,*  
<sup>1</sup>Odessa National Maritime University,  
 34, Mechnikova Str., Odessa, 65007, Ukraine,  
 phone +380 50 5980683,  
 e-mail: yarovenko@3g.ua, chernikov@onmu.odessa.ua,  
 roman.varbanets@gmail.com, zarickayalena@ukr.net

*How to cite this article:*

Yarovenko V.A., Chernikov P.S., Varbanets R.A., Zaritskaya E.I. Optimal control of the electric ships' propulsion motors during reversal. *Electrical engineering & electromechanics*, 2018, no.6, pp. 38-46. **doi: 10.20998/2074-272X.2018.6.05**.

N.I. Suprunovska, M.A. Shcherba

## APPLICATION OF VYSHNEGRADSKY'S DIAGRAMS FOR TRANSIENT ANALYSIS IN ELECTRIC DISCHARGE INSTALLATIONS WITH STOCHASTIC LOAD

*Purpose.* To analyze the transient processes in the discharge circuit of reservoir capacitor of electric discharge installations at a change in the circuit configuration during the discharge as well as to determine the appropriate circuit parameters for which the discharge process described by the third-order differential equation remains a damped oscillatory process. *Methodology.* We have applied the concepts of theoretical electrical engineering, the principles of theory of electrical circuits, theory of automatic control systems and mathematical simulation in the software package MathCAD 12. *Results.* We have obtained the analytical expressions and graphical dependencies that allow us to determine a relationship between the value of the element parameters of the discharge circuit of installations with an additional active-inductive chain and the character of the transient discharge process without solving a third-order differential equation. *Originality.* Using Vyshnegradsky's criteria and their graphical representations in the form of diagrams, we have proposed the procedure for determining the inductance value in additional chain shunting the capacitor of electric discharge installation in order to avoid the undesirable aperiodic discharge transient process in the stochastic load. *Practical value.* The use of this approach makes it possible to determine the ranges of the expedient change in the additional inductance at different load resistances for the realization of transient process required by the technology – the oscillatory discharge of the reservoir capacitor through the load. References 10, tables 1, figures 3.

*Key words:* electric discharge installation, capacitor discharge, transients, Vyshnegradsky's diagram, stochastic load.

*Цель.* Целью статьи является анализ переходных процессов в разрядной цепи накопительного конденсатора электроразрядных установок при изменении ее конфигурации во время разряда и определение целесообразных параметров цепи, при которых процесс разряда, описываемый дифференциальным уравнением третьего порядка, остается затухающим колебательным процессом. *Методика.* Для проведения исследований использовались научные положения теоретической электротехники, теория электрических цепей, теория систем автоматического регулирования и математическое моделирование в программном пакете MathCAD 12. *Результаты.* Получены аналитические выражения и графические зависимости, устанавливающие связь между значениями параметров элементов разрядной цепи установок с дополнительной активно-индуктивной цепочкой и характером переходного процесса разряда конденсатора без решения дифференциального уравнения третьего порядка. *Научная новизна.* Используя критерии Вышнеградского и их графические изображения в виде диаграмм, предложена методика определения величины индуктивности дополнительной цепочки, шунтирующей конденсатор электроразрядной установки, для исключения его нежелательного аperiodического разряда на стохастическую нагрузку. *Практическое значение.* Использование данного подхода позволяет определить диапазоны целесообразного изменения дополнительной индуктивности при различных сопротивлениях нагрузки для реализации необходимого для технологии переходного процесса – колебательного разряда накопительного конденсатора на нагрузку. Библи. 10, табл. 1, рис. 3.

*Ключевые слова:* электроразрядная установка, разряд конденсатора, переходные процессы, диаграмма Вышнеградского, стохастическая нагрузка.

**Introduction.** In the electric discharge installations (EDI) with reservoir capacitors, in particular in the semiconductor (thyristor) installations for volumetric electro-spark dispersion (VESD) of the metals, the oscillatory discharge of capacitor with a small reverse recharge (less than 30 % in voltage) is the most efficient technologically and energetically mode of discharge through electric spark load [1-6]. In this case, there is a fast natural locking of the discharge semiconductor switch, which makes it possible to quickly carry out the subsequent charge of the capacitor and further its discharge through the load [1, 4-6]. Thus, we can realize a high frequency of charge-discharge cycles and stability of the duration of discharge currents in the EDI load.

At the same time the resistance of such load as a metal granular layer can stochastically increase several times during discharge. As a result, a so-called idle discharge through the load, i.e., a long-term discharge with a low current without sparking can occur [1, 4, 6-8]. Since the increase in active resistance of load decreases the  $Q$ -factor of the discharge circuit, then the oscillatory capacitor discharge transient can become aperiodic one, and discharge duration can increase many times. Because of such long capacitor discharges, we can not to realize

high frequency and stability of charge-discharge cycles, and thus the yield of spark-eroded powders.

To reduce the discharge pulse duration in such EDI, we have proposed to connect an additional shunt chain  $VT_2-L_2-R_2$  in parallel to the capacitor at a certain time  $t_1$  as shown in Fig. 1. The parameters of the additional chain must be chosen from the condition for avoiding of aperiodic capacitor discharge.

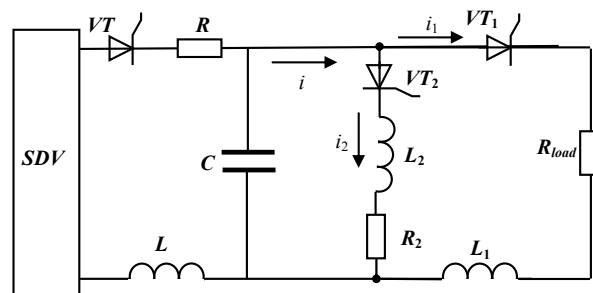


Fig. 1. Electric schematic diagram of EDI with additional  $RL$ -chain shunting the capacitor

The **purpose** of this paper is to analyze the transient processes in the discharge circuit of reservoir capacitor of

electric discharge installations at a change in the circuit configuration during the discharge as well as to determine the appropriate circuit parameters for which the discharge process described by third-order differential equation remains a damped oscillatory process.

**Transient analysis of capacitor discharge through the load when the capacitor is shunted by the RL-chain.** As an example, we have performed the transient analysis of the capacitor discharge through the load in the thyristor installation for VESD with an additional parallel active-inductive chain. In the installation for VESD, whose electrical circuit is shown in Fig. 1, the capacitor  $C$  is charged to a voltage  $U_0$  from a shaper of direct voltage (SDV). Then, after switching on the discharge thyristor  $VT_1$ , the capacitor  $C$  is discharged through the load with the resistance  $R_{load}$  and discharge circuit inductance  $L_1$ , which is usually 1–5  $\mu$ H.

We have assumed that the resistance  $R_{load}$  (that take into account not only the resistance of the electric spark load, but the active resistance of the circuit wires) remains unchanged during the discharge, but could change discontinuously between the discharges. It has been also assumed that the thyristor  $VT_2$  was locked until the time  $t_1$ , and the discharge process was aperiodic, that is, the  $Q$ -factor of the  $C$ - $VT_1$ - $R_{load}$ - $L_1$ - $C$  discharge circuit  $Q_1 < 0.5$ .

During the discharge transient analysis, we have believed that the thyristors  $VT_1$  and  $VT_2$  were ideal switches, that is, the commutation occurred instantaneously and without power loss.

Expressions for the voltage of the capacitor  $u_C(t)$  and the current  $i(t)$  in the discharge circuit are [10]:

$$u_C(t) = U_0 \left( p_1 e^{p_1 t} - p_2 e^{p_2 t} \right) / (p_1 - p_2), \quad (1)$$

$$i(t) = U_0 \left( e^{p_1 t} - e^{p_2 t} \right) / L_1 (p_1 - p_2), \quad (2)$$

where  $U_0$  is the initial capacitor voltage;  $p_1$  and  $p_2$  are the roots of the characteristic equation of this circuit:

$$p_1 = -R_{load} / 2L_1 + \sqrt{R_{load}^2 / 4L_1^2 - 1/L_1 C},$$

$$p_2 = -R_{load} / 2L_1 - \sqrt{R_{load}^2 / 4L_1^2 - 1/L_1 C}.$$

At point in time  $t = t_1$ , when the current in the circuit is equal to a certain value  $i(t_1) = I_1$ , and the capacitor voltage has a certain value  $u_C(t_1) = U_1$ , the thyristor  $VT_2$  unlocks and an additional  $L_2 R_2$ -chain is connected to the circuit, that is, the circuit changes its configuration.

In new transient process, which started at  $t \geq t_1$  in the circuit with the changed configuration, the following system of equations is valid according to the second Kirchhoff's law:

$$\begin{cases} u_C + u_{L_2} + u_{R_2} = 0; \\ u_C + u_{L_1} + u_{R_{load}} = 0. \end{cases} \quad (3)$$

As  $u_{L_1} = L_1 di_1/dt$ ,  $u_{L_2} = L_2 di_2/dt$ ,  $u_{R_{load}} = R_{load} i_1$ ,  $u_{R_2} = R_2 i_2$ , then system (3) can be written as:

$$\begin{cases} u_C + L_2 di_2/dt + R_2 i_2 = 0; \\ u_C + L_1 di_1/dt + R_{load} i_1 = 0. \end{cases} \quad (4)$$

Since according to first Kirchhoff's law  $i = i_1 + i_2$ , and the current  $i$  flowing through the capacitor is

$i = C du_C/dt$ , we can write the following expression:

$$du_C/dt = i_1/C + i_2/C. \quad (5)$$

Let us perform the differentiation of the system (4):

$$\begin{cases} du_C/dt + L_2 d^2 i_2/dt^2 + R_2 di_2/dt = 0; \\ du_C/dt + L_1 d^2 i_1/dt^2 + R_{load} di_1/dt = 0. \end{cases} \quad (6)$$

After substituting (5) in (6) and performing the transformations, we obtain the system:

$$\begin{cases} i_1 = -CL_2 d^2 i_2/dt^2 - CR_2 di_2/dt - i_2; \\ i_2 = -CL_1 d^2 i_1/dt^2 - CR_{load} di_1/dt - i_1. \end{cases} \quad (7)$$

Let us perform the differentiation of second equation of system (7) once, and then twice:

$$di_2/dt = -CL_1 d^3 i_1/dt^3 - CR_{load} d^2 i_1/dt^2 - di_1/dt, \quad (8)$$

$$d^2 i_2/dt^2 = -CL_1 d^4 i_1/dt^4 - CR_{load} d^3 i_1/dt^3 - d^2 i_1/dt^2. \quad (9)$$

Substituting (8), (9) and the second equation of system (7) into the first equation of this system and performing the transformations, we get

$$CL_1 L_2 d^4 i_1/dt^4 + C(L_1 R_2 + L_2 R_{load}) d^3 i_1/dt^3 + (L_1 + L_2 + CR_{load} R_2) d^2 i_1/dt^2 + (R_{load} + R_2) di_1/dt = 0.$$

After integrating this expression, we have

$$CL_1 L_2 d^3 i_1/dt^3 + C(L_1 R_2 + L_2 R_{load}) d^2 i_1/dt^2 + (L_1 + L_2 + CR_{load} R_2) di_1/dt + (R_{load} + R_2) i_1 + A_i = 0, \quad (10)$$

where  $A_i$  is a constant of integration, which we define from the final conditions.

Since at  $t = \infty$  the capacitor is discharged to zero and all currents in the circuit (as well as their derivatives) are 0, then  $A_i = 0$ , and equation (10) takes the form

$$CL_1 L_2 d^3 i_1/dt^3 + C(L_1 R_2 + L_2 R_{load}) d^2 i_1/dt^2 + (L_1 + L_2 + CR_{load} R_2) di_1/dt + (R_{load} + R_2) i_1 = 0. \quad (11)$$

Thus, we have obtained a third-order differential equation whose characteristic equation can be written as

$$a_0 p^3 + a_1 p^2 + a_2 p + a_3 = 0, \quad (12)$$

where  $a_0 = CL_1 L_2$ ,  $a_1 = C(L_1 R_2 + L_2 R_{load})$ ,

$$a_2 = L_1 + L_2 + CR_{load} R_2, \quad a_3 = R_{load} + R_2.$$

For delimitation of areas with different types of transients, which are described by the third-order differential equations, in many cases it is expedient to use Vyshnegradsky's diagrams [10]. Vyshnegradsky's criterion and its graphic representation in the form of diagrams allow us to judge the influence of parameters of third-order system on its stability without solving the differential equation.

Bringing the equation (12) to a normalized form and introducing a new variable

$$q = p \cdot \sqrt[3]{a_0/a_3}, \quad (13)$$

we obtain, as a result, the normalized equation

$$q^3 + Aq^2 + Bq + 1 = 0, \quad (14)$$

where  $A = a_1/\sqrt[3]{a_3 a_0^2}$  and  $B = a_2/\sqrt[3]{a_0 a_3^2}$  coefficients are called the Vyshnegradsky's parameters.

On the plane of  $A$  and  $B$  parameters we can plot a Vyshnegradsky's diagram that display the regions of stable and unstable operation of the system described by a third-order differential equation whose characteristic equation has the form (12).

The stability conditions for the third-order system, formulated by Vyshnegradsky, are

$$A > 0, B > 0, \text{ and } AB > 1. \quad (15)$$

The equation for oscillatory stability threshold is

$$AB = 1 \text{ at } A > 0 \text{ and } B > 0.$$

This is an equilateral hyperbola, for which the coordinate axes are the asymptotes (Fig. 2). The region of system stability according to conditions (15) lies above this curve.

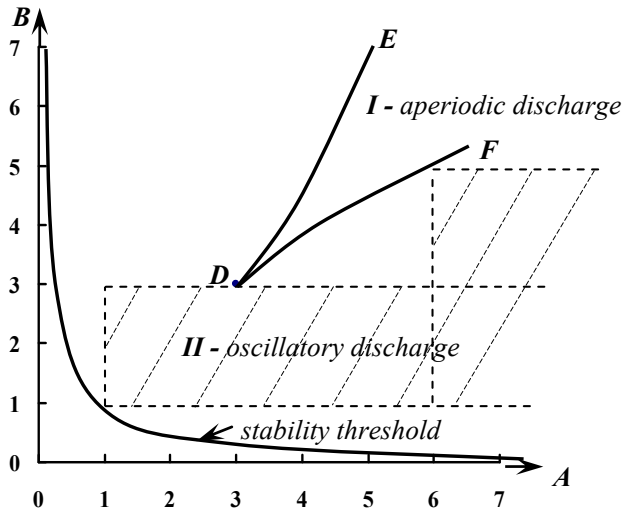


Fig. 2. Vyshnegradsky's diagram for the system, described by third-order differential equation

The stability region can be divided into separate parts corresponding to different combinations of the roots of the characteristic equation. It should be noted that at the point  $D$ , where  $A = 3$  and  $B = 3$ , the characteristic equation (14) takes the form  $(q + 1)^3 = 0$ . Consequently, at this point all three roots are equal  $q_1 = q_2 = q_3 = -1$ . In this case, for the initial equation (13), we obtain

$$p_1 = p_2 = p_3 = -\sqrt[3]{a_3/a_0}.$$

In the general case, two options are possible: 1) all three roots are real; 2) one root is real and two are complex. The boundary between these two cases is determined by the vanishing discriminant of the third-degree equation (14), which can be received, for example, from the Cardano's formula for solving the cubic equation:

$$A^2B^2 - 4(A^3 + B^3) + 18AB - 27 = 0.$$

This equation gives two curves in the plane of the  $A$  and  $B$  parameters:  $DE$ -curve and  $DF$ -one (Fig. 2). Inside of  $EDF$  region, the discriminant is positive. Consequently, in this region there are three real roots (region  $I$ ). In the remaining part of the plane, the discriminant is negative, which corresponds to the presence of a pair of complex roots (region  $II$ ).

In region  $I$ , where all roots are real, an aperiodic transient process takes place, and in region  $II$ , where there are one real and two complex roots, the transient process is oscillatory.

Calculating the value of Vyshnegradsky's parameters at changing the parameters of the discharge circuit (parameters of  $R_2L_2$ -chain connected to the capacitor), we can immediately conclude whether they are in the stability region of the system and if this is the case, then in which part of the region they are located (aperiodic discharge region  $I$  or oscillatory one  $II$ ).

Hence, when the load resistance increases stochastically during the discharge of the capacitor we can easily choose the necessary parameters  $R_2L_2$ -chain for connecting to the capacitor in order to prevent a long-term discharge with a low current without sparking in the load.

The investigations carried out in the installation for the volumetric electro-spark dispersion of aluminum in water with the following parameters:  $L_1 = 5 \mu\text{H}$ ,  $C = 100 \mu\text{F}$ , showed that resistance of the load, which is a layer of aluminum granules located between the electrodes, can vary within  $R_{load} = 0.2 - 5 \text{ Ohm}$ . Therefore, the  $Q$ -factor of the discharge circuit  $C-VT_1-R_{load}-L_1-C$ :  $Q_1$  can be in the range of  $1.118 - 0.045$ . That is, the discharge of the capacitor with certain changes in the load resistance can be aperiodic ( $Q_1 < 0.5$ ). That's why, it is necessary to connect an additional active-inductive chain in order to change the nature of the discharge process. The resistance  $R_2$  of such a chain takes into account the active resistances of both the wires of the inductive coil  $L_2$ , and the wires connecting this coil to the discharge circuit. This value is about  $0.001 \text{ Ohm}$ .

Fig. 3 shows the values of the Vyshnegradsky's parameters calculated using the software package Mathcad 12 for the discharge circuit  $C-VT_1-R_{load}-L_1-C$  with the parameters  $C = 10^{-4} \text{ F}$ ,  $L_1 = 5 \cdot 10^{-6} \text{ H}$ ,  $R_{load} = 5 \text{ Ohm}$ ,  $2.5 \text{ Ohm}$ , and  $1 \text{ Ohm}$ . The initial  $Q$ -factors are, respectively,  $Q_1 = 0.045$ ,  $0.089$ , and  $0.224$ , i.e. the capacitor discharge is aperiodic and for changing the discharge character it is necessary to connect an additional active-inductive chain. The resistance of the additional chain was assumed to be  $R_2 = 0,001 \text{ Ohm}$ , and the inductance value varied in the range  $L_2 = 10^{-7} \div 14 \cdot 10^{-4} \text{ H}$ .

According to Fig. 2 in zones defined by conditions, for example  $\begin{cases} A > 1 \\ 1 < B < 3 \end{cases}$  or  $\begin{cases} A > 6 \\ 1 < B < 5 \end{cases}$ , the discharge of

the capacitor when the additional active-inductive circuit is connected becomes an oscillatory. Further, according to the dependences shown in Fig. 3, the inductance values  $L_2$  satisfying the above conditions are determined.

The results of the analysis of the value ranges of the additional inductance  $L_2$ , which are required for the realization of the oscillatory discharge of the capacitor in the circuit with different load resistance, are given in Table. 1.

According to the proposed procedure, Vyshnegradsky's diagrams can be used to estimate the transient processes in the circuits of electrical discharge installations with different parameters and configuration.

Since the oscillatory discharge duration is proportional to the circuit inductance value, then in order to ensure short-term discharges, the appropriate values of  $L_2$  should be minimum values from corresponding ranges:  $103 \mu\text{H}$ ,  $48 \mu\text{H}$ ,  $15 \mu\text{H}$ .

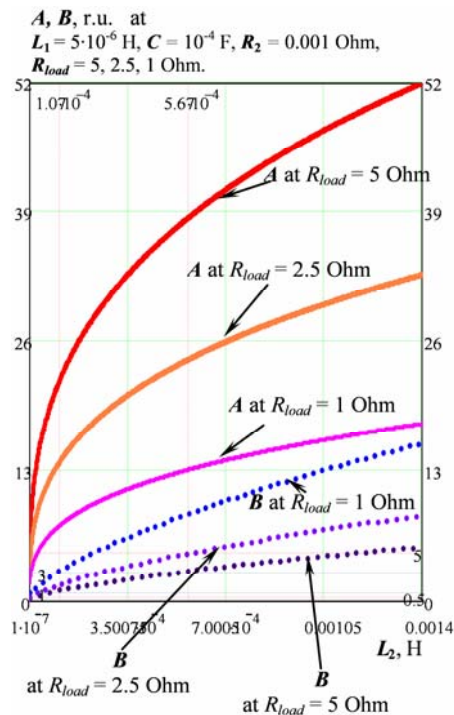


Fig. 3. The calculated values of the Vyshnegradsky's parameters for a discharge circuit with  $L_1 = 5 \cdot 10^{-6}$  H,  $C = 10^{-4}$  F,  $R_{load} = 5$  Ohm, 2.5 Ohm, 1 Ohm

Table 1  
Value ranges of additional inductance  $L_2$  for different load resistance  $R_{load}$

$R_{load}$ , Ohm	$L_2$ , $\mu$ H at $\begin{cases} A > 1 \\ 1 < B < 3 \end{cases}$	$L_2$ , $\mu$ H at $\begin{cases} A > 6 \\ 1 < B < 5 \end{cases}$
5	103 – 567	103 – 1240
2.5	48 – 281	48 – 617
1	15 – 109	55 – 242

### Conclusions.

1. In the discharge circuit of the capacitor of electric discharge installations whose load resistance can increase randomly, a low-current discharge (so-called idle discharge) through the load may occur. In order to transfer such a discharge into the required high-current and quickly damped discharge, we have connected the additional inductance to the discharge circuit.

2. To determine the value of the additional inductance, it is advisable to apply Vyshnegradsky's criteria and their graphic representations in the form of diagrams. This approach allows us to determine the range of values of such inductance for various load resistances in order to transfer aperiodic long-term capacitor discharge through the load in a short-term oscillatory discharge without solving a third-order differential equation.

3. As an example, we have performed a transient analysis in the discharge circuit of installation for volumetric electro-spark dispersion of the metals in a liquid with parameters  $C = 10^{-4}$  F,  $L_1 = 5 \cdot 10^{-6}$  H,  $R_2 = 0.001$  Ohm. We have calculated the Vyshnegradsky's parameters for load resistance of the installation  $R_{load} = 5$  Ohm, 2.5 Ohm, and 1 Ohm. Using the Vyshnegradsky's diagram, we have determined the ranges of the values of the additional

### How to cite this article:

Suprunovska N.I., Shcherba M.A. Application of Vyshnegradsky's diagrams for transient analysis in electric discharge installations with stochastic load. *Electrical engineering & electromechanics*, 2018, no.6, pp. 47-50. doi: 10.20998/2074-272X.2018.6.06.

inductance  $L_2$  for the realization of the oscillatory discharge of capacitor of the installation with a change in its stochastic load resistance.

Appropriate values of  $L_2$  are the minimum values from the corresponding ranges: 103  $\mu$ H, 48  $\mu$ H, 15  $\mu$ H.

### REFERENCES

- Shcherba A.A. *Printsipy postroeniia i stabilizatsii parametrov poluprovodnikovykh elektroimpul'snykh sistem elektroiskrovogo dispergirovaniia sloia tokoprovodiashchih materialov. Stabilizatsiia parametrov elektricheskoi energii*. [Principles of the construction and stabilization of the parameters of semiconductor electro-pulse systems of electro-spark dispersion of a layer of conductive materials. Stabilization of electrical energy parameters]. Kyiv, Institute of Electrodynamics of Academy of Sciences of Ukraine Publ., 1991, pp. 12-30. (Rus).
- Casanueva R., Azcondo F.J., Branas C., Bracho S. Analysis, Design and Experimental Results of a High-Frequency Power Supply for Spark Erosion. *IEEE Transactions on Power Electronics*, 2005, vol.20, no.2, pp. 361-369. doi: 10.1109/tpe.2004.842992.
- Sen B., Kiyawat N., Singh P.K., Mitra S., Ye J.H., Purkait P. Developments in electric power supply configurations for electrical-discharge-machining (EDM). *The Fifth International Conference on Power Electronics and Drive Systems PEDS 2003*. Singapore, 17-20 November 2003, vol.1, pp. 659-664. doi: 10.1109/PEDS.2003.1282955.
- Ivashchenko D.S., Shcherba A.A., Suprunovska N.I. Analyzing probabilistic properties of electrical characteristics in the circuits containing stochastic load. *Proceedings IEEE International Conference on Intelligent Energy and Power Systems (IEPS-2016)*, June 7-11, 2016, Kyiv, Ukraine, pp. 45-48. doi: 10.1109/IEPS.2016.7521887.
- Nguyen P.-K., Jin S., Berkowitz A. E. MnBi particles with high energy density made by spark erosion. *Journal of Applied Physics*, 2014, vol.115, no.17, p. 17A756. doi: 10.1063/1.4868330.
- Shcherba A.A., Suprunovska N.I. Study features of transients in the circuits of semiconductor discharge pulses generators with nonlinear electro-spark load. *Proceedings IEEE International Conference on Intelligent Energy and Power Systems (IEPS-2014)*, June 2-6, 2014, Kyiv, Ukraine, pp. 50-54. doi: 10.1109/IEPS.2014.6874200.
- Shydlovska N.A., Zakharchenko S.M., Cherkasky O.P. Physical prerequisites for constructing mathematical models of electrical resistance of plasma-erosion loadings. *Technical electrodynamics*, 2017, no.2, pp. 5-12. (Ukr). doi: 10.15407/techned2017.02.005.
- Shcherba A.A., Suprunovska N.I., Ivashchenko D.S. Modeling of nonlinear resistance of electro-spark load taking into account its changes during discharge current flowing in the load and at zero current in it. *Technical electrodynamics*, 2014, no.5, pp. 23-25. (Rus).
- Besekersky V.A., Popov Ye.P. *Teoriia sistem avtomaticheskogo regulirovaniia* [Theory of automatic control systems]. Moscow, Nauka Publ., 1975. 768 p. (Rus).
- Demirchian K.S., Neiman L.R., Korovkin N.V., Chechurin V.L. *Teoreticheskie osnovy elektrotehniki* [Theory of Electrical Engineering]. St. Petersburg, Piter Publ., 2009. 512 p. (Rus).

Received 21.07.2018

N.I. Suprunovska<sup>1</sup>, Doctor of Technical Science,

M.A. Shcherba<sup>1</sup>, Candidate of Technical Science,

<sup>1</sup>The Institute of Electrodynamics of the NAS of Ukraine,

56, prospect Peremogy, Kiev, 03057, Ukraine,

phone +380 44 3662493,

e-mail: iednat1@gmail.com, m.shcherba@gmail.com

K.V. Chunikhin

## ON THE INFLUENCE OF THE LEVEL OF AN EXTERNAL MAGNETIC FIELD AND THE LENGTH ON THE MAGNETIC MOMENT OF CYLINDRICAL CORES

**Purpose.** Analysis of inhomogeneous magnetization of long cylindrical permalloy 50N cores by a uniform constant magnetic field and the influence of length and field level on their magnetic moment. **Methodology.** The magnetostatic field of a non-uniformly magnetized in a uniform magnetic field long cylindrical core of an electromagnet of a spacecraft control system is considered. To calculate this field, a transformation of the integral equation with respect to the density of fictitious magnetic charges, as well as an iterative algorithm for its numerical solution, are proposed. **Results.** The convergence of the algorithm and the fact that the magnetic moment of the core depends heavily on its length and the level of the external magnetic field is shown. We have made an analysis of the influence of the length of a permalloy 50N core in the entire range of the magnetization curve and the level of a uniform external magnetic field on the axial projection of the magnetic moment of the core. **Originality.** The use of an almost equal distribution of the axial projection of the resulting magnetic field in the cross sections of the greater part of the cylindrical core and its division into cylindrical elements can significantly reduce the order of the system of algebraic equations approximating the integral equation for the surface density of fictitious magnetic charges for its numerical solution. **Practical value.** Recommendations regarding the level of the external field created by the electromagnet coil, the increase of the magnetic moment in cases of long cores and the choice of the number of cylindrical elements depending on the length of the core are given. References 14, tables 1, figures 5.

**Key words:** electromagnet, spacecraft control system, non-uniformly magnetized core, integral equation, fictitious magnetic charge, magnetization curve, magnetic moment of the core.

*Рассмотрено магнитостатическое поле неоднородно намагниченного в однородном магнитном поле длинного цилиндрического сердечника электромагнита системы управления космическим аппаратом. Для расчета этого поля предложены преобразование интегрального уравнения относительно плотности фиктивных магнитных зарядов, а также итерационный алгоритм его численного решения. Сделан анализ влияния длины сердечника из пермаллоя 50Н во всем диапазоне кривой намагничивания и уровня внешнего магнитного поля на осевую проекцию магнитного момента сердечника, а также даны практические рекомендации относительно уровня внешнего поля, создаваемого катушкой электромагнита, и увеличения магнитного момента в случаях длинных сердечников. Библи. 14, табл. 1, рис. 5.*

*Ключевые слова:* электромагнит, система управления космическим аппаратом, неоднородно намагниченный сердечник, интегральное уравнение, фиктивный магнитный заряд, кривая намагничивания, магнитный момент сердечника.

**Introduction.** To control the spacecraft, DC electromagnets consisting of a coil and a long cylindrical core of a material with high magnetic permeability are used [1]. Dimensions, winding data and materials can be determined and selected based on the calculation of the magnetic field generated by the electromagnet. Such an electromagnet must have a certain magnetic moment, the main part of which is provided by the core [2]. In the well-known works, for the calculation of the magnetostatic field of the cores the methods of demagnetization coefficients [2, 3] and integral equations [1, 4, 5] are developed. To determine the demagnetization coefficients, it is necessary to carry out experiments, and numerical solutions of integral equations were obtained under the assumption of a constant magnetic permeability of the core material [1, 4]. In [5], the calculations were performed under the condition of relatively small changes in the magnetic permeability along the core volume.

The relevance of this paper lies in the fact that in well-known works the magnetization of cylindrical cores is insufficiently investigated in conditions of large changes in magnetic permeability and levels of an external magnetic field, which makes it difficult to design electromagnets for spacecraft control systems.

**The goal** of the work is analysis of inhomogeneous magnetization of long cylindrical permalloy 50N cores by a uniform constant magnetic field and the influence of length and field level on their magnetic moment.

**Transformation of the original integral equation taking into account the peculiarities of the magnetization of the core.** Consider a cylindrical core of length  $b$  and of radius  $R$  located in an unbounded nonmagnetic and nonconducting space coaxially with an external constant uniform magnetic field of strength  $\vec{H}_0$  (Fig. 1).

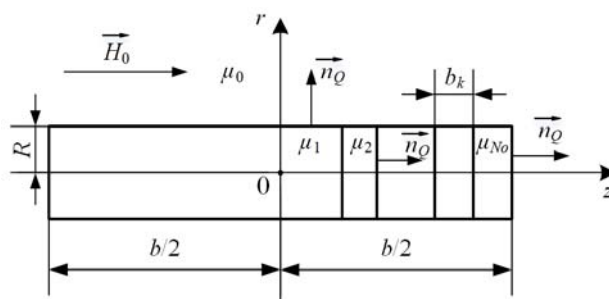


Fig. 1. Meridian section of the cylindrical core

The strength of the resulting magnetic field is represented as [6, 7]:

$$\vec{H} = \vec{H}_0 + \vec{H}_m, \quad (1)$$

where  $\vec{H}_m$  is the magnetic field strength due to the magnetic properties of the core («demagnetizing» field [2]).

The magnetic field  $\vec{H}$  is plane-meridian, and the vector field  $\vec{H}_m$  is potential and related to the scalar potential  $\varphi_m$  by

$$\vec{H}_m = -\text{grad } \varphi_m. \quad (2)$$

Using the electrostatic analogy [6, 8], we represent  $\varphi_m$  in the following form [9, 10]:

$$\varphi_m(Q) = \frac{1}{\pi\mu_0} \int_l \frac{\sigma_m(M)r_M K(k)}{\sqrt{(z_Q - z_M)^2 + (r_Q + r_M)^2}} dl_M, \quad (3)$$

where  $l, dl_M$  are the contour of the meridian section and its element with the center in the point  $M$ ;  $Q, M \in l$  are the observation point and the point with current coordinated;  $\sigma_m(M)$  is the surface density of fictitious magnetic charges;  $\mu_0$  is the magnetic constant;  $K(k)$  is the complete elliptic integral of the first kind of module  $k$  [11];

$$k = 2 \sqrt{\frac{r_Q r_M}{(z_Q - z_M)^2 + (r_Q + r_M)^2}};$$

$r_Q, r_M$  and  $z_Q, z_M$  are the radial and axial cylindrical coordinates of points  $Q$  and  $M$ .

Since the core material is isotropic, the relationship between  $\vec{H}$  and the magnetization  $\vec{J}$  is determined by the known dependence

$$\vec{J} = [\mu_r(H) - 1]\vec{H}, \quad (4)$$

where  $\mu_r(H)$  is the relative magnetic permeability.

To take into account the inhomogeneity of magnetization, we replace the nonlinear magnetized medium of the core with a piecewise homogeneous medium, which consists of  $2N_o$  homogeneous cylindrical elements with absolute magnetic permeability  $\mu_k$ ,

$k = \overline{1, N_o}$ , having a length  $b_k$ , and  $\sum_{k=1}^{N_o} b_k = b/2$  (Fig. 1).

Such a replacement allows to neglect volume fictitious magnetic charges and limit the definition of  $\sigma_m$ . In this case, the integral equation for  $\sigma_m$  takes the form [12]:

$$\begin{aligned} \sigma_m(Q) - \frac{\lambda_\mu}{\pi} \int_l \sigma_m(M) [S(Q, M) - S(Q, M')] dl_M = \\ = 2\mu_0 \lambda_\mu H_{0n}(Q), \end{aligned} \quad (5)$$

where  $l$  is the contour of the meridian section of the core in the first quarter of the coordinate plane  $zOr$ ;  $l = l_1 + l_2 + l_3$ ;  $l_{1,2}$  is the contour of the side and end surfaces;

$l_3 = \sum_{k=1}^{N_o-1} l_k^c$ ,  $l_k^c$  is the boundary between  $k$  and  $k+1$

cylindrical elements in the calculation region;  $H_{0n}(Q)$  is the normal projection of  $\vec{H}_0$  for  $Q \in l$ ;

$$\lambda_\mu = \begin{cases} (\mu_k - \mu_0)/(\mu_k + \mu_0), & Q \in l_1 \cup l_2; \\ (\mu_k - \mu_{k+1})/(\mu_k + \mu_{k+1}), & Q \in l_3; \end{cases}$$

$M'$  is the point symmetric to point  $M$  relative to the  $r$ -axis.

At  $Q \in l_1$  the first term of the kernel of the equation (5)

$S(Q, M) = \frac{k}{2} \sqrt{\frac{r_M}{r_Q^3}} \left[ K(k) + \frac{1}{k'^2} \left( \frac{r_M + r_Q}{2r_M} k^2 - 1 \right) E(k) \right]$ , and

at  $Q \in l_2 \cup l_3 - S(Q, M) = \frac{z_Q - z_M}{4\sqrt{r_Q^3 r_M}} \frac{k^3}{k'^2} E(k)$ , where  $E(k)$ ,

$k'$  is the complete elliptic integral of the second kind of modulus  $k$  and additional modulus of complete elliptic

integrals,  $k' = \sqrt{1 - k^2}$  [11]. The second term of the considered kernel  $S(Q, M')$  is determined by the same formulas as  $S(Q, M)$  if in them to replace the coordinates of the point  $M$  by  $M'$ .

The replacement of a non-uniformly magnetized core with a set of uniformly magnetized cylindrical elements was made on the basis of preliminary calculations, according to which at  $b/R \geq 16$  the axial projection of  $\vec{H}$  in the cross sections of the core along its entire length, except for small sections near the ends, is distributed almost uniformly. Considering this feature, as well as the well-known boundary condition about the jump of the normal projection of  $\vec{H}_m$  on the boundary between two magnetized media [13], we assume that  $\sigma_m$  is invariable for all  $l_k^c$ . Simplified by this assumption, equation (5) takes the following form:

$$\begin{aligned} \sigma_m(Q) - \frac{\lambda_\mu}{\pi} \int_{l-l_3} \sigma_m(M) [S(Q, M) - S(Q, M')] dl_M - \\ - \frac{\lambda_\mu}{\pi} \sum_{k=1}^{N_o-1} \sigma_m(M_k) \int_{l_k^c} [S(Q, M) - S(Q, M')] dl_M = \\ = 2\mu_0 \lambda_\mu H_{0n}(Q). \end{aligned} \quad (6)$$

The system of algebraic equations, with the help of which the integral equations are solved, for equation (6) has a much smaller order.

**An iterative algorithm for the numerical solution of a transformed integral equation.** The iteration algorithm cycle consists of the following main blocks. In the first block, for some initial values of  $\mu_k^{(0)}$ , we solve the integral equation (6). To do this, using the quadrature formula of rectangles, it was transformed into a system of algebraic equations of order  $N$  ( $N$  is the total number of nodes of the spatial mesh,  $N = N_1 + N_2 + N_3$ ,  $N_1$  is the number of nodes per  $l_1$ ,  $N_2$  - per  $l_2$ ,  $N_3$  - per  $l_3$ ,  $N_3 = N_o - 1$ ). When calculating each integral of the sum in the third term of the left-hand side of (6), 100 nodes were taken, and to take into account the edge effect at the cylinder ends, a non-uniform mesh was used. The obtained system of algebraic equations was solved by a direct method based on inverting the matrix of the left-hand sides and further multiplying the inverse matrix by a column vector of the right-hand sides.

In the second block we find the radial and axial projections of  $\vec{H}$

$$H_r(Q) = \frac{1}{2\pi\mu_0} \int_l \sigma_m(M) S_r(Q, M) dl_M, \quad (7)$$

$$H_z(Q) = H_0 + \frac{1}{2\pi\mu_0} \int_l \sigma_m(M) S_z(Q, M) dl_M, \quad (8)$$

and then the module of  $\vec{H}$  at each point inside the core.

In formulas (7) and (8), the functions  $S_r(Q, M)$  and  $S_z(Q, M)$  are determined using the same expressions as the kernel of the integral equation (5), respectively,  $Q \in I_1$  and  $Q \in I_2 \cup I_3$ .

In the third block, we determine average over the volume of each cylindrical element the relative and absolute magnetic permeabilities

$$\mu_{kr}^{-(j)} = \frac{2}{R^2 b_k} \int_{S_k} r_M \mu_r(M) dS_M, \quad \mu_k^{-(j)} = \mu_0 \mu_{kr}^{-(j)}, \quad (9, 10)$$

where  $S_k$  is the meridian area of the  $k$ -th cylindrical element;  $j$  is the iteration number.

To determine  $\mu_r$ , we use the magnetization curve of permalloy 50N [2]

$$J(H) = aH/(H + c), \quad (11)$$

from which with the help of a known connection between  $\vec{B}$ ,  $\vec{H}$  and  $\vec{J}$  on the basis of the model of magnetization by molecular currents, we find

$$\mu_r(H) = 1 + a/(H + c). \quad (12)$$

In dependencies (11), (12), shown using the logarithmic scale in Fig. 2 (a, b),  $J, H$  are the modules of  $\vec{J}$ ,  $\vec{H}$ ;  $a, c$  are the constants,  $a = 1.25 \cdot 10^6$  A/m,  $c = 40$  A/m.

Then we take  $\mu_k^{(j)} = \mu_k^{-(j)}$  and return to the first block of the algorithm. We continue iterations until the condition

$$|\mu_k^{(j)} - \mu_k^{(j-1)}| < \Delta, \quad j = 1, 2, \dots, n_{it}, \quad k = \overline{1, N_o}, \quad (13)$$

where  $\Delta$  is the specified discrepancy;  $n_{it}$  is the iteration number.

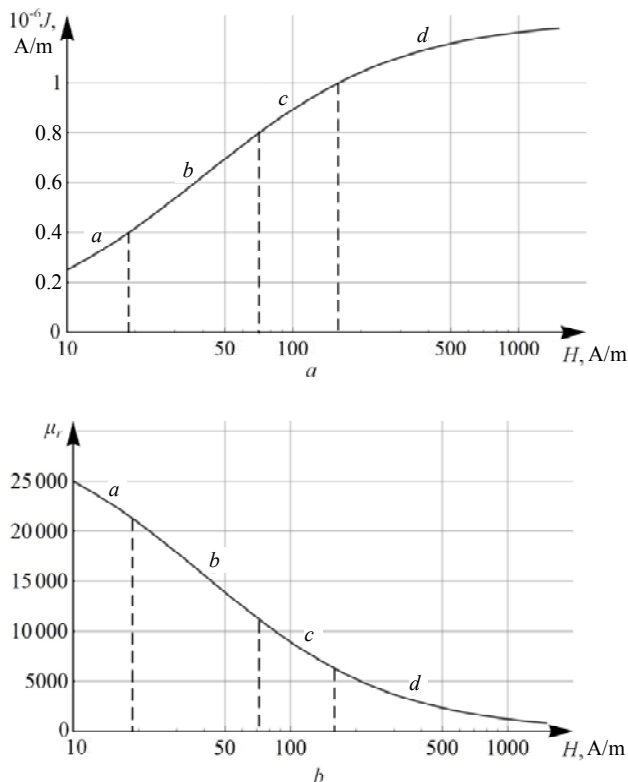


Fig. 2. Dependencies  $J(H) - a$  and  $\mu_r(H) - b$  for permalloy 50N

It is established that the iteration process converges to some values of  $\mu_k^{(it)}$  for any  $\mu_k^{(0)}$ , for which we have a numerical solution of (6). As explained below, the magnetic moment of the core is determined by the axial

projection of the magnetization  $J_z$ . After determining  $\sigma_m$  this projection can be calculated using formula (4), taking into account (8) and (12). The convergence of the iterations is illustrated by the curves in Fig. 3, constructed for the following initial data:  $R = 5$  mm (this size is assumed to be the same in subsequent calculations);  $b = 330$  mm;  $z^* = z/b$ . The values of  $b_k$  are hereinafter assumed to be the same. We see that with increasing  $N_o$ , the distributions of  $J_z$  converge. If it is necessary to clarify the influence of edge effects, the cylindrical elements at the edges of the core can be replaced by a set of ring elements. Note that in the work [5], when the integral equation regarding tangential projection of the magnetization was numerically solved in accordance with the recommendations of [14], the entire volume of the core was divided into ring elements.

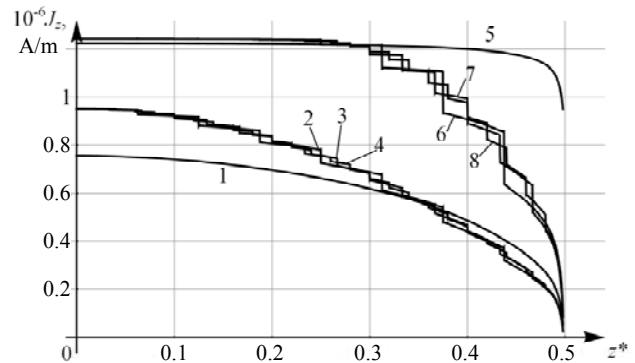


Fig. 3. Distribution of the axial projection of magnetization along the core axis at different  $N_o$  for  $H_0 = 1646.66$  A/m (curves 1-4) and  $H_0 = 6586.62$  A/m (curves 5-8); for curves 1 and 5, 2 and 6, 3 and 7, 4 and 8 values of  $N_o$  respectively equal to 1, 8, 15, 25

**The influence of the level of the external magnetic field and the length of the core on its magnetic moment.** Due to the axial symmetry of the field, the magnetic moment vector  $\vec{M}$  of the core under consideration has only an axial projection in cylindrical coordinates

$$M_z = 4\pi \int_S r_M J_z(M) dS_M, \quad (14)$$

where  $S$  is the part of the area of the meridian section in the positive half-plane  $z > 0$ .

Table 1 shows the values of  $M_z$  and the relative discrepancies  $\xi$  between  $M_z$  at  $N_o = 25$  (conventionally exact values) and  $M_z$  at smaller  $N_o$ . It follows from the above data that to ensure  $\xi \leq 1\%$  for all considered levels of  $H_0$  and values  $b = 80, 165$  and  $330$  mm,  $N_o$  should be taken equal to 4, 8 and 8, respectively. Note that for a core with a length 80 mm with  $N_o = 1$  the value of  $\xi \approx (1 \div 6)\%$  (obviously, this is also true for cores of not very different length).

Fig. 4, 5 show the influence of the level of the external field and the core length on the value of  $M_z$  (values of  $H_0$  are marked with dots on the abscissa axis in Fig. 4, and the corresponding values of  $M_z$  are shown on the curves). Calculations show that at each point of the core, with increasing  $H_0$  the strength of the resulting field always increases, but the magnetization depends on which

part of the magnetization curve  $H_z$  falls into (Fig. 2). In section  $a$  of the  $\mu_r(H)$  curve (Fig. 2, $b$ ), the magnetic permeability is maximum, which leads to large values of  $H_m$  and, as a consequence, small values of  $H$ . In the same part of the initial magnetization curve (Fig. 2, $a$ ), the latter corresponds to small values of  $J$ . At  $b = 80$  mm, this leads to relatively small magnetic moments  $M_z = 0.5 \div 2.8 \text{ A}\cdot\text{m}^2$  (Fig. 4, curve 1; Fig. 5).

Table 1

Values at different  $b, H_0, N_0$

$b, \text{ mm};$ $b/R$	$N_0$	$H_0, \text{ A/m}$			
		1646.66	3293.31	6586.62	9879.93
80; 16	25	0.500	0.989	1.937	2.845
	8	0.4998	0.9886	1.9342	2.8396
	$\xi, \%$	0.0392	0.0742	0.1348	0.1863
	4	0.499	0.986	1.926	2.822
	$\xi, \%$	0.150	0.294	0.562	0.803
	1	0.495	0.970	1.862	2.686
	$\xi, \%$	1.006	1.985	3.838	5.587
165; 33	25	3.090	5.927	10.839	13.043
	15	3.088	5.921	10.825	13.026
	$\xi, \%$	0.050	0.094	0.135	0.127
	8	3.083	5.904	10.776	12.972
	$\xi, \%$	0.213	0.396	0.585	0.540
	1	2.963	5.486	9.537	12.591
	$\xi, \%$	4.084	7.445	12.019	3.462
330; 66	25	17.863	25.330	28.394	29.546
	15	17.834	25.288	28.342	29.481
	$\xi, \%$	0.164	0.166	0.182	0.220
	8	17.765	25.186	28.202	29.331
	$\xi, \%$	0.551	0.568	0.677	0.728
	1	15.796	24.538	31.252	31.964
	$\xi, \%$	11.571	3.126	10.067	8.184

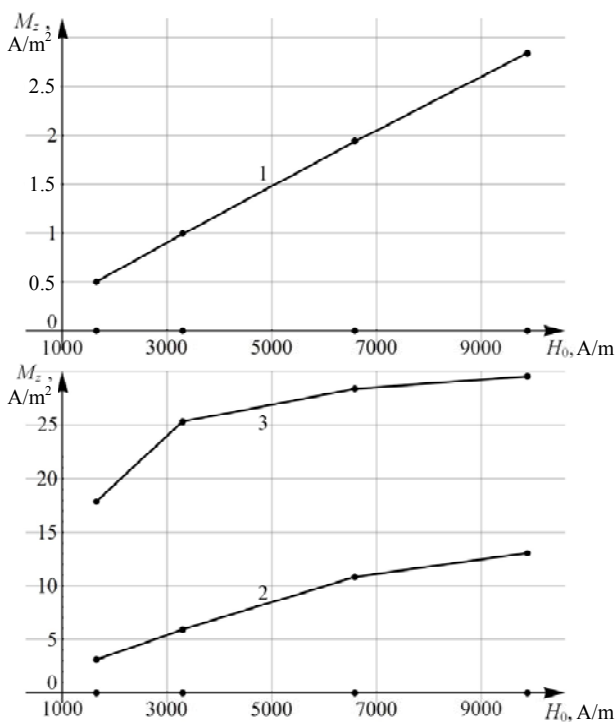


Fig. 4. Dependencies  $M_z(H_0)$  at  $N_0 = 25$ :  
curve 1 –  $b = 80$  mm, 2 –  $165$  mm, 3 –  $330$  mm

With an increase in the length of the core, we observe a significant increase in the magnetic moment (Fig. 4, curves 2, 3; Fig. 5), since the core points are magnetized either in all parts of the magnetization curve ( $b = 165$  mm), or in sections  $c, d$  ( $b = 330$  mm) with significantly larger  $J$  (Fig. 2, $a$ ). However, the growth of  $M_z$  of cores of greater length with increasing  $H_0$  slows down, since an increasing part of them is in a state of saturation. From Fig. 5 it follows that at  $b/R = (33 \div 66)$ , to achieve  $M_z \leq 18 \text{ A}\cdot\text{m}^2$ ,  $H_0 = 1646.66 \text{ A/m}$  is sufficient. For larger values of  $M_z$ , up to  $25 \text{ A}\cdot\text{m}^2$ ,  $H_0 = 3293.31 \text{ A/m}$  is required.

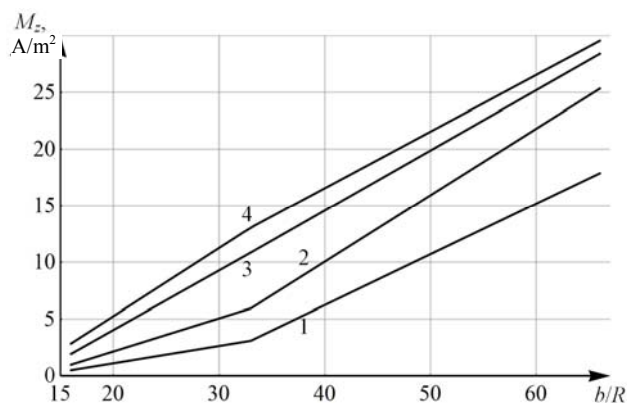


Fig. 5. Dependencies  $M_z(b/R)$  at  $N_0 = 25$ :  
curve 1 –  $H_0 = 1646.66 \text{ A/m}$ , 2 –  $3293.31 \text{ A/m}$ ,  
3 –  $6586.62 \text{ A/m}$ , 4 –  $9879.93 \text{ A/m}$

### Conclusions.

1. The choice of the sizes of the cylindrical cores of electromagnets of spacecraft control systems must be carried out on the basis of a given maximum value of the axial projection of the magnetic moment  $M_z$  and the magnetization curve of the core material.

2. The coil of an electromagnet should provide such levels of an external magnetic field at which the strength of the resulting magnetic field on the predominant part of the core is outside the saturation region of the magnetization curve and corresponds to a higher magnetization.

3. At  $R = 5$  mm, cores with a relative length of  $b/R < 33$  provide  $M_z \leq 13 \text{ A}\cdot\text{m}^2$ . In cases of  $b/R > 33$ , an increase in  $M_z$  can be achieved by increasing  $b/R$  at certain levels of the external magnetic field, which do not lead to the saturation of a significant part of the core (Fig. 4, 5).

### REFERENCES

1. Chadebec O., Rouve L.-L., Coulomb J.-L. New methods for a fast and easy computation of stray fields created by wound rods. *IEEE Transaction on Magnetics*, 2002, vol.38, no.2, pp. 517-520. doi: 10.1109/20.996136.
2. Kovalenko A.P. *Magnitnye sistemy upravleniia kosmicheskimi letatel'nymi apparatami* [Magnetic control systems for space vehicles]. Moscow, Mashinostroenie Publ., 1975. 248 p. (Rus).
3. Rozenblat M.A. Demagnetization factors for high permeability rods. *Technical Physics*, 1954, vol.24, no.4, pp. 637-661. (Rus).
4. Chen D.X., Pardo E., Sanchez A. Fluxmetric and magnetometric demagnetizing factors for cylinders. *Journal of Magnetism and Magnetic Materials*, 2006, vol.306, pp. 135-146. doi: 10.1016/j.jmmm.2006.02.235.

5. Matiuk V.F., Osipov A.A., Strelukhin A.V. Modeling of the magnetic state of a ferromagnetic rod in longitudinal constant magnetic field. *Technical Diagnostics and Non-Destructive Testing*, 2011, no.1, pp. 20-27. (Rus).
6. Grinberg G.A. *Izbrannyye voprosy matematicheskoi teorii elektricheskikh i magnitnykh iavlenii* [Selected questions of mathematical theory of electric and magnetic phenomena]. Moscow-Leningrad, Acad. of Sci. USSR Publ., 1948. 730 p. (Rus).
7. Tozoni O.V., Maergoiz I.D. *Raschet trekhmernykh elektromagnitnykh polei* [Calculation of three-dimensional electromagnetic fields]. Kiev, Tekhnika Publ., 1974. 352 p. (Rus).
8. Mikhailov V.M., Chunikhin K.V. On electrostatic analogy of magnetostatic field in inhomogeneous magnetized medium. *Electrical engineering & electromechanics*, 2017, no.5, pp. 38-40. (Rus). doi: **10.20998/2074-272X.2017.5.05**.
9. Jungerman J.A. Fourth-order uniform electric field form two charged rings. *Review of Scientific Instruments*, 1984, vol.55, no.9, pp. 1479-1482. doi: **10.1063/1.1137962**.
10. Mikhailov V.M. *Raschet elektricheskikh i magnitnykh polei s pomoshch'iu integral'nykh i integrodifferentsial'nykh uravnenii* [Calculation of electric and magnetic fields using integral and integrodifferential equations]. Kiev, UMC VO Publ., 1988. 60 p. (Rus).
11. Ianke E., Emde F., Lesh F. *Spetsial'nye funktsii* [Special functions]. Moscow, Nauka Publ., 1977. 344 p. (Rus).
12. Mikhailov V.M., Chunikhin K.V. Testing of numerical solution of the problem of determining sources of magnetostatic field in magnetized medium. *Electrical engineering & electromechanics*, 2017, no.6, pp. 42-46. (Rus). doi: **10.20998/2074-272X.2017.6.06**.
13. Polivanov K.M. *Teoreticheskie osnovy elektrotehniki, ch. 3. Teoriia elektromagnitnogo polia* [Theoretical foundations of electrical engineering, Part 3. Theory of electromagnetic field]. Moscow, Energiya Publ., 1969. 352 p. (Rus).
14. Kurbatov P.A., Arinchin S.A. *Chislennyi raschet elektromagnitnykh polei* [Numerical Calculation of Electromagnetic Fields]. Moscow, Energoatomizdat Publ., 1984. 168 p. (Rus).

*Received 16.08.2018*

*K.V. Chunikhin, Postgraduate Student,  
State Institution «Institute of Technical Problems  
of Magnetism of the NAS of Ukraine»,  
19, Industrialna Str., Kharkiv, 61106, Ukraine,  
phone +380 57 2992162,  
e-mail: kvchunikhin@gmail.com*

*How to cite this article:*

Chunikhin K.V. On the influence of the level of an external magnetic field and the length on the magnetic moment of cylindrical cores. *Electrical engineering & electromechanics*, 2018, no.6, pp. 51-55. doi: **10.20998/2074-272X.2018.6.07**.

M.I. Baranov

## A CHOICE OF SECTIONS OF ELECTRIC WIRES AND CABLES IN CIRCUITS OF DEVICES OF HIGH-VOLTAGE HIGH-CURRENT IMPULSE TECHNIQUE

**Purpose.** Implementation of calculation choice of sections of electric wires and cables in circuits of devices of high-voltage high-current impulse technique (HHIT), characterized flowing of pulsed current  $i_p(t)$  with different amplitude-temporal parameters (ATP). **Methodology.** Electrophysics bases of technique of high-voltage and high pulsed currents, theoretical bases of the electrical engineering, bases of electrical power engineering, technique of high electric and magnetic fields, and also measuring technique. **Results.** The results of the developed generalized electrical engineering investigations are resulted in a calculation choice on the condition of thermal resistibility of cable products of boundary permissible sections  $S_{Cil}$  of the electric uninsulated wires, and also insulated wires and cables with copper (aluminum) cores (shells) with polyvinyl chloride (PVC), rubber (R) and polyethylene (PET) insulation, on which in the circuits of HHIT the axial-flow of pulsed current  $i_p(t)$  flows with arbitrary ATP. On the basis of this approach the results of concrete choice of sections  $S_{Cil}$  are presented for the indicated electric wires (cables) of power circuits of HHIT with pulsed current, ATP of which with amplitudes of  $I_{mp} = (0.1-1000)$  kA change on an aperiodic law or law of damped sinusoid in nano-, micro- and millisecond temporal ranges. The results of calculation estimation present maximum permissible approximations of  $\delta_{Cil}$  of pulsed current  $i_p(t)$  of the examined temporal shapes in the indicated electric wires and cables of power circuits of HHIT. It is shown that the values of current approximations of  $\delta_{Cil}$  for the uninsulated copper (aluminum) wires in the nanosecond temporal range of ATP of pulsed currents  $i_p(t)$  are about 495 (293) kA/mm<sup>2</sup>, in the microsecond temporal range – 26 (15) kA/mm<sup>2</sup> and in a millisecond temporal range – 543 (320) A/mm<sup>2</sup>. By a calculation it is set that for the insulated wires (cables) with copper (aluminum) cores (shells) and PET with insulation the indicated current approximation of  $\delta_{Cil}$  is approximately: for the nanosecond range – 361 (233) kA/mm<sup>2</sup>; for the microsecond range – 19 (12) kA/mm<sup>2</sup>; for the millisecond range – 396 (256) A/mm<sup>2</sup>. **Originality.** Firstly by a calculation for the concrete temporal shapes of pulses of current  $i_p(t)$  in the discharge circuits of HHIT, changing in the wide range of the amplitudes  $I_{mp}$  on a aperiodic law or law of damped sinusoid, the numeral values of cross-sections  $S_{Cil}$  and current approximations of  $\delta_{Cil}$  are obtained for the uninsulated wires, insulated wires and cables with copper (aluminum) cores (shells) with PVC, R and PET insulation. **Practical value.** Application in practice of model tests of objects of electrical power engineering, aviation and space-rocket technique on resistibility to direct action of pulsed currents  $i_p(t)$  with different ATP of natural (currents of lightning) and artificial (discharge currents of HHIT) origin to increase electro-thermal resistibility of the electric uninsulated wires, and also the insulated wires and cables with PVC, R and PET insulation of HHIT widely applied in power circuits. References 13, tables 11, figures 2.

**Key words:** high-voltage high-current impulse technique, electric wires and cables, calculation choice of boundary permissible sections of wires and cables in the circuit of impulse technique.

*Приведены результаты разработанного обобщенного электротехнического подхода к расчетному выбору по условию термической стойкости предельно допустимых сечений  $S_{Cil}$  электрических неизолированных проводов, а также изолированных проводов и кабелей с поливинилхлоридной (ПВХ), резиновой (Р) и полиэтиленовой (ПЭТ) изоляцией с медными (алюминиевыми) жилами (оболочками), по которым в цепях высоковольтной сильнотоочной импульсной техники (ВСИТ) протекает аксиальный импульсный ток  $i_p(t)$  с произвольными амплитудно-временными параметрами (АВП). На основании данного подхода продемонстрированы результаты конкретного выбора сечений  $S_{Cil}$  для указанных электрических проводов (кабелей) силовых цепей ВСИТ с импульсным током, АВП которого с амплитудами  $I_{mp}=(0,1-1000)$  кА изменяются по аperiodическому закону или закону затухающей синусоиды в нано-, микро- и миллисекундному временных диапазонах. Представлены результаты расчетной оценки предельно допустимых плотностей  $\delta_{Cil}$  импульсного тока  $i_p(t)$  рассматриваемых временных форм в указанных электрических проводах и кабелях силовых цепей ВСИТ. Полученные результаты будут способствовать повышению электротермической стойкости электрических неизолированных проводов, а также изолированных проводов и кабелей с ПВХ, Р и ПЭТ изоляцией, широко применяемых в силовых цепях ВСИТ. Библи. 13, табл. 11, рис. 2.*

**Ключевые слова:** высоковольтная сильнотоочная импульсная техника, электрические провода и кабели, расчетный выбор предельно допустимых сечений проводов и кабелей в цепях импульсной техники.

**Introduction.** One of the challenges in the field of high-voltage high-current impulse technology (HHIT) is a reasonable choice of cross-sections  $S_C$  of used in it electrical wires and cables. It is known that in wires and cables in the area of HHIT can flow in normal and emergency modes of operation of such equipment pulsed currents  $i_p(t)$  with different amplitude-temporal parameters (ATP). In this case, the amplitudes  $I_{mp}$  of these currents can vary in the range from hundreds of amperes to thousands of kiloamperes, and their duration  $\tau_p$  varies from tens of nanoseconds to hundreds of milliseconds [1, 2]. The well-known approach for choosing sections  $S_C$  of electrical wires (cables) for short-term modes of their operation, used now in traditional industrial electric power engineering, is based on the thermal resistance of

cable-conductor products (CCP) under the conditions of a short circuit (SC) current acting on it with specified ATP [3]. In this case, the thermal resistibility of electrical wires and cables is limited by the maximum permissible short-term temperature  $\theta_{IS}$  of heating of the parts of wires (cables) at SC. In Table 1, according to the results of [3], the numerical values of the temperature  $\theta_{IS}$  of heating are given for the main conductive and insulating materials of electrical wires and cables at SC. From the data of Table 1 it can be seen that the value of  $\theta_{IS}$  should not exceed for used in power electric circuits with current frequency of 50 Hz uninsulated copper and aluminum cores (wires) in SC mode the highest level of 250 °C and 200 °C, and for

© M.I. Baranov

cables (insulated wires) with copper and aluminum cores and PVC (R), PET insulation, respectively, the level of 150 °C and 120 °C [3].

Table 1

The values of the maximum permissible short-term temperature  $\theta_{IS}$  of heating for the main conductor and insulation materials of wires (cables) of industrial electric power circuits under the action of SC [3]

No.	Name of the wire (cable) part	$\theta_{IS}$ , °C
1	Tire (core), copper, uninsulated at stresses less 20 N/mm <sup>2</sup>	250
2	Tire (core), aluminum, uninsulated at stresses less 10 N/mm <sup>2</sup>	200
3	Cable and insulated wire with copper (aluminum) cores and polyvinyl chloride (PVC) or rubber (R) insulation	150
4	Cable and insulated wire with copper (aluminum) cores and polyethylene (PET) Insulated	120
5	Aluminum part of the steel-aluminum wires of power lines	200

We point out that in the industrial electric power industry, the long-term permissible temperature  $\theta_{II}$  of heating the conductive and insulating parts of electrical wires and cables is limited by the conditions for reliable operation of electrical contacts and contact connections or by the conditions of their insulation [3]. In Table 2, according to the data of [3], the well-known numerical values of the heating temperature  $\theta_{II}$  for the main types of electrical wires and cables used in the field of modern power engineering are given.

Table 2

The values of long-term permissible temperature  $\theta_{II}$  for the main types of electrical wires (cables) [3]

No.	Name of the wire (cable) or the core	$\theta_{II}$ , °C
1	Wires (cores) uninsulated with any current-carrying tires (parts)	70
2	Cables (wires) with copper (aluminum) tires, PVC, R and PET insulation	65
3	Cables with impregnated cable insulation paper for voltage up to 6 kV	65
4	Cables with impregnated cable insulation paper for voltage up to 35 kV	50

From the data of Table 2 it follows that the maximum long-term permissible temperature  $\theta_{II}$  of heating for uninsulated wires and cables with PVC, PET and R insulation, which are under current load in industrial electric power circuits, should not exceed respectively the level of 70 °C and 65 °C. Taking into account the data of Table 1, 2, as well as the condition that the wire (cable) before the impulse effect of SC current on it was fully electrically loaded and had temperature  $\theta_{II}$ , and at SC it heated to temperature  $\theta_{IS}$ , in [3] to select the minimum permissible cross-section  $S_{Imin}$  of electrical wire (cable) wire the following calculated ratio is recommended:

$$S_{Imin} = B_k^{1/2} / C_k, \quad (1)$$

where  $B_k = \int_0^{t_k} i_k^2(t) dt$  is the Joule (action) integral of the SC

current  $i_k(t)$  with duration  $t_k$  (a technique of calculation of  $B_k$  is presented in [3]), A<sup>2</sup>·s;  $C_k$  is the coefficient (A·s<sup>1/2</sup>/mm<sup>2</sup>), whose numerical values are given in Table 3.

Table 3

The values of the coefficient  $C_k$  for the main types of electrical wires and cables of industrial electric power circuits under the action of SC [3]

No.	Name of the wire (cable) and the core	$C_k$ , A·s <sup>1/2</sup> /mm <sup>2</sup>
1	Wires (cores), copper, uninsulated	170
2	Wires (cores), aluminum, uninsulated	90
3	Cables (insulated wires) with PVC and R insulation and copper cores	120
4	Cables (insulated wires) with PVC and R insulation and aluminum cores	75
5	Cables (insulated wires) with PET insulation and copper cores	103
6	Cables (insulated wires) with PET insulation and aluminum cores	65

Taking into account the fact that ATP of pulsed currents  $i_p(t)$ , used in the field of HHIT, usually do not correspond to ATP of SC current in industrial electric network, application of (1) and data of Table 3 for the calculation determination of sections  $S_C$  of electrical wires (cables) in the HHIT circuits is essentially impossible technical way. In this regard, an approximate calculation of sections  $S_C$  of electrical wires and cables of HHIT for various ATPs of the pulsed current  $i_p(t)$  flowing through them is an actual applied scientific and technical problem.

**The goal of the paper** is performing a calculation selection of sections  $S_C$  of electrical wires and cables in circuits of HHIT devices, characterized by the flow of pulsed current  $i_p(t)$  with various ATPs.

**1. Problem definition.** We consider the widely used in electric circuits of HHIT uninsulated copper and aluminum wires, as well as insulated wires and cables with copper (aluminum) inner cores and outer shells, having PVC, R and PET insulation [1, 2]. It is assumed that in the round solid or split copper (aluminum) cores and shells of these wires and cables of HHIT electric circuits in their longitudinal direction pulsed currents  $i_p(t)$  flow, ATPs of which correspond to nano-, micro- or millisecond time ranges with amplitudes  $I_{mp}$ , varying in a wide range from 0.1 kA to 1 MA. We believe that the wires and cables under investigation are placed in the surrounding air environment, the temperature of which is  $\theta_0=20$  °C. We use the assumption that in the first approximation the pulsed current  $i_p(t)$  is almost uniformly distributed over the cross-section  $S_{Ci}$  of the core ( $i=1$ ) and the shell ( $i=2$ ) of the wire (cable). One of the rationales of this assumption is that, for example, for a current pulse of a short lightning discharge of the temporal shape  $\tau_f/\tau_p=10$   $\mu$ s/350  $\mu$ s ( $\tau_f$ ,  $\tau_p$  are, respectively, the front duration at the level (0.1-0.9)  $I_{mp}$  and the current pulse duration at the level of 0.5  $I_{mp}$ ) the penetration depth  $\Delta_i$  of the azimuthal magnetic field of the specified artificial lightning current into the studied non-ferromagnetic materials of the wire (cable) is approximately 0.65 mm for copper and 0.82 mm for aluminum [4]. These numerical values of  $\Delta_i$

in practice can be commensurate with the real radii of the core and the wall thickness of the wire (cable) shell. For current pulses  $i_p(t)$ , related to the millisecond time range (as for SC currents in circuits of power facilities), the use of such an assumption in the calculation of the cross-sections  $S_{Ci}$  of wires (cables) becomes even more legitimate. Let us take advantage of the adiabatic nature of pulsed current  $i_p(t)$  with a duration of no more than 1000 ms in the materials of the cores (shells) of the considered CCP of electrothermal processes, under which the influence of heat transfer from the surfaces of their current-carrying parts having the current temperature  $\theta_{Ci} \geq \theta_0$  and thermal conductivity of their materials and insulation on Joule heating of the current-carrying parts of the cores (shells) of wires (cables) is neglected. We believe that the thermal resistivity of wires (cables) of electric circuits of HHIT when exposed to a pulsed current  $i_p(t)$  is limited by their maximum permissible short-term heating temperature  $\theta_{CIS}$ , depending on the degree of reduction of the mechanical strength of the core (shell) material and the thermal conditions of operation conditions of the CCP insulation in the mode of its short-term heating by a current pulse of nano-, micro- or millisecond duration, flowing through their current-carrying parts. As in [4], we assume that the value of temperature  $\theta_{CIS}$  corresponds to the maximum permissible short-term temperature  $\theta_{IS}$  of heating wires and cables by SC currents of industrial frequency (see Table 1) known from [3]. Then, in accordance with the data of Table 1, for uninsulated copper (aluminum) wires of circuits of HHIT, the value of  $\theta_{CIS}$  will be approximately 250 °C (200 °C), for their insulated wires (cables) with copper and aluminum cores (shells) and PVC (R) insulation  $\theta_{CIS} \approx 150$  °C, and for their CCP with the indicated conductors (shells) and PET insulation  $\theta_{CIS} \approx 120$  °C. It is required by calculation in an approximate form to determine the boundary permissible cross-sections  $S_{Cil}$  of current-carrying parts for uninsulated copper (aluminum) wires, as well as for insulated wires and cables with copper (aluminum) cores (shells) and PVC (R), PET insulation, used in HHIT circuits and experiencing a direct axial pulsed current  $i_p(t)$  of various amplitudes  $I_{mp}$  in the nano-, micro- and millisecond time ranges.

**2. A generalized approach to the choice of sections  $S_{Cil}$  of electrical wires (cables) in the field of HHIT.** For the boundary permissible cross-sections  $S_{Cil}$  of the current-carrying cores (shells) of the considered electric wires and cables with axial pulsed current  $i_p(t)$  of arbitrary ATPs, the following approximate calculated dependence [5] follows from the equation of their heat balance in the adiabatic mode:

$$S_{Cil} = (J_{Cil})^{1/2} / C_l, \quad (2)$$

where  $J_{Cil} = \int_0^{\tau_p} i_p^2(t) dt$  is the action integral of the pulsed current  $i_p(t)$  with duration  $\tau_p$  and given ATPs,  $A^2 \cdot s$ ;  $C_l = (J_{CIS} - J_{Cil})^{1/2}$ ,  $A \cdot s^{1/2} / m^2$ ;  $J_{CIS}$ ,  $J_{Cil}$  are, respectively, the current integrals for the current-carrying cores (shells) of the studied electric wires and cables of the HHIT power circuits, the maximum permissible short-term and long-term heating temperatures of the material of which

correspond to  $\theta_{IS}$  (see Table 1) and  $\theta_{ll}$  (see Table 2) values,  $A^2 \cdot s / m^4$ .

To find the numerical values of the  $J_{CIS}$  and  $J_{Cil}$  current integrals included in (2), the following analytical expressions can be used [2, 5]:

$$J_{CIS} = \gamma_{0i} \beta_{0i}^{-1} \ln[c_{0i} \beta_{0i} (\theta_{IS} - \theta_0) + 1]; \quad (3)$$

$$J_{Cil} = \gamma_{0i} \beta_{0i}^{-1} \ln[c_{0i} \beta_{0i} (\theta_{ll} - \theta_0) + 1], \quad (4)$$

where  $\gamma_{0i}$ ,  $c_{0i}$ ,  $\beta_{0i}$  are, respectively, the specific electrical conductivity, the specific volume heat capacity and the thermal coefficient of specific electrical conductivity of the core (shell) material of the wire (cable) of the HHIT electrical circuit under study before they are subjected to a pulsed current  $i_p(t)$  with arbitrary ATPs.

Table 4 presents numerical values of  $\gamma_{0i}$ ,  $c_{0i}$  and  $\beta_{0i}$  at temperature  $\theta_0 = 20$  °C [2, 6].

Table 4

The main thermophysical characteristics of the material of the current-carrying cores (shells) of electric uninsulated wires and insulated wires as well as cables of power circuits of HHIT at  $\theta_0 = 20$  °C [2, 6]

Material of the core (shell) of the wire (cable)	Values $\gamma_{0i}$ , $10^7 \cdot (\Omega \cdot m)^{-1}$	Values $c_{0i}$ , $10^6 \cdot J / (m^3 \cdot ^\circ C)$	Values $\beta_{0i}$ , $10^{-9} \cdot m^3 / J$
Copper	5.81	3.92	1.31
Aluminum	3.61	2.70	2.14

As for the calculation definition in (2) of the integral of action  $J_{Cil}$  of the pulsed current  $i_p(t)$  with arbitrary ATPs, for the case of its change over time  $t$  according to the aperiodic law of the form

$$i_p(t) = k_{p1} I_{mp} [\exp(-\alpha_1 t) - \exp(-\alpha_2 t)], \quad (5)$$

where  $\alpha_1 \approx 0.76 / \tau_p$ ,  $\alpha_2 \approx 2.37 / \tau_f$  are, respectively, the shape coefficients of the aperiodic current pulse with given ATPs flowing in the electric circuit of the HHIT;  $k_{p1} = [(\alpha_1 / \alpha_2)^m - (\alpha_1 / \alpha_2)^n]^{-1}$  is the normalization factor;  $m = \alpha_1 / (\alpha_2 - \alpha_1)$ ;  $n = \alpha_2 / (\alpha_2 - \alpha_1)$ ; the calculated expression for the integral of action  $J_{Cil}$  of the current pulse  $i_p(t)$  flowing in the HHIT circuit takes the following convenient analytical form [7]:

$$J_{Cil} \approx k_{p1}^2 I_{mp}^2 [0.658 \tau_p - 0.633 \tau_f], \quad (6)$$

where  $\tau_f$ ,  $\tau_p$  are respectively, the durations of the front and the half-fall of the current pulse  $i_p(t)$ .

In the case of a change in time  $t$  of the acting on the materials of the wire (cable) of the HHIT pulsed current  $i_p(t)$  according to the law of a damped sinusoid of the form

$$i_p(t) = k_{p2} I_{mp1} \exp(-\delta t) \sin(\omega t), \quad (7)$$

where  $\delta = \Delta_p / T_p$  is the current attenuation coefficient;  $\omega = 2\pi / T_p$  is the circular frequency of the current oscillations;  $T_p$  is the period of the current oscillations;  $\Delta_p = \ln(I_{mp1} / I_{mp3})$  is the logarithmic decrement of pulsed current oscillations with the first  $I_{mp1}$  and the third  $I_{mp3}$  amplitudes in the HHIT circuit;  $k_{p2} = [\exp(-\Delta_p / 2\pi \arctg \Delta_p / 2\pi) \cdot \sin(\arctg \Delta_p / 2\pi)]^{-1}$  is the normalization factor for damped sinusoidal current; the calculated expression for the integral of action  $J_{Cil}$  of the current pulse  $i_p(t)$  flowing in the HHIT circuit takes the following simple analytical form [5]:

$$J_{Cil} \approx k_{p2}^2 I_{mp1}^2 [T_p (4\Delta_p)^{-1} - \Delta_p T_p (4\Delta_p^2 + 16\pi^2)^{-1}]. \quad (8)$$

From (4) it can be seen that at  $\theta_{iI}=\theta_0=20^\circ\text{C}$  (wires and cables are de-energized) the value of the current integral  $J_{CiI}=0$ , which will lead by (2) to a decrease in the cross-section  $S_{CiI}$ .

Knowing from normative documents or experimental data the numerical values of  $I_{mp}$ ,  $\tau_f$ ,  $\tau_p$ ,  $\Delta_p$ ,  $T_p$ , taking into account the estimates of the values of the normalizing coefficients  $k_{p1}$  and  $k_{p2}$  by (2)-(8) for the specified temporal shapes of the pulsed current  $i_p(t)$ , we can calculate in the approximate form (with an error of up to 5 %), the boundary permissible cross-sections  $S_{CiI}$  of the conductive wires (shells) of wires and cables used in the electric circuits of HHIT. Finding the values of the  $S_{CiI}$  sections, taking into account the accepted assumptions, the maximum permissible pulsed current densities of the pulsed current  $i_p(t)$  of one or another shape in electrical wires (cables) of the HHIT circuits can be determined in the first approximation from the dependence like  $\delta_{CiI}\approx I_{mp}/S_{CiI}$ .

**3. The choice of cross-sections  $S_{CiI}$  of electrical wires (cables) for nanosecond current pulses in the field of HHIT.** First, we will focus on the selection of the  $S_{CiI}$  sections of the wires (cables) under consideration, along copper (aluminum) cores (shells) under the conditions  $J_{CiI}=0$  or  $J_{CiI}\neq 0$ , the axial aperiodic current pulse of the time shape  $\tau/\tau_p=5\text{ ns}/200\text{ ns}$  flows [8]. Note that at one time this nanosecond current pulse  $i_p(t)$  of both polarities was used when imitating in HHIT discharge circuits with the necessary air field-formation systems and, accordingly, in their working air volumes with powerful electromagnetic pulse (EMP) dimensions of the high-altitude nuclear explosion (HNE) [9, 10]. From (5) we find that for this calculation case, the form coefficients  $\alpha_1$  and  $\alpha_2$  of the current pulse  $i_p(t)$  take the following numerical values:  $\alpha_1\approx 3.8\cdot 10^6\text{ cs}^{-1}$ ;  $\alpha_2\approx 4.7\cdot 10^8\text{ s}^{-1}$ . Here, for this current pulse, the normalizing coefficient  $k_{p1}$  is approximately equal to  $k_{p1}\approx 1.049$ . Table 5 presents by (6) the numerical values of the action integral  $J_{CiA}$  for a series of values of the amplitude  $I_{mp}$  of the considered powerful nanosecond current pulse of the time shape 5 ns/200 ns used in testing military and civilian objects for resistibility to EMP of HNE [9, 10].

Table 5

The values of the integral of action  $J_{CiA}$  for nanosecond aperiodic current pulse of the shape 5 ns/200 ns

The value of the amplitude $I_{mp}$ of the current pulse of the shape 5 ns/200 ns, kA	The value of the integral of action $J_{CiA}$ of the current pulse 5 ns/200 ns, $\text{A}^2\cdot\text{s}$
1	0.141
10	14.13
30	$1.27\cdot 10^2$
50	$3.53\cdot 10^2$
70	$6.92\cdot 10^2$
100	$1.41\cdot 10^3$
200	$5.65\cdot 10^3$
500	$3.53\cdot 10^4$
1000	$1.41\cdot 10^5$

Table 6 shows the calculated by (2) the numerical values of the coefficient  $C_i$  for uninsulated wires with copper (aluminum) cores and insulated wires (cables)

with copper (aluminum) cores (shells) with PVC, R and PET insulation for the cases of their preliminary current load ( $J_{CiI}\neq 0$ ) or full de-energizing ( $J_{CiI}=0$ ).

Comparison of data of Table 3, 6 indicates that the numerical values of the coefficients  $C_k$  и  $C_i$  for the considered wires and cables in the case when  $J_{CiI}\neq 0$  and the value of this integral of the current is determined from (4) differ from 3 to 8 %. In the case when  $J_{CiI}=0$  (the case traditional for HHIT), these differences increase and range from 9 to 26 %. In Table 7 based on (2) and calculated data of Table 5, 6 at  $J_{CiI}=0$  (wires and cables in the HHIT power circuit are without prior current load) the results of the selection of the boundary permissible cross-sections  $S_{CiI}$  for the wires (cables) in the HHIT circuits under study, along which a powerful nanosecond current pulse of the time shape of 5 ns/200 ns with amplitude  $I_{mp}$  equal to 10, 50, 100, and 500 kA are presented.

Table 6

The values of the coefficient  $C_i$  values for uninsulated wires, insulated wires (cables) with copper (aluminum) cores (shells) in HHIT circuits with nano-, micro- and millisecond current pulses

Insulation type in the wire (cable) of the HHIT power circuit	Material of the core (shell) of the wire (cable)	Values of $C_i$ , $10^8\text{ A}\cdot\text{s}^{1/2}/\text{m}^2$	
		$J_{CiI}=0$	$J_{CiI}\neq 0$
Without insulation	Copper	1.860	1.563
	Aluminum	1.096	0.880
PVC, R	Copper	1.506	1.160
	Aluminum	0.972	0.745
PET	Copper	1.355	0.957
	Aluminum	0.877	0.616

Table 7

The values of the boundary permissible cross-sections  $S_{CiI}$  for wires (cables) with copper (aluminum) cores (shells) in HHIC circuits with a nanosecond current pulse of the shape 5 ns/200 ns, the amplitude of which varies in a wide range from 10 kA to 500 kA

Insulation type in the wire (cable) of the HHIT power circuit	Material of the core (shell) of the wire (cable)	Values of the cross-section $S_{CiI}$ , $\text{mm}^2$			
		Amplitude $I_{mp}$ of the current pulse 5 ns/200 ns, kA			
		10	50	100	500
Without insulation	Copper	0.020	0.101	0.202	1.010
	Aluminum	0.034	0.171	0.342	1.714
PVC, R	Copper	0.025	0.125	0.250	1.250
	Aluminum	0.039	0.193	0.386	1.933
PET	Copper	0.028	0.138	0.278	1.386
	Aluminum	0.043	0.214	0.428	2.142

From the data of Table 7 it follows that the estimated maximum allowable density  $\delta_{CiI}\approx I_{mp}/S_{CiI}$  of a nanosecond current pulse of the shape 5 ns/200 ns for uninsulated wires with copper and aluminum cores is approximately 495 kA/mm<sup>2</sup> and 293 kA/mm<sup>2</sup>, and for cables with copper (aluminum) cores (shells) and PET insulation 361 (233) kA/mm<sup>2</sup>.

**4. The choice of cross-sections  $S_{CiI}$  of electrical wires (cables) for microsecond current pulses in the field of HHIT.** Fig. 1 shows a typical oscillogram of a

pulsed  $A$ - component of an artificial lightning current reproduced in the discharge circuit of a powerful lightning current generator (LCG) for testing aeronautical and rocket-space technology objects for lightning resistibility in accordance with the requirements of US SAE ARP 5412: 2013 [11] and SAE ARP 5416: 2013 [12]. It can be seen that the indicated component of the pulsed current  $i_p(t)$  of the lightning simulated under laboratory conditions in time  $t$  varies according to the damped sinusoid law. We make the choice of cross-sections  $S_{Cil}$  of wires and cables for the discharge circuit of the LCG applicable to a given current pulse  $i_p(t)$ .

From the experimental data presented in Fig. 1, we find that for the bipolar oscillatory current pulse used in the calculations of the cross-sections  $S_{Cil}$ ,  $\Delta_p = \ln(I_{mp1}/I_{mp3}) = 2.505$ . Then by (7) for this current the coefficient  $k_{p2} = 1.731$ . Table 8 shows the numerical values of the integral of action  $J_{CIA}$  calculated by (8) for a given microsecond current pulse [13], changing according to the law of a damped sinusoid.

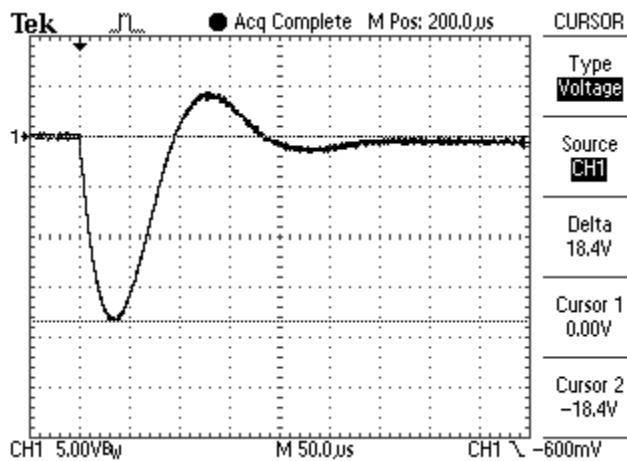


Fig. 1. A typical oscillogram of a microsecond pulsed  $A$ - component of an artificial lightning current flowing in a discharge circuit of a high-voltage LCG ( $I_{mp1} \approx -207$  kA;  $I_{mp3} \approx -16.9$  kA;  $T_p \approx 185$   $\mu$ s; vertical scale 56.3 kA/division; horizontal scale 50  $\mu$ s/division) [13]

Table 8

The values of the integral of action  $J_{CIA}$  for current pulse  $i_p(t)$ , changing in the microsecond time range according to the law of damped sinusoid of the form (7)

The value of the first amplitude $I_{mp1}$ of the damped sinusoidal current pulse, kA	The value of the integral of action $J_{CIA}$ of the current pulse of the form (7), $A^2 \cdot s$
10	$4.77 \cdot 10^3$
30	$4.29 \cdot 10^4$
50	$1.19 \cdot 10^5$
70	$2.34 \cdot 10^5$
100	$4.77 \cdot 10^5$
207	$2.05 \cdot 10^6$
300	$4.29 \cdot 10^6$
500	$11.92 \cdot 10^6$
700	$23.4 \cdot 10^6$
1000	$47.7 \cdot 10^6$

Using the calculated data for the coefficient  $C_b$ , given in Table 6, (2) and summarized in Table 8 the results of determining the integral of action  $J_{CIA}$ , we find

the boundary permissible cross-sections  $S_{Cil}$  for the wires (cables) under study in HHIT circuits, in which a microsecond current pulse of the form (7) flows with ATPs corresponding to the data typical of Fig. 1. In Table 9 at  $J_{Cil} = 0$ , the results of such a determination of the boundary permissible cross-sections of  $S_{Cil}$  for the wires and cables under consideration used in the discharge circuits of HHIT are presented.

From the presented in Table 9 the calculated data, it follows that the estimated maximum allowable density  $\delta_{Cil} \approx I_{mp1}/S_{Cil}$  of the microsecond pulsed current  $i_p(t)$  with the ATP corresponding to the data in Fig. 1, for uninsulated wires with copper and aluminum cores is approximately 26 kA/mm<sup>2</sup> and 15 kA/mm<sup>2</sup>, and for cables with copper (aluminum) cores (shells) and PET insulation 19 (12) kA/mm<sup>2</sup>.

Table 9

The values of the boundary permissible  $S_{Cil}$  cross-sections for wires (cables) with copper (aluminum) cores (shells) in HHIT circuits with a microsecond current pulse of the form (7), the first amplitude  $I_{mp1}$  of which varies in a wide range from 30 kA to 207 kA

Insulation type in the wire (cable) of the HHIT power circuit	Material of the core (shell) of the wire (cable)	The values of the cross-section $S_{Cil}$ , mm <sup>2</sup>			
		The first amplitude $I_{mp1}$ of the current pulse of the form (7), kA			
		30	50	100	207
Without insulation	Copper	1.113	1.854	3.713	7.698
	Aluminum	1.889	3.147	6.301	13.06
PVC, R	Copper	1.375	2.290	4.586	9.507
	Aluminum	2.131	3.549	7.105	14.73
PET	Copper	1.528	2.546	5.097	10.57
	Aluminum	2.362	3.933	7.875	16.32

**5. The choice of cross-sections  $S_{Cil}$  of electrical wires (cables) for millisecond current pulses in the field of HHIT.** Fig. 2 shows a typical oscillogram of a long-term  $C$ -component of the artificial lightning current generated according to the requirements of [11, 12] in the discharge circuit of the LCG for the purpose of the experimental determination of lightning resistibility of aerospace equipment objects in flight conditions in air. It can be seen that the aperiodic current pulse  $i_p(t)$  of the negative polarity of this component in the composition of the total artificial lightning discharge current varies in a millisecond time range. Its amplitude  $I_{mp}$  which corresponds to the time  $t_{mp} \approx 11$  ms, is about 835 A. At the same time, the duration of the front of the test current pulse is approximately  $\tau_f \approx 7$  ms, and its duration at the level of  $0.5 I_{mp}$  is  $\tau_p \approx 160$  ms. According to the requirements of [11, 12], the total duration of the flow of the specified component of the current pulse of artificial lightning in the conductors of the discharge circuit of a powerful high-voltage LCG reaches about 1000 ms. On the basis of the proposed electrical engineering approach, we perform the choice of cross-sections  $S_{Cil}$  of wires (cables) for a discharge circuit of the LCG involved in generating the specified current pulse  $i_p(t)$ .

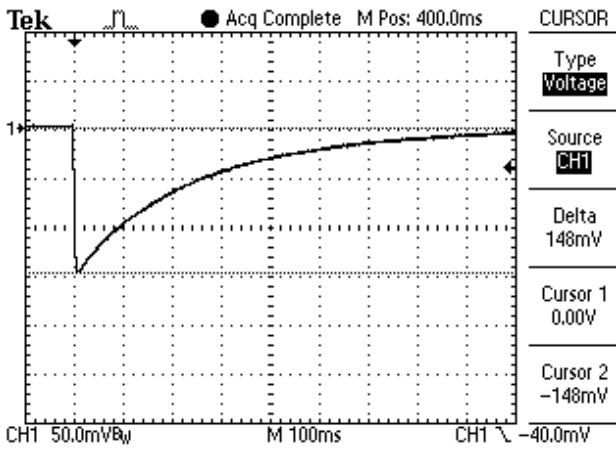


Fig. 2. A typical oscillogram of a millisecond long-term C-component of an artificial lightning current flowing in a discharge circuit of a powerful high-voltage LCG ( $I_{mp} \approx -835$  A;  $\tau_f \approx 7$  ms;  $\tau_p \approx 160$  ms; vertical scale 282 A/division; horizontal scale 100 ms/division) [13]

From (5) at  $\tau_f \approx 7$  ms and  $\tau_p \approx 160$  ms, we find that  $\alpha_1 \approx 4.75$  s<sup>-1</sup> and  $\alpha_2 \approx 338 \cdot 10^2$  s<sup>-1</sup>. Then the normalizing coefficient  $k_{p1}$  takes a numerical value of approximately  $k_{p1} \approx 1.077$ . Using (5) and varying the value of the current amplitude  $I_{mp}$ , it is possible to calculate the numerical indices of the integral of action  $J_{CIA}$  for the considered millisecond current pulse  $i_p(t)$ . Table 10 shows the numerical values of  $J_{CIA}$  for a number of amplitudes of  $I_{mp}$  of a given pulse current  $i_p(t)$ .

Table 10

Values of the integral of action  $J_{CIA}$  for unipolar current pulse  $i_p(t)$ , varying in millisecond time range by aperiodic low

The values of the amplitude $I_{mp}$ of the unipolar millisecond aperiodic current pulse 7 ms/160 ms, A	The values of the integral of action $J_{CIA}$ of the millisecond current pulse 7 ms/160 ms, A <sup>2</sup> ·s
100	$1.17 \cdot 10^3$
200	$4.68 \cdot 10^3$
300	$1.05 \cdot 10^4$
500	$2.92 \cdot 10^4$
700	$5.73 \cdot 10^4$
835	$8.15 \cdot 10^4$
1000	$1.17 \cdot 10^5$

Further, assuming that  $J_{Cil}=0$  (the wires and cables in the discharge circuit of HHIT are previously de-energized), we use the results of an approximate calculation of the coefficient  $C_l$ , summarized in Table 6. Taking into account these numerical values of  $C_l$  and the data of Table 10, according to (2), in the accepted approximation, it is possible to find the boundary permissible cross-sections  $S_{Cil}$  for uninsulated and insulated wires and cables with copper (aluminum) cores (shells) with PVC, R and PET insulation, which are subjected to an axial millisecond aperiodic current pulse  $i_p(t)$ , which ATPs correspond to the data of Fig. 2. Table 11 shows the numerical values of the boundary permissible cross-sections  $S_{Cil}$  for the indicated wires (cables) with a millisecond aperiodic current pulse  $i_p(t)$ , found in the manner described above. Based on the ratio of the form  $\delta_{Cil} \approx I_{mp}/S_{Cil}$ , the data of Table 11 allow us to estimate the

numerical values of the maximum permissible densities  $\delta_{Cil}$  in wires (cables), through which a millisecond aperiodic current pulse  $i_p(t)$  with amplitude  $I_{mp}$ , varying in the range (100-1000) A, flows in the longitudinal direction.

Table 11

The values of boundary allowable cross-sections  $S_{Cil}$  for uninsulated wires and insulated wires (cables) with copper (aluminum) cores (shells) in HHIT circuits with a millisecond aperiodic current pulse of 7 ms/160 ms, amplitude  $I_{mp}$  of which varies in the range from 100 A to 1000 A

Insulation type in the wire (cable) of the HHIT power circuit	Material of the core (shell) of the wire (cable)	The value of the cross-section $S_{Cil}$ , mm <sup>2</sup>			
		Amplitude $I_{mp}$ of the current pulse 7 ms/160 ms, A			
		100	500	835	1000
Without insulation	Copper	0.184	0.919	1.535	1.839
	Aluminum	0.312	1.559	2.605	3.121
PVC, R	Copper	0.227	1.135	1.896	2.271
	Aluminum	0.352	1.758	2.937	3.519
PET	Copper	0.252	1.261	2.107	2.524
	Aluminum	0.390	1.948	3.255	3.900

From the data of Table 11 it follows that the estimated maximum permissible density  $\delta_{Cil}$  of the millisecond aperiodic current pulse  $i_p(t)$  with the ATPs corresponding to the data in Fig. 2, for uninsulated wires with copper and aluminum conductors is approximately 543 A/mm<sup>2</sup> and 320 A/mm<sup>2</sup>, and for cables with copper (aluminum) cores (shells) and PET insulation 396 (256) A/mm<sup>2</sup>.

The results of experimental studies in discharge circuits of HHIT with pulsed currents  $i_p(t)$  of micro- and millisecond duration of electrothermal resistibility of prototypes of uninsulated wires, insulated wires and cables with copper cores (shells) with PVC and PET insulation, presented by the author in [5, 13], confirm the validity of the basic calculation data on the choice of the cross-sections  $S_{Cil}$  presented in Table 9, 11.

### Conclusions.

1. The presented generalized electrical engineering approach allows, according to the condition of thermal resistibility of CCP, to carry out an approximate calculation choice of boundary permissible cross-sections  $S_{Cil}$  of uninsulated wires, insulated wires and cables with copper (aluminum) cores (shells) with PVC, R and PET insulation, the current-carrying parts of which are affected axial current pulse  $i_p(t)$ , ATPs of which with different amplitudes  $I_{mp}$  can vary in nano-, micro- and millisecond time ranges.

2. Using the examples of the change in time  $t$  of the pulsed current  $i_p(t)$  flowing through the specified wires (cables) according to aperiodic law or the damped sinusoid law, the possibilities of the proposed electrical engineering approach to the specific choice of the boundary permissible cross-sections  $S_{Cil}$  for the considered types of uninsulated wires, insulated wires and cables widely used in the discharge circuits of HHIT are demonstrated.

3. It is shown that, in the first approximation, the maximum permissible densities  $\delta_{Cil} \approx I_{mp}/S_{Cil}$  of the

considered temporal shapes of pulsed current  $i_p(t)$  in copper (aluminum) cores of non-insulated wires for the nanosecond range are numerically about 495 (293) kA/mm<sup>2</sup>, for the microsecond range 26 (15) kA/mm<sup>2</sup> and for the millisecond range 543 (320) A/mm<sup>2</sup>. For insulated wires (cables) with copper (aluminum) cores (shells) and PET insulation, the numerical values of the maximum permissible densities  $\delta_{Cil}$  of the considered pulsed currents  $i_p(t)$  for the nanosecond range are about 361 (233) A/mm<sup>2</sup>, for the microsecond range 19 (12) kA/mm<sup>2</sup> and for the millisecond range 396 (256) A/mm<sup>2</sup>.

#### REFERENCES

1. Mesiats G.A. *Impul'snaia energetika i elektronika* [Pulsed power and electronics]. Moscow, Nauka Publ., 2004. 704 p. (Rus).
2. Baranov M.I. *Izbrannye voprosy elektrofiziki. Tom 3: Teorija i praktika elektrofizicheskikh zadach* [Selected topics of Electrophysics. Vol. 3: Theory and practice of electrophysics tasks]. Kharkiv, Tochka Publ., 2014. 400 p. (Rus).
3. Orlov I.N. *Elektrotehnicheskij spravochnik. Proizvodstvo i raspredelenie elektricheskoi energii. Tom 3, Kn. 1* [Electrical engineering handbook. Production and distribution of electric energy. Vol. 3, Book 1. Ed. I.N. Orlov]. Moscow, Ergoatomizdat Publ., 1988. 880 p. (Rus).
4. Baranov M.I., Rudakov S.V. Electrothermal action of the pulse of the current of a short artificial-lightning stroke on test specimens of wires and cables of electric power objects. *Journal of Engineering Physics and Thermophysics*, 2018, vol.91, no.2, pp. 544-555. doi: 10.1007/s10891-018-1775-2.
5. Baranov M.I., Kravchenko V.I. Electrothermal resistance wire and cable to the aircraft to the striking action pulsed current lightning. *Elektrichestvo*, 2013, no.10, pp. 7-15. (Rus).
6. Knopfel' G. *Sverkhshil'nye impul'snye magnitnye polia* [Ultra strong pulsed magnetic fields]. Moscow, Mir Publ., 1972. 391 p. (Rus).
7. Baranov M.I., Kniaziev V.V., Rudakov S.V. Calculation and experimental estimation of results of electro-thermal action of rationed by the international standard IEC 62305-1-2010 impulse current of short blow of artificial lightning on the thin-walled coverage from stainless steel. *Electrical engineering & electromechanics*, 2017, no.1, pp. 31-38. (Rus). doi: 10.20998/2074-272X.2017.1.06.
8. Baranov M.I. *Izbrannye voprosy elektrofiziki: Monografija v 2-h tomah. Tom 2, Kn. 1: Teorija elektrofizicheskikh effektov i zadach* [Selected topics of Electrophysics: Monograph in 2 vols. Vol. 2, book. 1: Theory of electrophysics effects and tasks]. Kharkov, NTU «KhPI» Publ., 2009. 384 p. (Rus).
9. Ricketts L.U., Bridges J.E., Mayletta J. *Elektromagnitnij impul's i metody zashchity* [Electromagnetic pulse and methods of protection]. Moscow, Atomizdat Publ., 1979. 328 p. (Rus).
10. Myrova L.O., Chepizhenko A.Z. *Obespechenie stojkosti apparatury svyazi k ionyzyruyushchim i elektromagnitnim izlucheniyam* [Ensuring stability of communications equipment to the ionizing and electromagnetic of radiations]. Moscow, Radio and Communications Publ., 1988. 296 p. (Rus).
11. SAE ARP 5412: 2013. Aircraft Lightning Environment and Related Test Waveforms. SAE Aerospace. USA, 2013. – pp. 1-56.
12. SAE ARP 5416: 2013. Aircraft Lightning Test Methods. SAE Aerospace. USA, 2013. – pp. 1-145.
13. Baranov M.I., Kravchenko V.I., Nosenko M.A. Experimental research into electrothermal stability of aircraft metallic elements against direct action of artificial lightning current. Part 2: stability of copper wires and cables. *Electrical Engineering & Electromechanics*, 2011, no.2, pp. 46-55. (Rus). doi: 10.20998/2074-272X.2011.2.11.

Received 07.08.2018

M.I. Baranov, Doctor of Technical Science, Professor, Scientific-&-Research Planning-&-Design Institute «Molniya», National Technical University «Kharkiv Polytechnic Institute», 47, Shevchenko Str., Kharkiv, 61013, Ukraine, phone +380 57 7076841, e-mail: baranovmi@kpi.kharkov.ua

#### How to cite this article:

Baranov M.I. A choice of sections of electric wires and cables in circuits of devices of high-voltage high-current impulse technique. *Electrical engineering & electromechanics*, 2018, no.6, pp. 56-62. doi: 10.20998/2074-272X.2018.6.08.

G.V. Bezprozvannykh, A.N. Boyko, A.V. Roginskiy

## EFFECT OF A DIELECTRIC BARRIER ON THE ELECTRIC FIELD DISTRIBUTION IN HIGH-VOLTAGE COMPOSITE INSULATION OF ELECTRIC MACHINES

*Introduction. Modern high-voltage systems for composite insulation of electrical machines consist of tape glass mica paper materials (dry or pre-impregnated). The electrical characteristics of a multilayer composite insulation system are determined by both the fractional content of the individual components and their electrophysical properties. Purpose. The analysis of the influence of electrophysical characteristics and thickness (fraction) of the dielectric barrier on the distribution of the electric field in the composite high-voltage insulation of electrical machines. Methodology. Simulation of surface charge accumulation at the interface between the substrate and the dielectric barrier is based on the Maxwell–Wagner theory for interfacial polarization. Practical value. The influence of the electrophysical characteristics and thickness of the dielectric barrier on the distribution of the electric field has been established. In the steady state, the electric field strength in the dielectric barrier exceeds the average value by 50 %. In the region of small transition times (up to 1 s), the relative dielectric constant of the barrier has a significant effect on the distribution of the electric field. The use of a dielectric barrier with a higher dielectric constant and fractional content in comparison with the substrate leads to an increase in electric field strength by 5 % relative to the average value in composite insulation. Experimental studies of the long-term electrical strength of glass mica-belt ribbons in the cured (thermosetting) state are consistent with the simulation results. Composite insulation based on glass fiber mica tape with a high content of the mica barrier and fiberglass of smaller thickness has (8-16) % higher values of long-term electric strength. References 9, figures 5.*

**Key words:** high-voltage composite insulation, dielectric barrier, fiberglass substrate, interfacial polarization, electric field distribution, long-term electrical strength.

*Представлены результаты распределения электрического поля в высоковольтной композитной изоляции на основе предложенной математической модели накопления поверхностного заряда на границе раздела подложка – барьер. В установившемся режиме напряженность электрического поля в диэлектрическом барьере может превышать среднее значение на 50 % в зависимости от электрофизических характеристик и толщины компонентов. Показано, что в области малых времен переходного процесса на характер распределения электрического поля влияют как относительная диэлектрическая проницаемость, так и толщина диэлектрического барьера. Экспериментальная проверка выполнена для пяти типоразмеров стеклослюдобумажной ленты по 5-ть макетов в каждой. Установлено, что композитная изоляция с повышенным содержанием слюдинитового барьера и стеклотканью меньшей толщины имеет на (8-16) % более высокие значения длительной электрической прочности. Библ. 9, рис. 5.*

**Ключевые слова:** высоковольтная композитная изоляция, диэлектрический барьер, стекловолнистая подложка, межфазная поляризация, распределение электрического поля, длительная электрическая прочность.

**Introduction.** Modern high-voltage systems for composite insulation of electrical machines consist of ribbon glass mica paper materials (dry or pre-impregnated) [1, 2]. The main function of such insulation is the preservation of long-term electrical strength under the conditions of long-lasting thermal, mechanical and thermomechanical effects. High-voltage insulation should also have the necessary level of manufacturability and relatively low cost while maintaining high technical and operational characteristics.

Use as a dielectric barrier of mica paper is cost-effective, as it is made from waste of scarce and fairly expensive splinter mica [1]. Compared with materials based on splinter mica, micaceous and mica plastics papers have a greater thickness uniformity, increased and more uniform electrical strength. The combination of good elasticity and mechanical strength allows to obtain a dense, monolithic thermosetting insulation [2]. Flat mica particles form a dielectric barrier and, depending on the conditions, are bound by various impregnating compositions and substrates. The binder can be introduced into the composition of the tape either in advance, then the tape is called pre-impregnated (Resin Rich), or introduced into the dry tapes after they have been processed in the process of vacuum-pressure impregnation [1].

Epoxy resins (diano, cycloaliphatic and epoxy drawing) are used as a binder, which have high mechanical properties, good adhesion to various materials, sufficient heat resistance (class B and F) and corona resistance, have a slight shrinkage ratio (3-5) % [2].

The mechanical strength is provided by the glass fabric substrate, which is a reinforcing material in such a system. It also contains most of the binder in the case of impregnated tape. Composite insulation, made with the use of glass fiber materials, has an increased tensile strength and flexural strength. Glass fiber materials are highly thermally resistant [1, 2].

The electrical characteristics of a multilayer composite insulation system are determined by both the fractional content of the individual components and their electrophysical properties.

**Problem definition.** The real interface between the substrate and the dielectric barrier has a surface layer of finite thickness, within which the thermodynamic parameters (concentration of components, pressure and temperature) undergo drastic changes. The surface layers of each phase with a thickness of about 0.5 nm have special properties, since they are in the field of action of the molecular forces of the neighboring phase (the so-called Rebinder effect) [3].

© G.V. Bezprozvannykh, A.N. Boyko, A.V. Roginskiy

The desire of a heterogeneous system to reduce the surface energy causes an appropriate orientation of polar molecules, ions and electrons in the boundary layer, as a result of which the contacting phases acquire charges of opposite sign, but of equal value. At the interface between the substrate and the dielectric barrier, as on the interfacial surfaces, a double electric layer arises as a result of the interaction of the contacting phases due to excess surface energy [4] with the corresponding electric potential, surface charge density, capacity [5-7].

**The goal of the paper** is analysis of the influence of electrophysical characteristics and thickness (fraction) of the dielectric barrier on the distribution of the electric field in the composite high-voltage insulation of electrical machines.

**Mathematical model of surface charge accumulation at the flat interface between two dielectrics.** A high-voltage thermosetting composite insulation of electrical machine can be represented in the form of two layers of dielectric: a glass fiber substrate (1) with an impregnating compound (3) and a mica paper tape (2) as a dielectric barrier (Fig. 1). The anisotropy of the properties of mica in this case is weakly expressed.

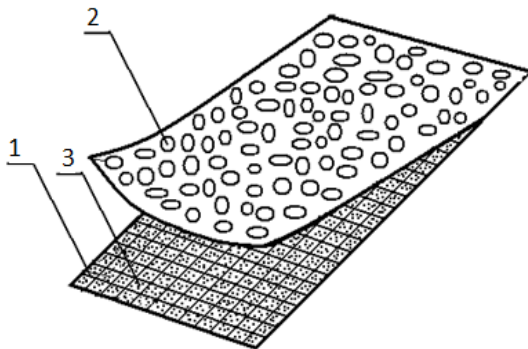


Fig. 1. Schematic representation of the three-component insulation by a double layer tape

The most common approach in simulating the accumulation of surface charge at the interface of two dielectric media is based on the Maxwell–Wagner theory for interfacial polarization [8].

The hypothetical configuration of the interface between two flat isotropic dielectrics with electrodes is represented by a Maxwell capacitor (Fig. 2). In such a system, the insulation properties change depending on the step function at the interface of the media [8].

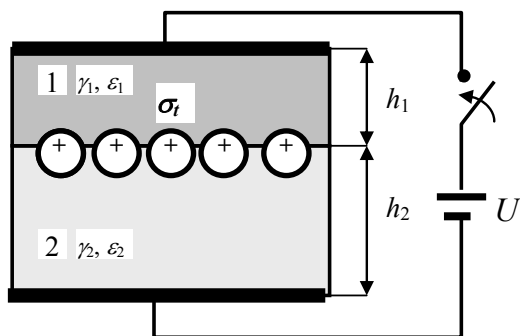


Fig. 2. Representation of the accumulation of surface charges at the interface of two isotropic dielectrics when switched on under constant voltage  $U$

At the dielectric interface, the dielectric permeability  $\varepsilon$  (or the polarization vector) varies in steps [8, 9]. The jump of the normal component of the electric displacement vector  $\mathbf{D}$  is equal to the surface density  $\sigma$  of electric charges. The tangential component of the electric field strength vector is continuous at any interface

$$D_{2n} - D_{1n} = \sigma, \quad E_{1t} = E_{2t}, \quad (1)$$

where  $D_{2n}, D_{1n}$  are the normal components of the electric displacement vector:  $D_{2n} = \varepsilon_0 \varepsilon_2 E_{2n}, D_{1n} = \varepsilon_0 \varepsilon_1 E_{1n}$ ,  $\varepsilon_0 = 8.85 \cdot 10^{-12}$  F/m is the electric constant;  $\varepsilon_1, \varepsilon_2$  are the dielectric permeabilities of dielectrics,  $\sigma$  is the surface density of electric charges;  $E_{1n}, E_{2n}$  are the normal,  $E_{1t}, E_{2t}$  are the tangential components of the electric field strength vector of the first and the second dielectrics, respectively.

At the moment of switching on the capacitor to the voltage source  $U$ , the surface density  $\sigma$  of electric charges is zero, as a result, in accordance with (1), the electric field strength in the layers is proportional to the dielectric permeability [8]

$$E_{1n} \varepsilon_1 = E_{2n} \varepsilon_2. \quad (2)$$

At the next instant, the conduction current with the corresponding density  $J$  begins to influence the distribution of the electric field in the layers

$$J_1 = \gamma_1 E_1, \quad J_2 = \gamma_2 E_2, \quad (3)$$

where  $\gamma_1$  and  $\gamma_2$  are the conductivities of each dielectric, S/m.

Since the current densities are not equal (the electrophysical properties of dielectrics are different), a space charge accumulates at the interface between the dielectrics. The transient ends with the balancing of the currents  $J_1$  and  $J_2$ , as well as the stabilization of the surface charge at the interface of the dielectrics. For the steady state, the electric field strength in the layers is proportional to the conductivity

$$\gamma_1 E_1 = \gamma_2 E_2. \quad (4)$$

From the initial moment and steady state, the total current in the first and second dielectrics is the same and has two components: active, which is caused by conduction current (leakage current), and reactive, due to displacement current (absorption current). Thus, the total current density will be determined as

$$J = \gamma_1 E_1 + \varepsilon_0 \varepsilon_1 \frac{dE_1}{dt} = \gamma_2 E_2 + \varepsilon_0 \varepsilon_2 \frac{dE_2}{dt}. \quad (5)$$

The sum of the voltage drop across each layer is equal to the applied DC voltage

$$E_1 h_1 + E_2 h_2 = U, \quad (6)$$

where  $h_1, h_2$  are the dielectric thickness.

When combining (5) and (6), the differential equation for  $E_1$  is

$$\frac{dE_1}{dt} \varepsilon_0 (\varepsilon_1 h_2 + \varepsilon_2 h_1) + E_1 (\gamma_1 h_2 + \gamma_2 h_1) = \gamma_2 U, \quad (7)$$

whose solution is searched in the form

$$E_1(t) = A e^{-\left(\frac{\gamma_1 h_2 + \gamma_2 h_1}{\varepsilon_0 (\varepsilon_1 h_2 + \varepsilon_2 h_1)} t\right)} + U \frac{\gamma_2}{(\gamma_1 h_2 + \gamma_2 h_1)}, \quad (8)$$

where  $A$  is the integration constant, which, taking into account the initial conditions at time  $t = 0$  and (2), (6) is defined as

$$A = U \left( \frac{\varepsilon_2}{\varepsilon_1 h_2 - \varepsilon_2 h_1} - \frac{\gamma_2}{\gamma_1 h_2 + \gamma_2 h_1} \right). \quad (9)$$

After substituting (9) into (8), the electric field strength in the first layer of a two-layer dielectric varies with time in accordance with (10)

$$E_{1t} = U \frac{\gamma_2}{\gamma_1 h_2 + \gamma_2 h_1} + U \frac{h_1 \cdot (\varepsilon_2 \gamma_1 - \varepsilon_1 \gamma_2)}{(\varepsilon_1 h_2 + \varepsilon_2 h_1) \cdot (\gamma_1 h_2 + \gamma_2 h_1)} e^{-t/\tau}, \quad (10)$$

and in the second one in accordance with (11)

$$E_{2t} = U \frac{\gamma_1}{\gamma_1 d_2 + \gamma_2 d_1} + U \frac{d_2 \cdot (\varepsilon_1 \gamma_2 - \varepsilon_2 \gamma_1)}{(\varepsilon_1 d_2 + \varepsilon_2 d_1) \cdot (\gamma_1 d_2 + \gamma_2 d_1)} e^{-t/\tau}, \quad (11)$$

where  $\tau$  is the time constant, s

$$\tau = \varepsilon_0 \frac{\varepsilon_1 h_2 + \varepsilon_2 h_1}{\gamma_1 h_2 + \gamma_2 h_1}. \quad (12)$$

The density of the total current, which consists of the current of absorption and leakage due to the presence of free charges, is determined by the formula (13)

$$J(t) = U \frac{h_1 h_2 (\varepsilon_1 \gamma_2 - \varepsilon_2 \gamma_1)}{(\varepsilon_1 h_2 + \varepsilon_2 h_1)^2 (\gamma_1 h_2 + \gamma_2 h_1)} \times \exp(-t/\tau) + U \frac{\gamma_1 \gamma_2}{\gamma_1 h_2 + \gamma_2 h_1} = J_{abs} + J_{cond}. \quad (13)$$

The time variation of the surface charge density  $\sigma(t)$  at the interface between two dielectrics can be written as

$$\sigma(t) = \varepsilon_0 \frac{\varepsilon_1 \gamma_2 - \varepsilon_2 \gamma_1}{\gamma_1 h_2 + \gamma_2 h_1} \cdot U (1 - e^{-t/\tau}). \quad (14)$$

**The effect of electrophysical characteristics and thickness of the dielectric barrier on the distribution of the electric field in high-voltage composite insulation.** Fig. 3 shows the simulation results for two cases: curves 1 – the identity of the electrical characteristics of the barrier and the substrate:  $\varepsilon_1 = \varepsilon_2 = 4.5$ ;  $\gamma_1 = \gamma_2 = 2 \cdot 10^{-13}$  S/m; curves 2, 2' – different:  $\varepsilon_1 = 4.5$ ;  $\varepsilon_2 = 3.8$ ;  $\gamma_1 = 2 \cdot 10^{-13}$  S/m,  $\gamma_2 = 2 \cdot 10^{-12}$  S/m. Indexes 1 relate to the barrier, 2 – to the substrate. The thickness of the dielectric barrier is  $h_1 = 0.1$  mm, of the glass fiber substrate is  $h_2 = 0.05$  mm. Curve 2 corresponds to the distribution of the electric field in the barrier, curve 2' in the substrate (Fig. 3,b). The calculations were performed for the average electric field strength  $E_{mid} = 15$  kV/mm in composite insulation.

If the electrical characteristics are identical, surface charges do not accumulate at the interface between dielectric media (curve 1, Fig. 3,a) and the electric field is equal to the average value:  $E = E_{mid} = 15$  kV/mm (curve 1, Fig. 3,b). The transient is absent.

In the case of different characteristics, a transient of a duration of about 10 s is observed. In the steady state, the surface charge density is  $0.85$  mC/m<sup>2</sup> (curve 2, Fig. 3,a), the electric field strength in the dielectric barrier exceeds the average value by 50 % (curve 2, Fig. 3,b), in the substrate it is insignificantly small (curve 2', Fig. 3,b).

Fig. 4 shows the dynamics of the time variation of the electric field distribution with varying conductivity, relative dielectric permeability and thickness of the dielectric barrier.

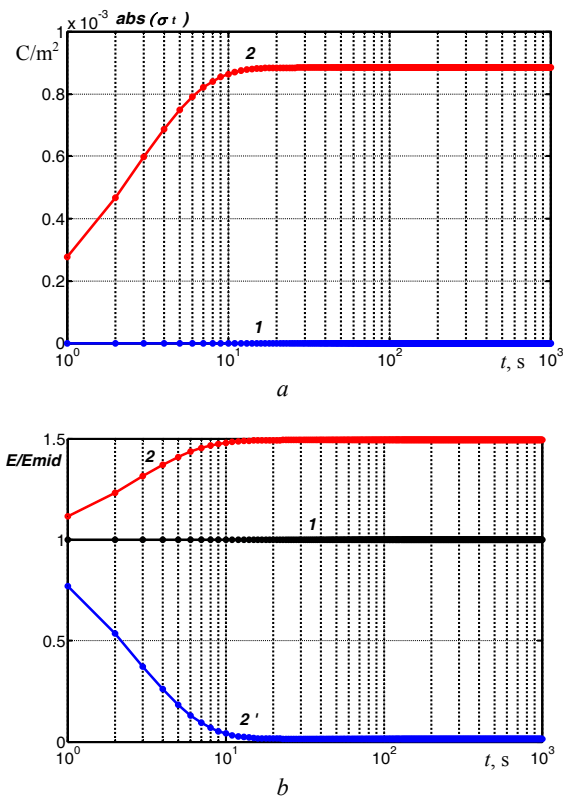


Fig. 3. The distribution of surface charge density (a) and the electric field strength (b) at the interface between the substrate and the dielectric barrier

In Fig. 4, a, b curves 1 and 2 correspond:  $\varepsilon_1 = 4.5$ ,  $\varepsilon_2 = 3.8$ ,  $\gamma_1 = 2 \cdot 10^{-13}$  S/m,  $\gamma_2 = 2 \cdot 10^{-12}$  S/m; curves 1' and 2' –  $\varepsilon_1 = 4.5$ ,  $\varepsilon_2 = 3.8$ ,  $\gamma_1 = 2 \cdot 10^{-13}$  S/m,  $\gamma_2 = 2 \cdot 10^{-11}$  S/m, respectively. The thickness of the dielectric barrier is assumed to be  $h_1 = 0.1$  mm, of the substrate is  $h_2 = 0.05$  mm. The share content of mica in this case is 67 % of the total volume of composite insulation.

The effect of relative dielectric permeability and barrier thickness on the distribution of the electric field is shown in Fig. 4, c. Curves 1 and 2 correspond to the characteristics:  $\varepsilon_1 = 4.5$ ,  $\varepsilon_2 = 3.8$ ,  $\gamma_1 = 2 \cdot 10^{-13}$  S/m,  $\gamma_2 = 2 \cdot 10^{-12}$  S/m,  $h_1 = 0.1$  mm,  $h_2 = 0.05$  mm. Curves 1' and 2':  $\varepsilon_1 = 3.8$ ,  $\varepsilon_2 = 4.5$ ,  $\gamma_1 = 2 \cdot 10^{-13}$  S/m,  $\gamma_2 = 2 \cdot 10^{-12}$  S/m;  $h_1 = 0.1$  mm,  $h_2 = 0.05$  mm. Curves 1'' and 2'':  $\varepsilon_1 = 4.5$ ,  $\varepsilon_2 = 3.8$ ,  $\gamma_1 = 2 \cdot 10^{-13}$  S/m,  $\gamma_2 = 2 \cdot 10^{-12}$  S/m,  $h_1 = 0.05$  mm,  $h_2 = 0.1$  mm.

In the region of short transient times (10 ms – 1 s), the nature of the distribution of the electric field is significantly affected by the ratio between the dielectric permeabilities of the barrier and the substrate, with their constant thickness. In the case when  $\varepsilon_1 < \varepsilon_2$ , the electric field strength in the barrier exceeds the average value of 1.05, while in the substrate it is 1.1 times, respectively (compare curves 1' and 2, Fig. 4, c). This fact is especially important when working under alternating voltage: a dielectric barrier provides long-term dielectric strength of composite insulation.

A decrease in the thickness of the dielectric barrier (fractional content), provided that  $\varepsilon_1 > \varepsilon_2$ , leads to an increase in the electric field, although it «unloads» the substrate electrically (compare curves 1'' and 1' in Fig. 4, c).

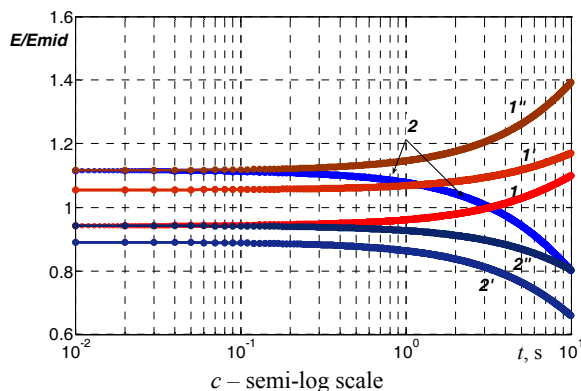
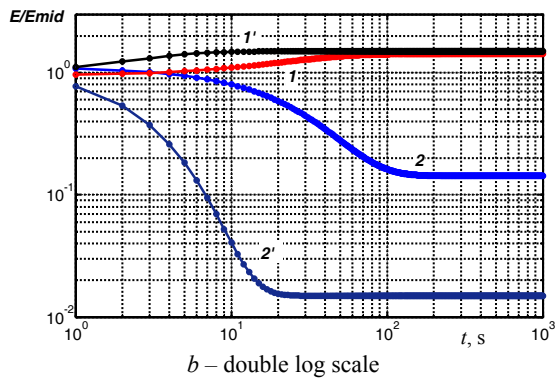
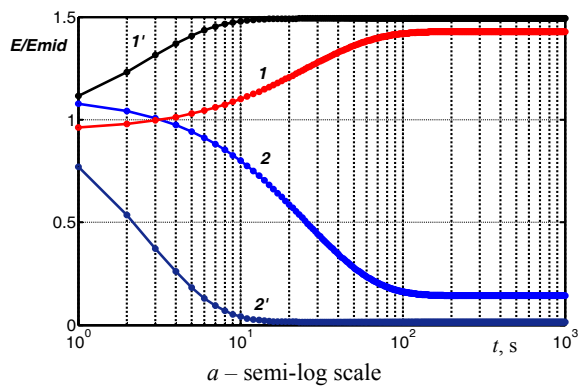


Fig. 4. The effect on the distribution of the electric field of the electrophysical characteristics and thickness of the components at the interface between the substrate and the dielectric barrier

**Experimental verification of the effect of the fractional content of mica paper tape on the long-term electrical strength of composite high-voltage insulation samples.** For testing tapes in the cured state, 5 layouts were made with each glass-mica paper tape of different thickness from different manufacturers: 1 –  $h = 0.15$  mm, 2 –  $h = 0.14$  mm, 3 –  $h = 0.14$  mm, 4 –  $h = 0.18$  mm, 5 –  $h = 0.18$  mm.

The layouts are copper busbars of  $6 \times 30 \times 800$  mm size, which are isolated on the ЛИСИ-4 tape insulation machine with a tape heated to temperature of  $50-60^\circ\text{C}$  and tension of  $40-60$  N. Layouts, covered with slats on wide faces, are pressured by hydrostatic method. Long-term electrical strength of the finished layouts is determined with continuous exposure under voltage from the calculation  $15$  kV/mm at industrial frequency.

The correctness of the adequacy of the results of modeling on direct current by experimental research on alternating current is permissible, since in the region of

short transient times, the influence of both the electrophysical characteristics and the fraction of the dielectric barrier on the distribution of the electric field in the composite insulation is manifested (see Fig. 4, a-c) [long-term electrical strength at 50 Hz alternating current is lower in comparison with constant current due to large losses due to the polarization process].

Fig. 5 shows the results of tests of long-term electrical strength of the layouts, depending on the thickness of the composite insulation. The integral distribution functions of long-term electric strength are shown in Fig. 5, a, average values in Fig. 5, b.

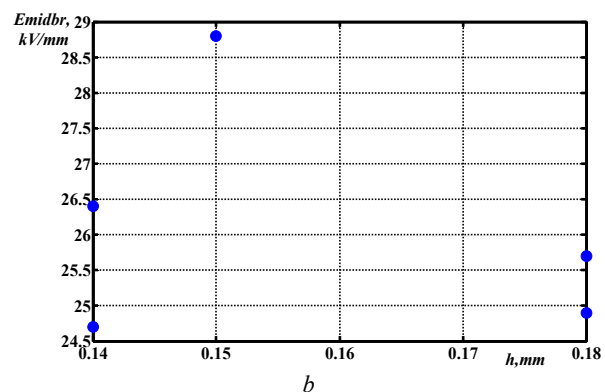
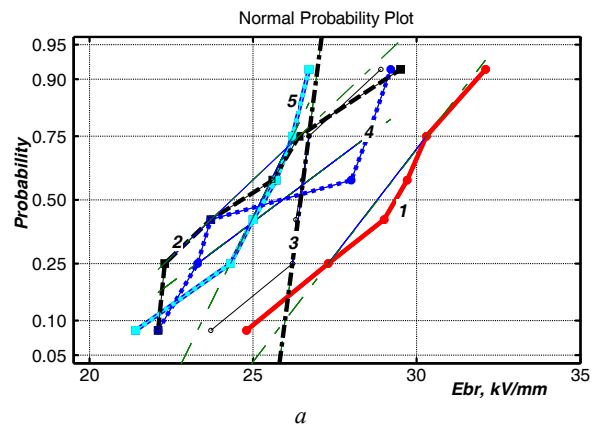


Fig. 5. The effect of the micaceous barrier on the long-term electrical strength of the composite high-voltage insulation of electrical machines

The smallest scatter of the values of the breakdown electric strength is for insulation systems with thickness  $h = 0.14$  mm (curve 3, Fig. 5, a), which may be due to a more uniform thickness of glass-mica paper tape due to the use of a different type of binder. The slope of the integral distribution function of the electrical strength of the layouts with this insulation system differs significantly from the rest (compare curve 3 with curves 1, 2, 4, 5 in Fig. 5, a).

For sample thickness of composite insulation  $h = 0.15$  mm (curve 1, Fig. 5, a) the greatest value of long-term electric strength is observed: at the level of 50 % probability, the average value is  $28.75$  kV/mm (Fig. 5, b). In this layout, a tape with a high content of the micaceous barrier and a less thick fiberglass (in accordance with the technical description on the tape) are used.

**Conclusions.** For the first time, the distribution of the electric field in high-voltage composite insulation of

electrical machines is obtained on the basis of the proposed mathematical model of surface charge accumulation at a flat interface between the substrate and the dielectric barrier.

It is established that in the steady state the electric field strength in the barrier exceeds the average value by 50 % depending on the electrophysical characteristics and thickness of the components.

In the region of short transient times (up to 1 s), the relative dielectric permeability of the barrier has a significant effect on the distribution of the electric field in composite insulation. The use of a dielectric barrier with higher dielectric permeability and fractional content in comparison with the substrate leads to an increase of 5 % of the electric field relative to the average value.

Experimental studies of the long-term electrical strength of layouts of glass mica tapes in the cured (thermosetting) state are consistent with the simulation results.

Composite insulation based on glass fiber mica tape with a high content of the mica barrier and fiberglass of smaller thickness has (8 – 16) % higher values of long-term electrical strength.

#### REFERENCES

1. Ogonkov V.G., Serebryannikov S.V. *Elektroizolatsionnye materialy i sistemy izoliatsii dlia elektricheskikh mashin. V dvukh knigakh. Kn. 2* [Electrical insulation materials and insulation systems for electrical machines. In 2 books. Book 2]. Moscow, Publishing house MEI, 2012. 304 p. (Rus).
2. Pak V.M., Trubachev S.G. *Novye materialy i sistemy izoliatsii vysokovol'tnykh elektricheskikh mashin* [New materials and systems for isolation of high-voltage electrical machines]. Moscow, Energoatomizdat Publ., 2007. 416 p. (Rus).
3. Rebinder P.A. *O vliianii izmenenii poverkhnostnoi energii na spainost', tverdost' i drugie svoistva kristallov* [On the effect of changes in surface energy on the cleavage, hardness and other

properties of crystals]. Congress of Russian physicists. The list of reports submitted to the congress, with a brief summary. Moscow - Leningrad, 1928. 29p. (Rus).

4. Gibbs J.V. *Termodinamika. Statisticheskaya mekhanika* [Thermodynamics. Statistical mechanics]. Moscow, Nauka Publ., 1982. 584 p. (Rus).

5. Mikhailov V.M. Initial relations and approximate boundary conditions for calculating the field in systems with thin layers. *Electricity*, 2007, no.3, pp. 49-55. (Rus).

6. Kim Yong Dar, Kalmykov V.L. Study of the electric field of an insulating structure with thin extended areas. *Bulletin of NTU «KhPI»*, 2005, no.42, pp. 65-70. (Rus).

7. Bezprozvannykh G.V., Boyko A.N. Distribution of surface density of charges on the interface between contacting isolated conductors of the cables. *Technical Electrodynamics*, 2014, no.6. pp. 18-23. (Rus).

8. Hippel A.R. *Dielektriki i volny* [Dielectrics and waves]. Moscow, Publ. House of Foreign Literature, 1960. 439 p. (Rus).

9. Demirchian K.S., Neiman L.R., Korovkin N.V., Chechurin V.L. *Teoreticheskie osnovy elektrotehniki: V 3-kh t. Uchebnik dlia vuzov* [Theoretical bases of electrical engineering. In 3 vols.]. St. Petersburg, Piter Publ, 2003. 463 p. (Rus).

Received 14.07.2018

G.V. Bezprozvannykh<sup>1</sup>, Doctor of Technical Science, Professor,  
A.N. Boyko<sup>2</sup>, Candidate of Technical Science,  
A.V. Roginskiy<sup>3</sup>, Postgraduate Student,

<sup>1</sup> National Technical University «Kharkiv Polytechnic Institute»,  
2, Kyrpychova Str., Kharkiv, 61002, Ukraine,

e-mail: bezprozvannykh@kpi.kharkov.ua

<sup>2</sup> Company «WebMeridian in Ukraine»,

13, Chernyshevskogo Str., Kharkiv, 61002, Ukraine,

<sup>3</sup> SE Plant Electrotyazhmash,

299, Moskovsky Ave., Kharkiv, 61089, Ukraine,

e-mail: roginskiy.av@gmail.com

#### How to cite this article:

Bezprozvannykh G.V., Boyko A.N., Roginskiy A.V. Effect of a dielectric barrier on the electric field distribution in high-voltage composite insulation of electric machines. *Electrical engineering & electromechanics*, 2018, no.6, pp. 63-67. doi: 10.20998/2074-272X.2018.6.09.

M. Dehghani, M. Mardaneh, Z. Montazeri, A. Ehsanifar, M.J. Ebadi, O.M. Grechko

## SPRING SEARCH ALGORITHM FOR SIMULTANEOUS PLACEMENT OF DISTRIBUTED GENERATION AND CAPACITORS

*Purpose.* In this paper, for simultaneous placement of distributed generation (DG) and capacitors, a new approach based on Spring Search Algorithm (SSA), is presented. This method is contained two stages using two sensitive index  $S_v$  and  $S_s$ .  $S_v$  and  $S_s$  are calculated according to nominal voltage and network losses. In the first stage, candidate buses are determined for installation DG and capacitors according to  $S_v$  and  $S_s$ . Then in the second stage, placement and sizing of distributed generation and capacitors are specified using SSA. The spring search algorithm is among the optimization algorithms developed by the idea of laws of nature and the search factors are a set of objects. The proposed algorithm is tested on 33-bus and 69-bus radial distribution networks. The test results indicate good performance of the proposed method. References 30, tables 4, figures 4.

*Key words:* DG placement, capacitor placement, distribution network, SSA, sensitive index, two-stage simultaneous placement.

*Цель.* В статье для одновременного размещения распределенной генерации и конденсаторов представлен новый подход, основанный на «пружинном» алгоритме поиска (Spring Search Algorithm, SSA). Данный метод состоит из двух этапов с использованием двух показателей чувствительности  $S_v$  и  $S_s$ . Показатели чувствительности  $S_v$  и  $S_s$  рассчитываются в соответствии с номинальным напряжением и потерями в сети. На первом этапе определяются шины-кандидаты для установки распределенной генерации и конденсаторов согласно  $S_v$  и  $S_s$ . Затем, на втором этапе размещение и калибровка распределенной генерации и конденсаторов выполняются с использованием алгоритма SSA. «Пружинный» алгоритм поиска входит в число алгоритмов оптимизации, разработанных на основе идей законов природы, а факторы поиска представляют собой набор объектов. Предлагаемый алгоритм тестируется на радиальных распределительных сетях с 33 и 69 шинами. Результаты тестирования показывают хорошую эффективность предложенного метода. Библ. 30, табл. 4, рис. 4.

*Ключевые слова:* размещение распределенной генерации, размещение конденсаторов, распределительная сеть, «пружинный» алгоритм поиска SSA, показатель чувствительности, двухэтапное одновременное размещение.

**Introduction.** Lately, electricity trading and connecting distributed generation (DG) to the distribution network has been placed under private investors' scope of interest. Besides, placing capacitors within medium voltage networks is a paramount factor, which is noticed highly by distribution companies. Noticeably since the DG and capacitor are related to each other as sources of active and reactive power, performing their placement at the same time makes more optimal solution found.

**Placement of DGs.** The distribution system planning requires DGs to be placed properly within the distribution system. In definition, DG known as a small generator is responsible of generating Stand Alone and On Grid electricity [1].

In placing DGs, some methods can be used. [2, 3] refers to the sizing and analytical method by which DGs can be placed and sized properly. The objective function of the mentioned reference is minimizing the loss. In [4], DGs are placed by considering some objective functions known as increasing the spinning reserve, improving the voltage profile, decreasing the load flow and decreasing the transmission loss. In [5], based on the fuzzy logic the algorithm known as Bellman-zadeh is used for DGs placement. Reference [6], uses the load flow method by applying the voltage profile and the power loss such that it computes some objective function optimal paramount factors first, then decreases the transmission loss and finally improves the voltage profile. The method of DGs placement in [7], is based on the voltage stability analysis known as a security measure. It is proper to mention that energy efficiency can be improved by applying two strategies known as conservation voltage reduction (CVR) and DG integration. In [8], CVR and DG placement are studied to find their interaction in minimizing the load

consumption of distribution networks. It is noted that the afore-mentioned process is performed by keeping the lowest voltage level within the predefined range. [9], refers highly to the economic and network-driven DG placement planning. Its viewpoint is from the local distribution company (DISCO) considering reliability level and the electrical distribution network power loss.

**Placement of Capacitor.** Capacitors have long been applied within the industrial plants and commercial establishments for the purpose of a power factor (PF) improvement. Besides, electric utilities use capacitor to control the feeder voltage and to improve the distribution system efficiency. Based on studies conducted in recent decades [10-22], there are different models and mathematical solution techniques for the capacitor placement. More elaborately, Schmill [19], applied a uniform characteristics feeder comprising a uniform load distribution. He used the two-thirds rule that is he used a single capacitor along with the two-thirds of the feeder length. In [12], dynamic programming (DP) was used by Duran to arrive at the optimal solution.

However, the application of a uniform load and a fixed conductor size was abolished by Grainger and Lee [16], who searched to find the optimal solution by dividing the problem into three sub problems known as size, switching time, and location. Noticeably, these phases were successively solved. In [18], load data were gathered from the distribution feeder by Rembert and Rinker who used a reactive current recorder to compute the instantaneous apparent and reactive currents. Moreover, in order to find the optimal solution Sundhararajan [21], applied a directed grid search method to decrease the number of candidate nodes such that by rejecting other nodes, the top two or three nodes in each

lateral branch were merely used. Xu [22], in his method of capacitor banks placement could reduce the power loss. Indeed, the low-side of transformers was considered a proper location for the capacitor bank. Some other important factors were taken into account by Kaur [15], like cost, size and location of capacitor bank. Ultimately, he could compensate the reactive power demand by using the load. An integrated optimization method enjoying a sequential strategy and multi objectives was proposed and then applied by Su [20], who could optimally place and then control the delta-connected switched capacitors.

**Simultaneous placement of DGs and Capacitors.** A more optimal solution can be achieved if DGs and capacitors are placed properly at the same time. This ideal motivated many researchers to seek its performing procedure such that in [23], this ideal was sought within the radial distribution network with different load levels. The same investigation was done in [24], In this study through the simultaneous placement of DG and capacitor in a radial distribution network, researchers aimed to arrive at the optimal quantity, placement, and sizing. To fulfil this aim, researchers chose a new manner as the multi objective optimization problem, which encompassed the DG units', and capacitors' costs, power losses, and voltage stability margins. This problem performing process was to apply a developed genetic algorithm as the first stage in the proposed hierarchical optimization strategy. The other type of simultaneous capacitor banks and distributed generation allocation comprising the stochastic nature of DG was done in [25], in which the Tabu -search and genetic algorithms-based efficient hybrid method was proposed.

Likewise, in the present paper, a new method is suggested to simultaneously allocate DGs and Capacitors in distribution systems. Accordingly, concerning the nominal voltage of buses and network losses, two new sensitivity indexes are introduced. The first index is called the sensitivity index of voltage ( $S_v$ ) which is based on the buses nominal voltage. The second one is the sensitivity index of losses network, which is related to the network losses. The present methodology operates within two stages; in the first one, candidate buses are chosen to install DG and capacitors concerning both sensitivity indexes of  $S_v$  and  $S_s$ ; though, in the second stage, DG and capacitors placement and sizing are done by applying SSA. It is proper to mention that, the present study is indeed a case study using IEEE 33-bus of [7] and 69-bus of [25] and results are reported as well.

**Problem Formulation.** Minimizing the overall system loss and improving the system voltage profile are indeed two principal objectives of DGs optimal sizing and placement. Noticeably, in this process the bus and branch number must be minutely adjusted to find the answer of the load flow distribution (Fig. 1).

The process of branch numbering is as follows:

- choosing the root, swing or the slack bus when the main source is connected;
- ordering layers from the first layer of tree in which all branches connected to root bus;
- labelling the second layer of tree, which is connected to the first layer receiving end bus and so on.

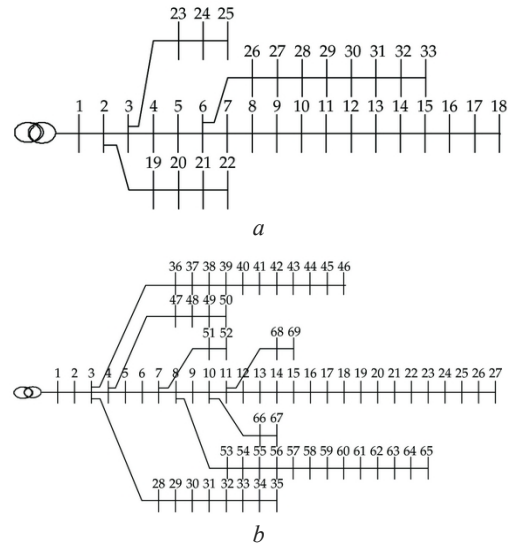


Fig.1. IEEE 33-bus distribution network (a); IEEE 69-bus distribution network (b)

In an assumed  $\Pi$  model of the network in which  $I$  branch is attached to  $k$  bus in one hand and to the  $m$  bus on the other hand,  $k$  bus is closer to the root bus that is the net power goes from  $k$  to  $m$  bus. Fig. 2 represents the power flow through the series impedance of the branch. These flows are represented in (1) and (2), elaborately.

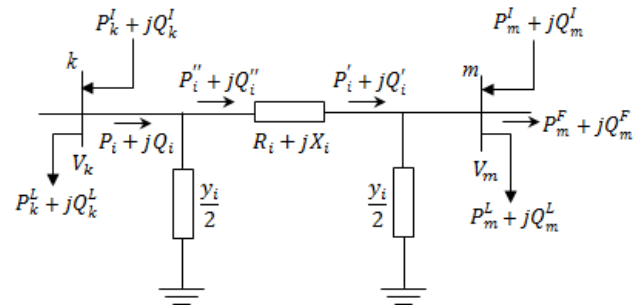


Fig. 2.  $\Pi$  model of a network

$$P_i' = P_m^L + P_m^F - P_m^I, \quad (1)$$

$$Q_i' = Q_m^L + Q_m^F - Q_m^I - V_m^2 \frac{y_i}{2}, \quad (2)$$

where  $L$ ,  $F$  and  $I$  subscripts represents the load, the flow and the injection respectively. Branch  $i$  let the power flow near bus  $k$ . This passage can be formulated as

$$P_i = P_i'' = P_i' + R_i \frac{P_i'^2 + Q_i'^2}{V_m^2}, \quad (3)$$

$$Q_i = Q_i'' - V_k^2 \frac{y_i}{2} = Q_i' + X_i \frac{P_i'^2 + Q_i'^2}{V_m^2} - V_k^2 \frac{Y_i}{2}, \quad (4)$$

In order to calculate the power flow quantity in each branch of tree, it is computed recursively in a backward/anti clock-wise direction. Thus, the bus  $m$  complex voltage is computed as

$$V_m = \left[ V_k - \frac{P_i'' R_i + Q_i'' X_i}{V_k^*} \right] - j \left[ \frac{P_i'' X_i - Q_i'' R_i}{V_k^*} \right]. \quad (5)$$

The strategy of finding the magnitude and angle of all buses voltages of the tree is to compute this complex voltage in a forward direction.

This computation is done iteratively again and again till the voltage difference at loop breaking points (breaking points of the tree) is placed within the acceptable limit. Hence the branch  $I$  active power loss ( $P_{Li}$ ) and reactive power loss ( $Q_{Li}$ ) are measured as

$$P_{Li} = P_i'' - P_i' = R_i \frac{P_i'^2 + Q_i'^2}{V_m^2}, \quad (6)$$

$$Q_{Li} = Q_i'' - Q_i' = X_i \frac{P_i'^2 + Q_i'^2}{V_m^2}. \quad (7)$$

Accordingly, quantities of the system net active, reactive and apparent power loss are

$$P_L = \sum_{i=1}^N P_{Li}; \quad (8)$$

$$Q_L = \sum_{i=1}^N Q_{Li}; \quad (9)$$

$$S_L = \left( P_L^2 + Q_L^2 \right)^{\frac{1}{2}}, \quad (10)$$

where  $S_L$  is the distribution system apparent power loss.

As mentioned, the major objective of the present problem is to minimize the net power loss and modify the voltage profile of the system. It is proper to re-mention that the present paper seeks some other minor objectives like optimal sizing and placement of DGs and capacitors.

SSA or the spring search Algorithm optimization technique is known as a robust and a very few user dependent parameter which has a very good convergence characteristic. Besides, it doesn't stagnate at the local minima. This characteristic is the major reason of selecting SSA to minimize the system the net power loss and to modify the voltage profile.

**Methodology.** In this study, stimulatory placement and sizing of DG and Capacitors are determined in two stages base on two sensitivity indexes.

*Sensitivity indexes*  $S_v$  and  $S_s$  are defined as

$$S_v^j = \sum_{i=1}^{NB} |V_i - 1|, \quad (11)$$

$$S_s^j = \frac{S_L^i}{S_L^b}, \quad (12)$$

where  $S_v^j$  is the sensitivity index of voltage in perchance Capacitor in Bus  $j$ ,  $NB$  is the number of buses,  $S_s^j$  is the sensitivity index of loss power in perchance DG in bus  $j$ ,  $S_L^i$  is the apparent power loss in perchance DG in bus  $j$ , and  $S_L^b$  is the apparent power loss in base case.

*First stage.* DGs and capacitors must be installed at the appropriate position. This position must have an acceptable impact on the characteristics of the network. So it is important to identify a suitable location for installing DGs and capacitors. In the first stage, candidate locations are determined. For this purpose  $S_v$  and  $S_s$  for all buses are calculated. Then, priorities of each bus for installing DG and capacitor are identified according to the  $S_v$  and  $S_s$ .

*Second stage.* In the first stage, priorities of buses are determined. Prioritization of Buses makes the search

space reduces and also increase accuracy. Now size and place of DGs and capacitors should be determined. For this purpose SSA is used. The objective function introduces as

$$\text{objective function} = k_1 S_s^n + k_2 S_v^n, \quad (13)$$

$$k_1 + k_2 = 1, \quad (14)$$

where  $k_1$  and  $k_2$  is the weight factors,  $S_v^n$  and  $S_s^n$  are the normalized sensitivity indexes.

**The Spring Force Optimization** [26, 27]. Optimization algorithms have been used in many applications in electrical engineering [28] such as operation of electrical energy [29] and energy management [30].

The SSA algorithm is explained in two phases: 1 – making an artificial system with the discrete time in the problem atmosphere, the initial positioning of objects, determining the governing laws and principles, and arranging parameters, 2 – passing the time until arriving at the stop time.

*Forming system, determining the laws, and adjustment of the parameter.* In the first step, the system atmosphere is determined. This atmosphere includes a multi- dimensional coordinates within the problem definition atmosphere. Any point in the space is the answer to the problem. Searching factors are a set of objects, which are attached to each other by springs. Indeed, each object is attached to any other objects by means of spring, and each object has the characteristics of the springs' position and stiffness coefficient attached to it. The object position is a point in the space where it is a solution of the problem. The springs' stiffness coefficients can be determined concerning the suitability of any two objects attached to one another.

After making the system, its governing laws are determined. It is supposed that the governing laws are merely the spring law and the motion law. The general schematic of these laws are approximately similar to the nature laws and it is defined as below:

*The spring force law (Hook law).* In physics, mechanics and the elastic material science, the spring force law is an approximate which shows that a material length change has a linear relationship with its imposed force. Most materials follow this rule with a good (acceptable) approximate till the imposed force is lower than their elastic ability. Any deviation from the Hook law can be increased by increasing deformations such that in many deformations when the material trespasses the linear elastic domain, the Hook law loses its applicability [23, 24]. In the present article, it is supposed that the Hook law is always satisfied.

*The motion laws.* The present movement of each object equals to the coefficient sum of the object last position and its dislocation. Any object dislocation can be determined concerning the spring force law [23].

Now assume the system as a set of  $m$  objects. The position of each object is a point in the space where it can be the answer to the optimization problem. In equation (15), the  $d$  position of  $I$  object is shown with  $x_i^d$

$$X_i = (x_i^1, \dots, x_i^d, \dots, x_i^n). \quad (15)$$

At first, the objects position is defined within the problem definition atmosphere randomly. These objects pave the way to arrive at the balance point (solution) concerning forces imposed to each other by spring.

In order to compute the spring stiffness, equation (16) is used

$$K_{i,j} = K_{\max} |F_n^i - F_n^j| \max(F_n^i, F_n^j), \quad (16)$$

where  $K_{i,j}$  is the spring stiffness between  $i$  and  $j$  objects,  $K_{\max}$  represents the maximum quantity of the spring stiffness which is determined regarding the problem type,  $F_n$  shows the normalised objective function, and  $F_n^i, F_n^j$  are the normalised objective functions of  $i$  and  $j$  objects.

In order to normalise the objective function, equations (17) and (18) are used:

$$F_n^i = \frac{f_{obj}^i}{\min(f_{obj})}; \quad (17)$$

$$F_n^i = \min(F_n^i) \times \frac{1}{F_n^i}, \quad (18)$$

where  $f_{obj}$  is the objective function and  $f_{obj}^i$  is the objective function quantity of object  $i$ .

In a problem with  $m$  variables, it is possible to suppose that the problem has  $m$  dimensions; hence, it is possible to define a coordinate for each dimension; thus, it is plausible to depict the equivalent of any system variable on the related coordinate. On each coordinate, the robust/strong points of the right side and left side of the object are determined concerning the comparison of the objective function quantity. The robust/strong points of each object are indeed those objects, which are in fact in a more optimal position, rather than the object itself. Therefore, on each coordinate, two total sum forces are imposed to the object: the right side sum forces and the left side sum forces. In order to compute these forces, there are

$$F_{total_R}^{j,d} = \sum_{i=1}^{n_R^d} K_{i,j} x_{i,j}^d; \quad (19)$$

$$F_{total_L}^{j,d} = \sum_{l=1}^{n_L^d} K_{l,j} x_{l,j}^d, \quad (20)$$

where, respectively,  $F_{total_R}^{j,d}$  and  $F_{total_L}^{j,d}$  are the resultant force imposed to object  $j$  from the right and left side at the dimension  $d$ ;  $n_R^d$  and  $n_L^d$  are respectively the number of right and left robust/strong points of  $d$ th dimension;  $K_{i,j}$  and  $K_{l,j}$  show the spring stiffness connected to  $j$  object on one hand and the strong points on the other hand.

Now by applying the Hook law in  $d$ th dimension, there are

$$dX_R^{j,d} = \frac{F_{total_R}^{j,d}}{K_{equal_R}^j}; \quad (21)$$

$$dX_L^{j,d} = \frac{F_{total_L}^{j,d}}{K_{equal_L}^j}, \quad (22)$$

where  $dX_R^{j,d}$  and  $dX_L^{j,d}$  are respectively the  $j$  object dislocation to the right and to the left in the  $d$ th dimension.

Therefore, there is

$$dX^{j,d} = dX_R^{j,d} + dX_L^{j,d}, \quad (23)$$

where  $dX^{j,d}$  is the  $j$  object ultimate dislocation along with the  $d$  dimension.

This dislocation quantity can be positive or negative concerning equation (23). Now, there is

$$X^{j,d} = X_0^{j,d} + r_1 \times dX^{j,d}, \quad (24)$$

where  $X^{j,d}$  is related to the new balance point place and time of the  $j$  object in the  $d$  dimension;  $X_0^{j,d}$  is the  $j$  object initial balance point along with the  $d$  dimension. Here, there is a random number with a constant distribution within  $[0,1]$  time span which is used to keep the random mode of the search.

*The passing of time and the parameter updating.* At the beginning of the system formation, any object is randomly placed in a point in the space where it is the answer to the problem. At each moment of the time, objects are assessed and then their dislocations are computed after calculating equations (16) to (23). At the later time, the object holds a place at that position. The present used parameter is the spring stiffness coefficient which is updated at each level based on equation (16). The stop point can be determined after passing a definite time. The spring force algorithm different steps are shown as below:

1. Determining the system atmosphere and the allocating the initial quantities;
2. The initial positioning of objects;
3. Assessing and normalising the objects suitability;
4. The  $k$  parameter updating;
5. Forming the spring force and motion laws for each object;
6. Computing the values of objects dislocations;
7. Updating the objects positions/locations;
8. Repeating steps 3 to 7 till the stop point is satisfied;
9. Ending.

**Simulation result.** In order to simulate the proposed problem, the IEEE 33-bus and IEEE 69-bus radial network is used. The networks data, including the resistance and reactance of the lines and the loads connected to nodes, were presented in [7, 25]. In order to show the importance of studying the simultaneous placement and sizing of the DG units and the capacitors, first, for the proposed networks, placement, and sizes of the DG units and the capacitors are presented separately, and finally, the simultaneous placement and sizing of the DGs and capacitors is determined and the results are compared.

*Placement and sizing of DG.* In this section, placement and sizing of DG units regarding the minimum value of the problem objective function are defined. The results for this case are shown in Table 1.

*Placement and sizing of Capacitor.* In this section, placement and sizing of capacitors regarding the minimum value of the problem objective function are defined. The results for this case are shown in Table 2.

Table 1

Network	Capacity (kW)	Bus No.
33-bus	1987.1971	14
	656.4803	30
	203.0234	31
69-bus	958.3215	60
	245.2561	61
	260.4957	62

Table 2

Network	Capacity (kVAr)	Bus No.
33-bus	551.1281	14
	986.8425	30
69-bus	746.4401	64
	654.3891	65

*Simultaneous placement and sizing of DG and Capacitors.* In this section, placement and sizing of DG units and capacitors regarding the minimum value of the problem objective function are defined. The results for this case are shown in Table 3.

Table 3

Network	Capacity (kW)	Bus No.	Capacity (kVAr)	Bus No.
33-bus	504.8423	14	892.5297	12
	489.5621	16	344.2624	30
	750.3225	32	–	–
69-bus	893.2986	60	786.5941	24
	221.2428	61	702.4423	25
	857.5422	62	–	–

Losses and  $S_V$  of the system different case of study are shown in Table 4. The voltages profile of network before and after the installation of the DGs and capacitors are shown in Fig. 3 and Fig. 4.

Table 4

Network	Case study	Power losses (kVA)	$S_V$
IEEE 33-Bus	Base	243.6003	1.7009
	DG	106.5249	0.5301
	CAPACITOR	155.1845	0.7368
	DG and CAPACITOR	78.6582	0.2162
IEEE 69-Bus	Base	247.0873	1.8367
	DG	83.7836	0.5513
	CAP	158.5726	0.7068
	DG and CAPACITOR	29.6673	0.1278

**Discussion.** According to the above simulation results, the operation from the network that is in the presence of DG provided better conditions than the operation in the presence of the capacitors, which shows that the role of DG is more effective than that of the capacitors. Also, the simulation results show that the optimal operation of the network occurs in the simultaneous expansion planning of DGs and capacitors. Comparing the results, it is obvious that optimal operation from the network is obtained by the simultaneous placement of DG units and capacitors.

**Conclusions.** In this paper, we have presented a new approach for simultaneous placement and sizing of distributed generation and capacitors. Two sensitive indexes has been defined based on voltage profile and power loss of the network. Proposed methodology has been implemented in two stages. In the first stage, the candidate

buses for installation DG and capacitors has been determined. Then in the second stage, the places and sizes of the DGs and Capacitors have been located using SSA. The proposed algorithm is tested on IEEE-33 bus and IEEE-69 bus distribution system. The voltage profile and power loss of the system has improved to acceptable limit.

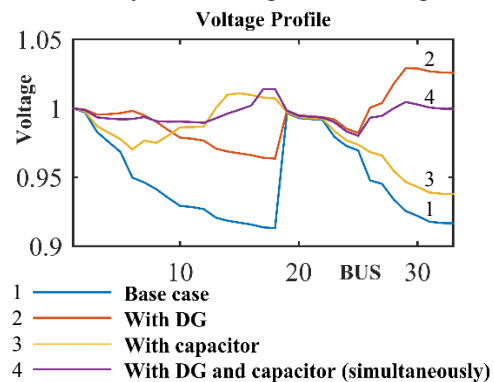


Fig. 3. Voltage profile of IEEE 33-Bus

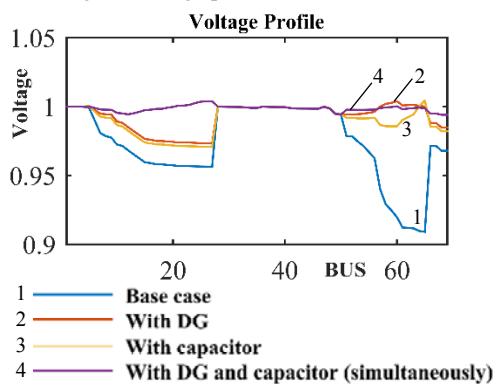


Fig. 4. Voltage profile of IEEE 69-Bus

## REFERENCES

1. Daly P.A. Morrison J. Understanding the potential benefits of distributed generation on power delivery systems. *2001 Rural Electric Power Conference*. Papers Presented at the 45th Annual Conference (Cat. No.01CH37214). doi: [10.1109/repcon.2001.949510](https://doi.org/10.1109/repcon.2001.949510).
2. Gözel T., Hocaoglu M.H. An analytical method for the sizing and siting of distributed generators in radial systems. *Electric Power Systems Research*, 2009, vol.79, no.6, pp. 912-918. doi: [10.1016/j.epsr.2008.12.007](https://doi.org/10.1016/j.epsr.2008.12.007).
3. Wang C., Nehrir M.H. Analytical approaches for optimal placement of distributed generation sources in power systems. *IEEE Transactions on Power Systems*, 2004, vol.19, no.4, pp. 2068-2076. doi: [10.1109/tpwrs.2004.836189](https://doi.org/10.1109/tpwrs.2004.836189).
4. Abou El-Ela A.A., Allam S.M., Shatla M.M. Maximal optimal benefits of distributed generation using genetic algorithms. *Electric Power Systems Research*, 2010, vol.80, no.7, pp. 869-877. doi: [10.1016/j.epsr.2009.12.021](https://doi.org/10.1016/j.epsr.2009.12.021).
5. Barin A., Pozzatti L.F., Canha L.N., Machado R.Q., Abaide A.R., Arend G. Multi-objective analysis of impacts of distributed generation placement on the operational characteristics of networks for distribution system planning. *International Journal of Electrical Power & Energy Systems*, 2010, vol.32, no.10, pp. 1157-1164. doi: [10.1016/j.ijepes.2010.06.015](https://doi.org/10.1016/j.ijepes.2010.06.015).
6. Ghosh S., Ghoshal S.P., Ghosh S. Optimal sizing and placement of distributed generation in a network system. *International Journal of Electrical Power & Energy Systems*, 2010, vol.32, no.8, pp. 849-856. doi: [10.1016/j.ijepes.2010.01.029](https://doi.org/10.1016/j.ijepes.2010.01.029).
7. Etehadi M., Ghasemi H., Vaez-Zadeh S. Voltage stability-based DG placement in distribution networks. *IEEE Transactions on Power Delivery*, 2013, vol.28, no.1, pp. 171-178. doi: [10.1109/tpwrd.2012.2214241](https://doi.org/10.1109/tpwrd.2012.2214241).
8. Wang Z., Chen B., Wang J., Begovic M.M. Stochastic DG placement for conservation voltage reduction based on multiple

- replications procedure. *IEEE Transactions on Power Delivery*, 2015, vol.30, no.3, pp. 1039-1047. doi: [10.1109/tpwrd.2014.2331275](https://doi.org/10.1109/tpwrd.2014.2331275).
9. Rahmani-andebili M. Distributed generation placement planning modeling feeder's failure rate and customer's load type. *IEEE Transactions on Industrial Electronics*, 2016, vol.63, no.3, pp. 1598-1606. doi: [10.1109/tie.2015.2498902](https://doi.org/10.1109/tie.2015.2498902).
10. Baran M.E., Wu F.F. Optimal capacitor placement on radial distribution systems. *IEEE Transactions on Power Delivery*, 1989, vol.4, no.1, pp. 725-734. doi: [10.1109/61.19265](https://doi.org/10.1109/61.19265).
11. Chiang H.-D., Wang J.-C., Cockings O., Shin H.-D. Optimal capacitor placements in distribution systems. I. A new formulation and the overall problem. *IEEE Transactions on Power Delivery*, 1990, vol.5, no.2, pp. 634-642. doi: [10.1109/61.53065](https://doi.org/10.1109/61.53065).
12. Dura H. Optimum number, location, and size of shunt capacitors in radial distribution feeders a dynamic programming approach. *IEEE Transactions on Power Apparatus and Systems*, 1968, vol.PAS-87, no.9, pp. 1769-1774. doi: [10.1109/tpas.1968.291982](https://doi.org/10.1109/tpas.1968.291982).
13. Fawzi T., El-sobki S., Abdel-halim M. New approach for the application of shunt capacitors to the primary distribution feeders. *IEEE Transactions on Power Apparatus and Systems*, 1983, vol.PAS-102, no.1, pp. 10-13. doi: [10.1109/tpas.1983.317991](https://doi.org/10.1109/tpas.1983.317991).
14. Kaplan M. Optimization of number, location, size, control type, and control setting of shunt capacitors on radial distribution feeders. *IEEE Transactions on Power Apparatus and Systems*, 1984, vol.PAS-103, no.9, pp. 2659-2665. doi: [10.1109/tpas.1984.318238](https://doi.org/10.1109/tpas.1984.318238).
15. Kaur H., Kumar P., Sharma A., Kamaiya N. A study on optimal capacitor placement in distribution system: Conventional and Artificial Intelligence techniques. *2015 International Conference on Computation of Power, Energy, Information and Communication (ICCPEIC)*, Apr. 2015. doi: [10.1109/iccpeic.2015.7259457](https://doi.org/10.1109/iccpeic.2015.7259457).
16. Lee S., Grainger J. Optimum placement of fixed and switched capacitors on primary distribution feeders. *IEEE Transactions on Power Apparatus and Systems*, 1981, vol.PAS-100, no.1, pp. 345-352. doi: [10.1109/tpas.1981.316862](https://doi.org/10.1109/tpas.1981.316862).
17. Ponnasikko M., Rao K.S. Optimal choice of fixed and switched shunt capacitors on radial distributors by the method of local variations. *IEEE Transactions on Power Apparatus and Systems*, 1983, vol.PAS-102, no.6, pp. 1607-1615. doi: [10.1109/tpas.1983.317890](https://doi.org/10.1109/tpas.1983.317890).
18. Rinker R.E., Rembert D.L. Using the reactive current profile of a feeder to determine optimal capacitor placement. *IEEE Transactions on Power Delivery*, 1988, vol.3, no.1, pp. 411-416. doi: [10.1109/61.4272](https://doi.org/10.1109/61.4272).
19. Schmill J.V. Optimum size and location of shunt capacitors on distribution feeders. *IEEE Transactions on Power Apparatus and Systems*, 1965, vol.84, no.9, pp. 825-832. doi: [10.1109/tpas.1965.4766262](https://doi.org/10.1109/tpas.1965.4766262).
20. Su X., Masoum M.A.S., Wolfs P.J. PSO and improved BSFS based sequential comprehensive placement and real-time multi-objective control of delta-connected switched capacitors in unbalanced radial MV distribution networks. *IEEE Transactions on Power Systems*, 2016, vol.31, no.1, pp. 612-622. doi: [10.1109/tpwrs.2015.2398361](https://doi.org/10.1109/tpwrs.2015.2398361).
21. Sundhararajan S., Pahwa A. Optimal selection of capacitors for radial distribution systems using a genetic algorithm. *IEEE Transactions on Power Systems*, 1994, vol.9, no.3, pp. 1499-1507. doi: [10.1109/59.336111](https://doi.org/10.1109/59.336111).
22. Xu Y., Dong Z.Y., Wong K.P., Liu E., Yue B. Optimal capacitor placement to distribution transformers for power loss reduction in radial distribution systems. *IEEE Transactions on Power Systems*, 2013, vol.28, no.4, pp. 4072-4079. doi: [10.1109/tpwrs.2013.2273502](https://doi.org/10.1109/tpwrs.2013.2273502).
23. Sajjadi S.M., Haghifam M.-R., Salehi J. Simultaneous placement of distributed generation and capacitors in distribution networks considering voltage stability index. *International Journal of Electrical Power & Energy Systems*, 2013, vol.46, pp. 366-375. doi: [10.1016/j.ijepes.2012.10.027](https://doi.org/10.1016/j.ijepes.2012.10.027).
24. Esmaelian H.R., Darjany O., Mohammadian M. Optimal placement and sizing of DG units and capacitors simultaneously in radial distribution networks based on the voltage stability security margin. *Turkish Journal of Electrical Engineering & Computer Science*, 2014, p. 1-14. doi: [10.3906/elk-1203-7](https://doi.org/10.3906/elk-1203-7).
25. Pereira B.R., Martins da Costa G.R.M., Contreras J., Mantovani J.R.S. Optimal distributed generation and reactive power allocation in electrical distribution systems. *IEEE Transactions on Sustainable Energy*, 2016, vol.7, no.3, pp. 975-984. doi: [10.1109/tste.2015.2512819](https://doi.org/10.1109/tste.2015.2512819).
26. Dehghani M., Montazeri Z., Dehghani A., Seifi A.R. Spring search algorithm: A new meta-heuristic optimization algorithm inspired by Hooke's law. *2017 IEEE 4th International Conference on Knowledge-Based Engineering and Innovation (KBEI)*. doi: [10.1109/kbei.2017.8324975](https://doi.org/10.1109/kbei.2017.8324975).
27. Dehghani M., Montazeri Z., Dehghani A., Nouri N., Seifi A. BSSA: Binary spring search algorithm. *2017 IEEE 4th International Conference on Knowledge-Based Engineering and Innovation (KBEI)*, Dec. 2017., pp. 0220-0224. doi: [10.1109/kbei.2017.8324977](https://doi.org/10.1109/kbei.2017.8324977).
28. Dehghani M., Montazeri Z., Ehsanifar A., Seifi A.R., Ebadi M.J., Grechko O.M. Planning of energy carriers based on final energy consumption using dynamic programming and particle swarm optimization. *Electrical engineering & electromechanics*, 2018, no.5, pp. 62-71. doi: [10.20998/2074-272X.2018.5.10](https://doi.org/10.20998/2074-272X.2018.5.10).
29. Montazeri Z., Niknam T. Optimal utilization of electrical energy from power plants based on final energy consumption using gravitational search algorithm. *Electrical engineering & electromechanics*, 2018, no.4, pp. 70-73. doi: [10.20998/2074-272X.2018.4.12](https://doi.org/10.20998/2074-272X.2018.4.12).
30. Montazeri Z., Niknam T. Energy carriers management based on energy consumption. *2017 IEEE 4th International Conference on Knowledge-Based Engineering and Innovation (KBEI)*, Dec. 2017. doi: [10.1109/kbei.2017.8325036](https://doi.org/10.1109/kbei.2017.8325036).

Received 14.07.2018

M. Dehghani<sup>1</sup>, Candidate of Power Engineering, PhD Student,  
M. Mardaneh<sup>1</sup>, Doctor of Power Engineering, Associate  
Professor,

Z. Montazeri<sup>2</sup>, Candidate of Power Engineering, M.Sc.,  
A. Ehsanifar<sup>3</sup>, Candidate of Power Engineering, M.Sc.,  
M.J. Ebadi<sup>4</sup>, Doctor of Applied Mathematics, Assistant  
Professor,

O.M. Grechko<sup>5</sup>, Candidate of Technical Science, Associate  
Professor,

<sup>1</sup> Department of Electrical and Electronics Engineering,  
Shiraz University of Technology, Shiraz, Iran,  
e-mail: adanbax@gmail.com, mardaneh@sutech.ac.ir

<sup>2</sup> Department of Electrical Engineering,  
Islamic Azad University of Marvdasht, Marvdasht, Iran,  
e-mail: Z.montazeri2002@gmail.com

<sup>3</sup> Department of Power and Control,  
Shiraz University, Shiraz, Iran,  
e-mail: ali.ehsanifar2020@gmail.com

<sup>4</sup> Faculty of Marine Science,  
Chabahar Maritime University, Chabahar, Iran,  
e-mail: ebadi@cmu.ac.ir

<sup>5</sup> National Technical University «Kharkiv Polytechnic Institute»,  
2, Kyrpychova Str., Kharkiv, 61002, Ukraine,  
e-mail: a.m.grechko@gmail.com

#### How to cite this article:

Dehghani M., Mardaneh M., Montazeri Z., Ehsanifar A., Ebadi M.J., Grechko O.M. Spring search algorithm for simultaneous placement of distributed generation and capacitors. *Electrical engineering & electromechanics*, 2018, no.6, pp. 68-73. doi: [10.20998/2074-272X.2018.6.10](https://doi.org/10.20998/2074-272X.2018.6.10).

**Матеріали приймаються за адресою:**

**Кафедра "Електричні апарати", НТУ "ХПИ", вул. Кирпичова, 21, м. Харків, 61002, Україна**

**Електронні варіанти матеріалів по e-mail: [a.m.grechko@gmail.com](mailto:a.m.grechko@gmail.com)**

**Довідки за телефонами: +38 050 653 49 82 Клименко Борис Володимирович**

**+38 067 359 46 96 Гречко Олександр Михайлович**

**Передплатний індекс: 01216**

